UNIVERSITY OF CALIFORNIA

SANTA CRUZ

FROM FAT TO MELANIN: A TALE OF TWO ANTAGONISTS, RELATED BUT DISTINCT

A dissertation submitted in partial satisfaction
of the requirements for the degree of

DOCTOR OF PHILOSOPHY

in

CHEMISTRY and BIOCHEMISTRY

by

Darren A. Thompson

December 2009

The Dissertation of Darren A. Thompson is approved:

_____
Professor Theodore R. Holman, Chair

_____
Professor Glenn L. Millhauser

_____
Professor R. Scott Lokey

_____
Tyrus Miller
Vice Provost and Dean of Graduate Studies

Table of Contents

List of Figures

FROM FAT TO MELANIN: A TALE OF TWO ANTAGONISTS, RELATED BUT DISTINCT

By

Darren A. Thompson

Abstract

The two endogenous antagonists, Agouti Signaling Protein (ASIP) and Agouti Related Protein (AgRP), have much in common, but they vary quite dramatically in physiology. Structurally the C-terminus of both proteins are highly homologous, both act at similar 7TM-GPCRs known collectively as the melanocortin receptors, but the *in vivo* function of the two antagonists are entirely dissimilar. ASIP regulates pigment type switching, while AgRP controls satiety. This dissertation demonstrates the first ever total chemical synthesis of AgRP from fish. It also establishes, for the first time, a bacterial expression system for ASIP procurement as well as validates a robust technique of ASIP production. In addition it provides proof that the three contiguous amino acid residues, Arg-Phe-Phe, from the active loop of AgRP are indeed responsible for much of the pharmacology. Lastly it helps illuminate the mechanism of melanocortin 4 receptor auto-activation.

Acknowledgements

The human brain is a fascinating organ, it can amplify the pitfalls of life so much so you are blinded to all things beautiful. On May 15 1998, in an abandoned San Francisco apartment, I fell victim to my own personal demons. Eleven years later, on the verge of great human achievement, I reflect on the people who have made contribution to this doctorate.

I thank Dr. Glenn Millhauser whose frank honesty in my class evaluation for Chemistry 05 – Analytical Chemistry back in the spring of 1992 supplied the incentive of aspiration.

I owe Michael Siani hugely for sitting at my comatose bedside long hours in the hospital and for demonstrating friendship.

To my parents, Jim and Alicia Good, many thanks for your patience. My sister, one of the smartest people I know, you have my gratitude for believing in me, even when I did not merit that faith. Merci Mary Thompson for being the family matriarch and never forgetting my birthday.

I worked with some truly excellent scientists at Gryphon Sciences, Gianinne Figliozi, Michael Siani, Drs. Reyna Simon, Lynne Canne-Bannen, Paolo Botti, Michael Carrasco, Jill Wilken, Steve Kent, Donald Low, Christie Hunter, etc.. I was co-author on 21 scientific papers in respected journals from less than two years labor. Thank you so much for sharing the wealth of scientific knowledge you so artfully possessed.

I thank members of the Millhauser Research Group past and present. Dr. Joseph McNulty for determining the NMR structures of ASIP and AgRP. Dr. Pilgrim Jackson for being a good human being. Dr. Bin Yu for making my trip to Beijing special by introducing me to Dejun Luv. I am grateful to Micah Visconte for

teaching me to use the DNA thermocycler. Matthew Nix for lively discussion and setting an example for future graduate students. Ann Spevacek, Chris Dudzik, Alex McDonald, and Eric Evans for sharing libations. Michael Madonna for being ridiculous and making me laugh. Dr. Eric Walter for fixing things and general expertise. Undergraduates Michael Mendoza, Hilary Rood, Nicolai Douglas, and Justin Bursch for invaluable assistance.

I'm appreciative of my collaborators, without who the biological activity could not be established, Drs. Gregory Barsh, Ira Gantz, Christian Vaisse, Jose-Miguel Cerda Reverter, and Christopher Kaelin.

Finally, since no one is an island, I thank my friends, Clint and Kari Steele, Tony Lialin, David Rogow, Victor Kenyon, Drs. Debraj Ghosh, Joshua DesChamps, Zachary Sharrett, Monica Lares, Joni Bock, Abraham Wolcott, Eefei Chen and others: a toast with champagne to you all.

Introduction

The melanocortin system (figure 0.1) consists of 5 seven trans-membrane G protein coupled receptors (MC1-5R), a series of agonists derived from the proopiomelanocortin (POMC) precursor protein, and two endogenous antagonists, Agouti Signaling Protein (ASIP) and Agouti Related Protein (AgRP). These two antagonists share similar sequences (figure 0.2) as well as related exon/intron genomic structures but distinct patterns of expression (*1, 2*) and dramatically different functions. In mice ASIP controls the type of melanin produced (figure 0.3) and AgRP functions in a satiety switch, in humans the role of ASIP is unclear, but AgRP has identical responsibilities.

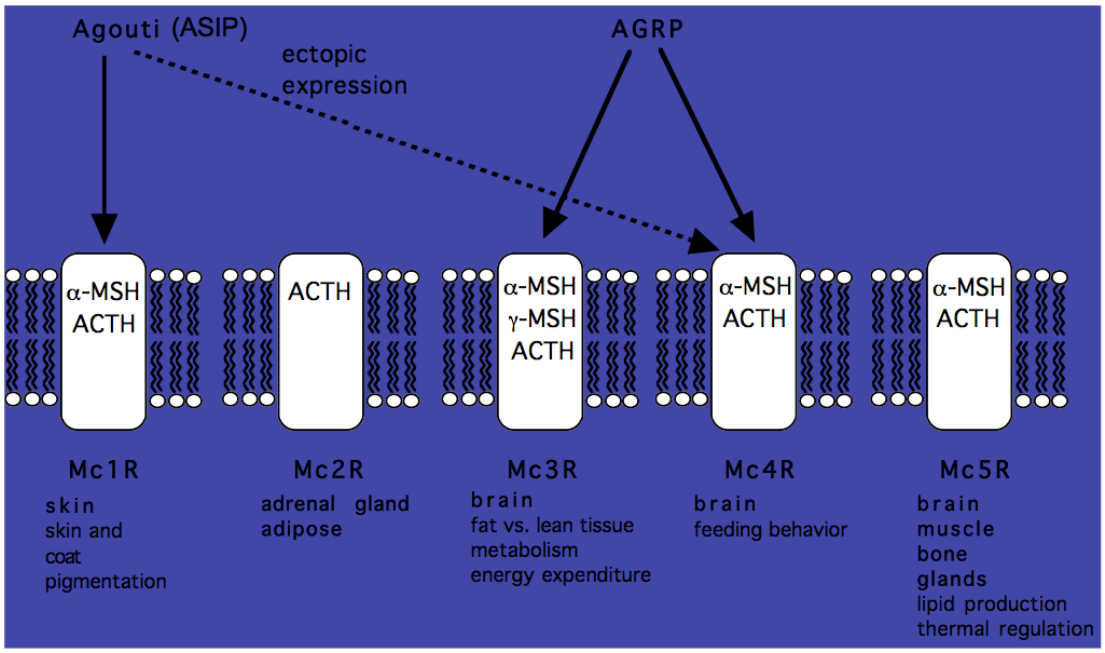

Figure 0.1. Diagram of the melanocortin system. The five receptors represented as rounded rectangles, with agonist peptides appearing inside rectangles, tissue specific expression and known function pasted beneath, and antagonists above. The solid arrows represent wild type activity, broken arrow indicates activity in the lethal yellow mouse.

Over the past decade I have contributed substantially to the AgRP knowledge base (*3-11*), but little to understanding the biochemistry of ASIP (*12*). All the published AgRP variants chemically synthesized by the Millhauser research group have been some form of the C-terminal domain. Quite serendipitously this turns out to be the in vivo processed portion of the active protein (*13*). This may not be the case with ASIP. There is a highly conserved region in the N-terminus of ASIP absent in AgRP (*14*). Western blots of protein secreted from mouse skin detect a band consistent with the full length protein (*15*). Interaction of ASIP with attractin requires the N-terminus (*17*). The wild type C-terminal domain of ASIP does not undergo spontaneous in vitro folding (*12*). All the AgRP analogues were made using SPPS, ASIP constructs needed another method of fabrication. Recombinant DNA technology provided an attractive alternative to organic synthesis. Typically, protein chemists are heavily invested in recombinant methods and move to SPPS as an option. However my career has been atypical, as I started out using organic synthesis and went to a recombinant system for ASIP production.

```
        10         20         30         40         50         60
MDVTRLLLAT LVSFLCFFTV HSHLALEETL GDDRSLRSNS SMNSLDFSSV SIVALNKKSK
        70         80         90        100        110        120
KISRKEAEKR KRSSKKKASM KKVARPPPPS PCVATRDSCK PPAPACCDPC ASCQCRFFGS
       130
ACTCRVLNPN C

        10         20         30         40         50         60
MLTAMLLSCV LLLALPPTLG VQMGVAPLKG IRRPDQALFP EFPGLSLNGL KKTTADRAEE
        70         80         90        100        110        120
VLLQKAEALA EVLDPQNRES RSPRRCVRLH ESCLGQQVPC CDPCATCYCR FFNAFCYCRK
       130
LGTATNLCSR T
```

```
CVATRDSCKPPAPACCDPCASCQCRFFGSACTCR-V-LNPN-C
CVRLHESCLGQQVPCCDPCATCYCRFFNAFCYCRKLGTATNLCSR T
```

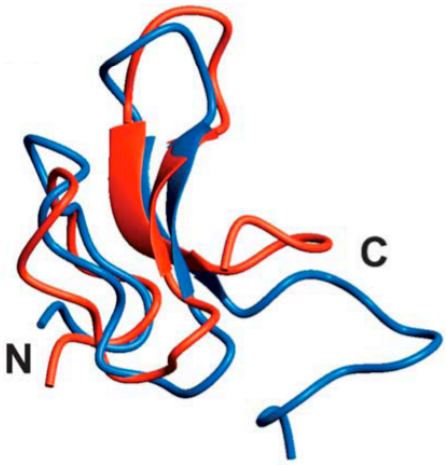

Figure 0.2. (Top) The full primary sequences of ASIP and AgRP from mouse, ASIP C-terminus in red, AgRP in blue. (Bottom left) Sequence alignment of the C-terminus for the two proteins beginning with the first cysteine. Identical residues highlighted in cyan. (Bottom right) Structural alignment of the C-terminus for the two proteins (PDB ID's 1HYK and 1Y7J), again ASIP in red, AgRP in blue.

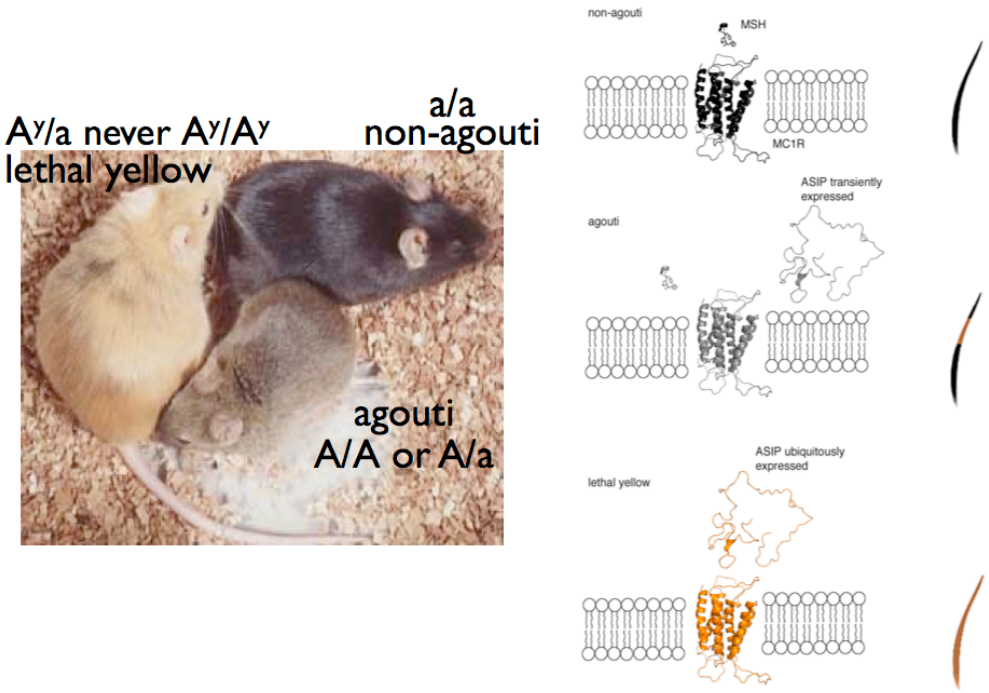

Figure 0.3. (Left) Representative phenotypes, along with genotypes, of mice and (Right) a model for coat color genesis. MC1R=melanocortin 1 receptor, MSH=melanocyte stimulating hormone, ASIP=agouti signaling protein.

Originally the title of my dissertation was "The Origin of the Mouse Mahogany Phenotype". This phenotype is intimately associated with ASIP. The mahogany phenotype refers to mice coat color and is caused by mutation in the attractin gene resulting in N-terminally truncated protein (*16*). Full length, wild type attractin has affinity for ASIP (*17*), leading to a hypothesis about ASIP involvement in generation of the mahogany phenotype. Briefly, as stated above, ASIP controls the type of melanin pigment produced. This happens through the MC1R, when this receptor is activated, eumelanin, or brown pigment, is produced; when it is antagonized (i.e. off) by ASIP, pheomelanin biosynthesis, or yellow pigment, dominates (*18*). Mahogany

mice over expressing ASIP are brown, normally ASIP over expression produces a yellow coat, a functional attractin molecule (i.e. one that binds ASIP) is necessary for MC1R antagonism by ASIP. Generating speculation of a ternary complex between MC1R, ASIP, and attractin. There is biochemical evidence supporting the binary complexes between MC1R/ASIP and attractin/ASIP, and genetic evidence of a ternary complex, nonetheless biochemical confirmation of the ternary interaction is required. Mahogany mice ectopically expressing ASIP are thin, in contrast, ubiquitous ASIP production usually results in obesity due to antagonism of MC4R, bolstering the ternary complex scenario, MC4R/ASIP/attractin. He et al. 2001 demonstrated the absence of a binary contact between attractin and AgRP, making an interaction between ASIP and attractin unlikely for the inhibition of MC4R, it is now generally accepted the weight loss observed in mahogany mice is caused by brain spongiform vacuolization (*19*). Other groups have proposed alternate explanations to explain the attractin role in pigmentation (*20*), it was my goal to produce sufficient ASIP to make a biochemical experiment feasible, and nail down the origin of the mouse mahogany phenotype, but that should be a thesis of a future graduate student.

The interaction of ASIP and attractin wholly depends on residues in the N-terminus, while the affinity for MC1R resides in the C-terminal half of the molecule. An experiment detailing the ternary complex must feature the full length protein. Figure 0.2 shows full length ASIP is 109 amino acids; as the first two chapters of this dissertation reveal, single chain SPPS can produce peptides and even small proteins, but 109 residues goes well beyond

the threshold of single chain SPPS. The reason for this is quite elementary, the addition of each successive amino acid to the growing peptide chain requires two organic reactions, a deprotection and a coupling, even if the yield of each were 99%, quite good for organic synthesis, the overall yield would be $.99^{218}$ x 100% or 11.2%. Native chemical ligation developed by Kent and co-workers solves this conundrum, but the majority of techniques stemming from his laboratory employ anhydrous HF (*21*). Giving a reason to try recombinant DNA methods. Another rationale for abandoning SPPS in favor of bacterial protein expression is I wanted to give it a try.

Chapter 1 is a rewritten, submitted manuscript by Baran Ersoy in the laboratory of Christian Vaisse. Chapter 2 is rewritten to emphasize my part in the research and is published by Jose-Miguel Cerda-Reverter. Chapters 3 and 4 detail my foray into the wonderful world of Molecular Biology. Chapter 5 is a paper I wrote describing several small molecule mimics of AgRP. Small molecules functioning like AgRP have recently found use in mouse models of cachexia and will eventually treat humans suffering from this and other wasting conditions (*22*). Although this dissertation touches on a number of subjects, I hope the reader realizes the overarching theme. I started my graduate school experience synthesizing AgRP, involved in fat, ended up making ASIP, involved in melanin, "from fat to melanin", both are antagonists, "a tale of two antagonists", with homologous sequences while having strikingly diverse functions, "related but distinct".

References

1. Miller, M. W., Duhl, D. M., Vrieling, H., Cordes, S. P., Ollmann, M. M., Winkes, B. M., and Barsh, G. S. (1993) Cloning of the mouse agouti gene

predicts a secreted protein ubiquitously expressed in mice carrying the lethal yellow mutation, *Genes Dev 7*, 454-467.
2. Ollmann, M. M., Wilson, B. D., Yang, Y. K., Kerns, J. A., Chen, Y., Gantz, I., and Barsh, G. S. (1997) Antagonism of central melanocortin receptors in vitro and in vivo by agouti-related protein, *Science 278*, 135-138.
3. Yang, Y. K., Thompson, D. A., Dickinson, C. J., Wilken, J., Barsh, G. S., Kent, S. B., and Gantz, I. (1999) Characterization of Agouti-related protein binding to melanocortin receptors, *Mol Endocrinol 13*, 148-155.
4. Bolin, K. A., Anderson, D. J., Trulson, J. A., Thompson, D. A., Wilken, J., Kent, S. B., Gantz, I., and Millhauser, G. L. (1999) NMR structure of a minimized human agouti related protein prepared by total chemical synthesis, *FEBS Lett 451*, 125-131.
5. McNulty, J. C., Thompson, D. A., Bolin, K. A., Wilken, J., Barsh, G. S., and Millhauser, G. L. (2001) High-resolution NMR structure of the chemically-synthesized melanocortin receptor binding domain AGRP(87-132) of the agouti-related protein, *Biochemistry 40*, 15520-15527.
6. Jackson, P. J., McNulty, J. C., Yang, Y. K., Thompson, D. A., Chai, B., Gantz, I., Barsh, G. S., and Millhauser, G. L. (2002) Design, pharmacology, and NMR structure of a minimized cystine knot with agouti-related protein activity, *Biochemistry 41*, 7565-7572.
7. Chai, B. X., Neubig, R. R., Millhauser, G. L., Thompson, D. A., Jackson, P. J., Barsh, G. S., Dickinson, C. J., Li, J. Y., Lai, Y. M., and Gantz, I. (2003) Inverse agonist activity of agouti and agouti-related protein, *Peptides 24*, 603-609.
8. Millhauser, G. L., McNulty, J. C., Jackson, P. J., Thompson, D. A., Barsh, G. S., and Gantz, I. (2003) Loops and links: structural insights into the remarkable function of the agouti-related protein, *Ann N Y Acad Sci 994*, 27-35.
9. Thompson, D. A., Chai, B. X., Rood, H. L., Siani, M. A., Douglas, N. R., Gantz, I., and Millhauser, G. L. (2003) Peptoid mimics of agouti related protein, *Bioorg Med Chem Lett 13*, 1409-1413.
10. Sanchez, E., Rubio, V. C., Thompson, D., Metz, J., Flik, G., Millhauser, G. L., and Cerda-Reverter, J. M. (2009) Phosphodiesterase inhibitor-dependent inverse agonism of agouti-related protein on melanocortin 4 receptor in sea bass (Dicentrarchus labrax), *Am J Physiol Regul Integr Comp Physiol 296*, R1293-1306.
11. Yang, Y. K., Dickinson, C. J., Zeng, Q., Li, J. Y., Thompson, D. A., and Gantz, I. (1999) Contribution of melanocortin receptor exoloops to Agouti-related protein binding, *J Biol Chem 274*, 14100-14106.
12. McNulty, J. C., Jackson, P. J., Thompson, D. A., Chai, B., Gantz, I., Barsh, G. S., Dawson, P. E., and Millhauser, G. L. (2005) Structures of the agouti signaling protein, *J Mol Biol 346*, 1059-1070.

13. Creemers, J. W., Pritchard, L. E., Gyte, A., Le Rouzic, P., Meulemans, S., Wardlaw, S. L., Zhu, X., Steiner, D. F., Davies, N., Armstrong, D., Lawrence, C. B., Luckman, S. M., Schmitz, C. A., Davies, R. A., Brennand, J. C., and White, A. (2006) Agouti-related protein is posttranslationally cleaved by proprotein convertase 1 to generate agouti-related protein (AGRP)83-132: interaction between AGRP83-132 and melanocortin receptors cannot be influenced by syndecan-3, *Endocrinology 147*, 1621-1631.
14. Jackson, P. J., Douglas, N. R., Chai, B., Binkley, J., Sidow, A., Barsh, G. S., and Millhauser, G. L. (2006) Structural and molecular evolutionary analysis of Agouti and Agouti-related proteins, *Chem Biol 13*, 1297-1305.
15. Ollmann, M. M., and Barsh, G. S. (1999) Down-regulation of melanocortin receptor signaling mediated by the amino terminus of Agouti protein in Xenopus melanophores, *J Biol Chem 274*, 15837-15846.
16. Gunn, T. M., Miller, K. A., He, L., Hyman, R. W., Davis, R. W., Azarani, A., Schlossman, S. F., Duke-Cohan, J. S., and Barsh, G. S. (1999) The mouse mahogany locus encodes a transmembrane form of human attractin, *Nature 398*, 152-156.
17. He, L., Gunn, T. M., Bouley, D. M., Lu, X. Y., Watson, S. J., Schlossman, S. F., Duke-Cohan, J. S., and Barsh, G. S. (2001) A biochemical function for attractin in agouti-induced pigmentation and obesity, *Nat Genet 27*, 40-47.
18. Millar, S. E., Miller, M. W., Stevens, M. E., and Barsh, G. S. (1995) Expression and transgenic studies of the mouse agouti gene provide insight into the mechanisms by which mammalian coat color patterns are generated, *Development 121*, 3223-3232.
19. Bronson, R. T., Donahue, L. R., Samples, R., Kim, J. H., and Naggert, J. K. (2001) Mice with mutations in the mahogany gene Atrn have cerebral spongiform changes, *J Neuropathol Exp Neurol 60*, 724-730.
20. Duke-Cohan, J. S., Kim, J. H., and Azouz, A. (2004) Attractin: cautionary tales for therapeutic intervention in molecules with pleiotropic functionality, *J Environ Pathol Toxicol Oncol 23*, 1-11.
21. Dawson, P. E., Muir, T. W., Clark-Lewis, I., and Kent, S. B. (1994) Synthesis of proteins by native chemical ligation, *Science 266*, 776-779.
22. Chen, C., Tucci, F. C., Jiang, W., Tran, J. A., Fleck, B. A., Hoare, S. R., Wen, J., Chen, T., Johns, M., Markison, S., Foster, A. C., Marinkovic, D., Chen, C. W., Arellano, M., Harman, J., Saunders, J., Bozigian, H., and Marks, D. (2008) Pharmacological and pharmacokinetic characterization of 2-piperazine-alpha-isopropyl benzylamine derivatives as melanocortin-4 receptor antagonists, *Bioorg Med Chem 16*, 5606-5618.

Chapter 1

Constitutive Activity of the Human Melanocortin 4 Receptor

(Much of the text and figures of this chapter appeared originally as "Expanding the role of the N-terminal domain in the evolution of Class A GPCR activity modulation." submitted to PLoS Biology. This work was done in the laboratory of Christian Vaisse and is reprinted with his permission. My role in this project was the synthesis of portions of the N-terminal domain, purification of said peptides, and development of methods to narrow in on the active residues in that domain.)

Introduction

Despite recognition of the problem and proposed solutions, obesity remains one of the chief health concerns in America (*1*) and the entire globe. The viability of a solution must be questioned if the problem still exists. Obesity is linked to increased risk for type II diabetes, elevated blood pressure, coronary artery disease, and stroke. The prevalence of these conditions have become so common that clinicians have coined a new term, metabolic syndrome, to describe these diseases.

Positive energy balance, consuming more calories than one utilizes, can lead to weight gain and eventually obesity. A source of positive energy balance is hyperphagia (i.e. overeating). Mice with hypothalamic targeted disruption of the melanocortin 4 receptor (MC4R) are hyperphagic and hence obese (*2*). The MC4R is a seven transmembrane G protein coupled receptor which, when activated, creates a satiety signal. Spontaneous, non-synonymous mutations in the coding region of MC4R are among the most common monogenic origins of obesity (*3*).

Basal activity of the MC4R contributes to tonic satiety and the absence of a constant foraging for food (*4*). The N-terminus of the MC4R is necessary for basal stimulation (*5*). A number of mutations in the N-terminus of MC4R are linked to human obesity, these include T11A, R18C, and R18L (*6*). A transmembrane tethered N-terminal construct of hMC4R transactivates a truncated receptor starting at residue 24. Somewhere in the first 23 amino acids is a region responsible for the receptor's constitutive activity. An

attractive technique for producing short peptides in large quantities is solid phase peptide synthesis.

Protein protein interaction can typically be narrowed down to just a few key residues. The constitutive activity of the MC4R is analogous to the agonist adrenocorticotrophic hormone (ACTH). ACTH is 39 amino acids in length, similar to the N-terminus of MC4R (figure 1.1), however all the binding energy comes from the contact of just 4 residues, 6-9 (His-Phe-Arg-Trp). Peptide synthesis can rapidly make regions of MC4R N-terminus and hone in on the sequence responsible for activating the receptor at the basal level.

Methods

MC4R ligands- Melanotan-II was obtained from Genscript (Piscataway, NJ). 1,2,3,4-tetrahydroisoquinoline (THIQ) was provided by Merck Research Labs (Rahway, NJ). Melanocyte stimulating hormone and AgRP were purchased from Phoenix Pharmaceuticals (Belmont, CA).

MC4R plasmid constructs- Wild-type (WT) and E42K human MC4R genes were cloned from genomic DNA into the vector pcDNA 3.1 as previously described (*7*). MC4R D1-24 was made as described, and the prolactin signal peptide and a Flag epitope tag (DYKDDDD) were added to both WT and MC4R D1-24 for identical membrane localization (Srinivasan et al. 2004).

Ligand binding assay- Ligand binding was carried out as previously described(*8*). Briefly, HEK293 cells were stably transfected with WT or mutant MC4R. Competitive binding was measured as a function of radiolabeled MC4R ligand displacement ([^{125}I]-NDP-αMSH, [^{125}I]-AgRP -

PerkinElmer Life and Analytical Sciences, Billerica, MA) in the presence of increasing concentrations of a competitive ligand. Gamma counter readings were normalized for non-specific binding and plotted as a percentage of maximum radioligand binding.

MC4R activity- MC4R activty was measured as previously described (*9*). Briefly, HEK293 cells were transiently transfected with WT or mutant MC4R plasmid, renilla luciferase, and a firefly luciferase reporter that is driven by a cAMP responsive element. After stimulation with a choice of ligand, luciferase activity was measured using the Steady-Glo Luciferase Assay System (Promega, Madison, WI) and a microplate luminescence counter (Packard Instrument, Downers Grove, IL). Firefly luciferase activity upon MC4R activation was normalized over the transfection efficiency by dividing the firefly luciferase activity by the renilla luciferase activity. The results were normalized to the percentage of the maximum stimulation observed.

Peptide synthesis- Fmoc-Asn(Trt)-OH, Fmoc-Arg(Pbf)-OH, Fmoc-Gly-OH, Fmoc-His(Trt)-OH, Fmoc-Leu-OH, Fmoc-Met-OH, Fmoc-Ser(tBu)-OH, Fmoc-Thr(tBu)-OH, Fmoc-Trp(Boc)-OH, Fmoc-Tyr(tBu)-OH, Fmoc-Val-OH and Rink Amide MBHA resin were purchased from Novabiochem (San Diego, CA). All peptides were assembled as amides on an Applied Biosystems (Foster City, CA) model 433a automated peptide synthesizer using modified cycles with HBTU/DIEA mediated coupling, DMF as solvent (Fisher or EM Science), and a deprotecting solution of 1:1:98 1,8-Diazabicyclo[5.4.0]undec-7-ene:Hexamethyleneimine:DMF. The proper molecular mass was confirmed

by a Waters (Milford, MA) ZMD ESI-MS. All peptides were lyophilized following HPLC purification.

Molecular modeling of MC4R A homology model of the seven transmembrane helices of the MCR4r was constructed based in the crystal structure of the β2-adrenergic receptor (PDB id P32245). The sequence alignment was based on the most conserved residues found in all class A GPCRs (*10*). Side chains were placed using SCWRL 3.0. Local geometries were optimized with 1026 steps of steepest descent energy minimization using the Gromas package.

Statistical Analysis- For the competitive ligand binding assay, best-fit estimates of the IC_{50} and its 95% confidence intervals were obtained by non-linear regression fitting of the one site competition curves using Prism 4. For MC4R activity dose response curves, best-fit estimates of the EC_{50}, IC_{50} and their 95% confidence intervals were obtained by non-linear regression fitting of the sigmoidal dose response (variable slope) curves using Prism 4.

RESULTS

The N-terminal domain of MC4R acts as a diffusible ligand.

We had previously demonstrated that the N-terminal domain of MC4R is a tethered ligand and is essential for the maintenance of its constitutive activity. Specifically, a receptor lacking the first 24 N-terminal amino acids (MC4R Δ1-24, Figure 1.1) responds normally to a panel of agonists and to AGRP antagonism of αMSH but has a low constitutive activity that can be rescued by co-expression of the MC4R N-terminal domain chimerically linked to the trans-membrane domain of CD-8. The activation of MC4R by its N-terminal domain resembles that of PAR1, in which unmasking of the active

site requires proteolytic cleavage by thrombin (*11*). In the case of PAR1, it had been shown that, in the absence of thrombin, exogenous addition of a synthetic peptide mimicking the unmasked active N-terminal domain can also lead to the activation of the receptor (*12*). To determine whether this could also be the case for MC4R, we tested whether a peptide mimicking amino acids 2 through 26 of the N-terminal domain would act as a partial agonist for MC4R Δ1-24. Indeed, at 100μM, MC4R2-26, but not MC4R20-39, increased the activity of MC4R Δ1-24 to the level of the constitutive activity of WT MC4R (Figure 1.2a). The low potency of the N-terminal domain activation (EC50=72μM) (Figure 1.2b) is compatible with the high local concentration in the tethered form and is similar to that observed in the case of PAR1.

Figure 1.1: The serpentine of MC4R outlining the studied amino acids. MC4R Δ1-24, ATG translational start site (dashed line). Naturally occurring obesity causing mutations (white on black). Mutations that cause premature termination of translation or frame shift are not shown. Residues implicated exclusively in the αMSH activation of MC4R (white on grey). Alanine mutagenesis targeted polar and aromatic amino acids (black on grey).

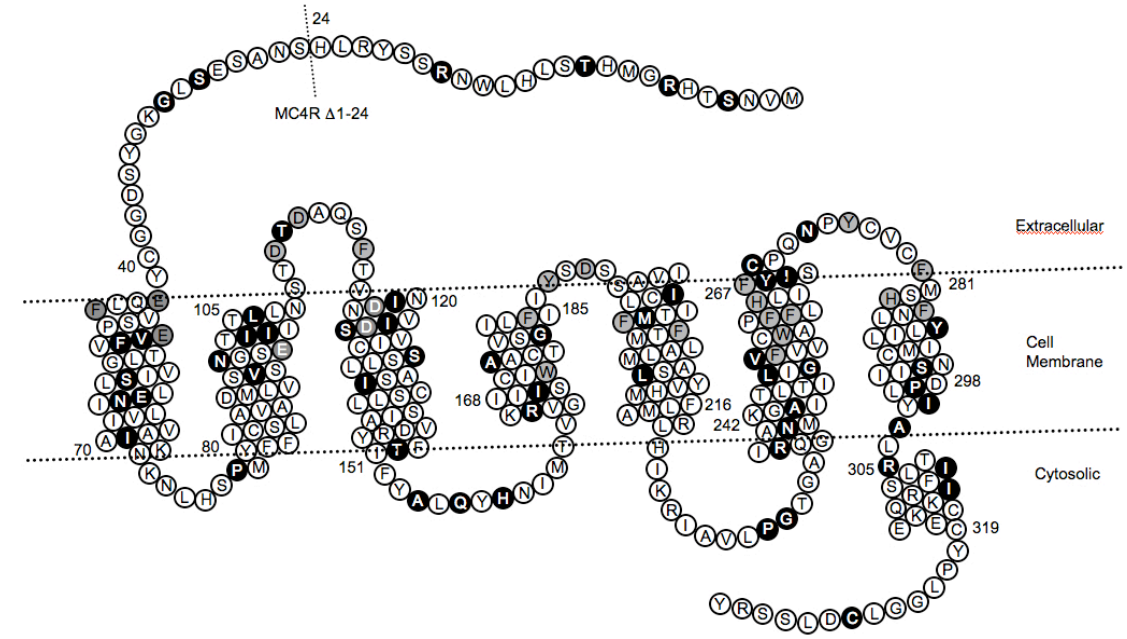

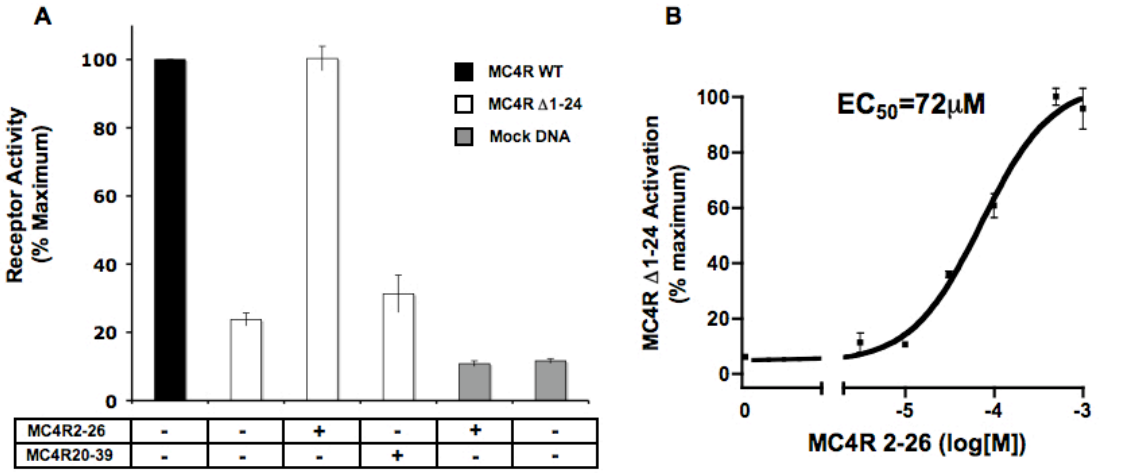

Figure 1.2: MC4R2-26 peptide is a partial agonist of MC4R Δ1-24. A) The full 2-39 amino acid sequence of MC4R N-terminal domain has been synthesized as two peptides: 2nd through 26th amino acids (MC4R2-26) and 20th through 39th amino acids (mock peptide). Stimulation of MC4R Δ1-24 with 2-26 vs. 20-39 N-terminal peptides. The assay control for background activation was done using pcDNA3.1 that encodes LacZ. B) MC4R2-26 dose response. MC4R Δ1-24 transfected cells were stimulated with increasing concentrations of MC4R2-26. Receptor activation is calculated as percentage of maximal activity recorded in the presence of MC4R2-26 (0.5mM).

AGRP antagonizes the diffusible MC4R2-26 N-terminal domain.

AGRP is both an antagonist of αMSH and an inverse-agonist at the MC4R (*13*). Its antagonist activity is independent of the N-terminal domain. Availability of an active diffusible N-terminal domain allowed us to test whether the inverse-agonist activity of AGRP could be exclusively assigned to antagonism of the N-terminal domain (Figure 1.3a). AgRP antagonized the activation of MC4R Δ1-24 by MC4R2-26 with an identical EC50 as that for the inverse agonism of AgRP on the WT receptor (Figure 1.3b). In addition, MC4R2-26 displaced radio-labeled AgRP with similar affinities for WT and Δ1-24 MC4R (Figure 1.3c). Together, these data indicate that the inverse agonist activity of AGRP at the MC4R can be attributed to its antagonism of the N-terminal domain of that receptor.

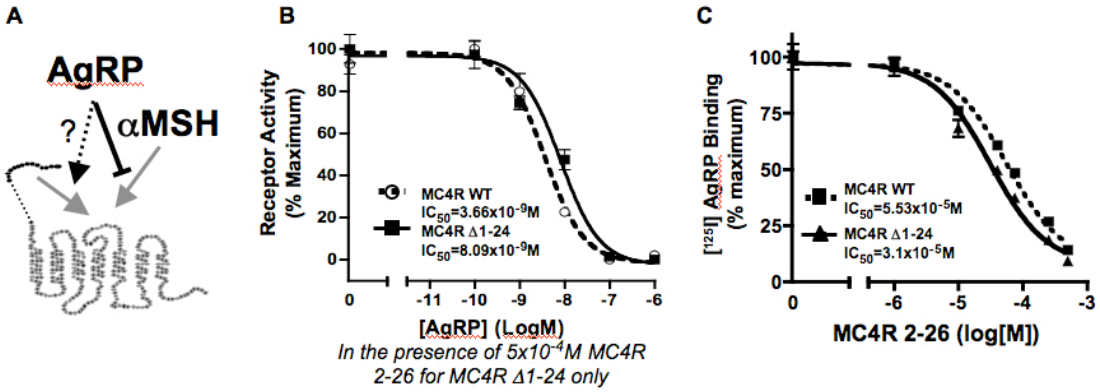

Figure 1.3: Independent modulation of MC4R2-26 activation. A) The model of Independent regulation of N-terminal domain by the AgRP. B) AgRP antagonism of MC4R2-26 activation of MC4R Δ1-24 compared to AgRP inverse agonism of WT MC4R. C) MC4R2-26 binding to Δ1-24 and WT MC4R. ^{125}I AgRP is used as the competitive radio-labeled ligand. Error bars represent standard error for the triplicate.

The MC4R2-26 activation site does not overlap with the αMSH activation site.

Three acidic residues in the second and third transmembrane domains of melanocortin receptors (E100 , D122 , and D126 in MC4R, Figure 1.1 - white on grey) are essential for their activation by melanocortins. Alanine substitution of these residues impairs αMSH binding and activation but does not decrease the constitutive activity of the receptor. To determine if the activation site of MC4R by its N-terminal domain overlaps with αMSH, we tested whether these mutations also affected activation by the N-terminal domain. When introduced into MC4RΔ1-24, E100A, D122A and D126A impaired activation of the receptor by αMSH but not by MC4R2-26 (Figure 1.4) demonstrating that these three residues are not implicated in activation by the N-terminal domain.

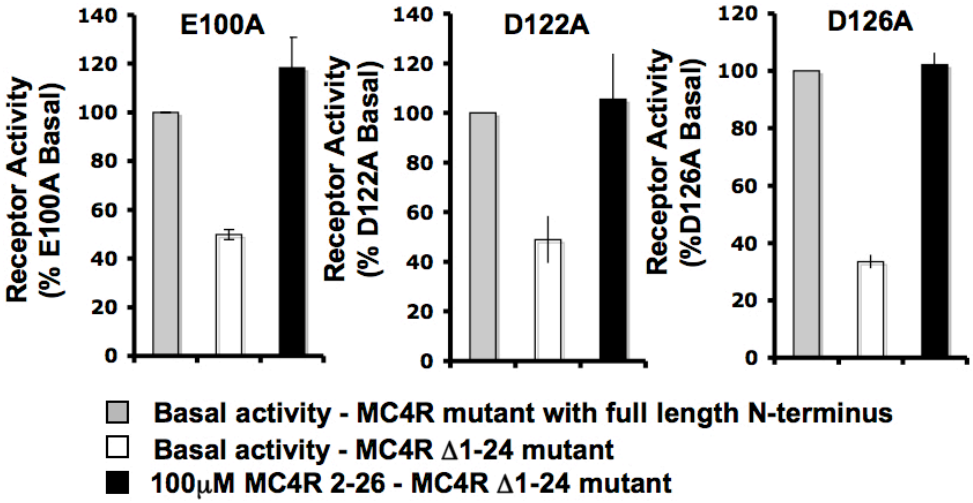

Figure 1.4: The basal activity of full length E100A, D122A, and D126A MC4Rs (black). The basal activity of truncated Δ1-24 MC4R E100A, Δ1-24 MC4R D122A, and Δ1-24 MC4R D126A (white). MC4R2-26 stimulation of truncated Δ1-24 MC4R E100A, Δ1-24 MC4R D122A, Δ1-24 MC4R D126A (grey). Error bars represent standard error for the triplicate.

The peptide sequence HLWNRS is the minimum activating sequence of the N-terminal domain of MC4R.

To further outline the molecular basis of the N-terminal activation of MC4R, we first delineated the minimal activating region of the N-terminal domain. We tested overlapping peptides spanning the MC4R N-terminus for their activity at MC4R Δ1-24. Setting hexapeptides as the shortest sequence length, all possible combinations produced 9 smaller overlapping peptides in addition to the original MC4R2-26 peptide (Figure 1.5). While MC4R2-26 showed the greatest activity, some of its segments failed to activate MC4R Δ1-24 (Figure 1.5). All activating peptides shared the common sequence His14-Leu15-Trp16-Asn17-Arg18-Ser19 (MC4R14-19). Notably, this minimal activating sequence encompasses the most conserved portion of the N-terminal region throughout several species (Figure 1.6), encompasses Arg18, a previously described genetic "hotspot" for obesity-causing mutations in the MC4R and can be targeted by a specific antibody with relevant physiological consequences as antibodies against the overlapping rat MC4R11-25 act as inverse agonists in vitro and lead to increased food intake and body weight in rats (*14*).

We further determined the relative role of specific amino-acids within this minimal activating sequence. Substitutions of His14, Arg18 and W16 significantly decreased the activity of MC4R14-19 suggesting that N-terminal domain activation may be due to interaction with accessible aromatic or charged residues in the transmembrane core of the receptor (Figure 1.5).

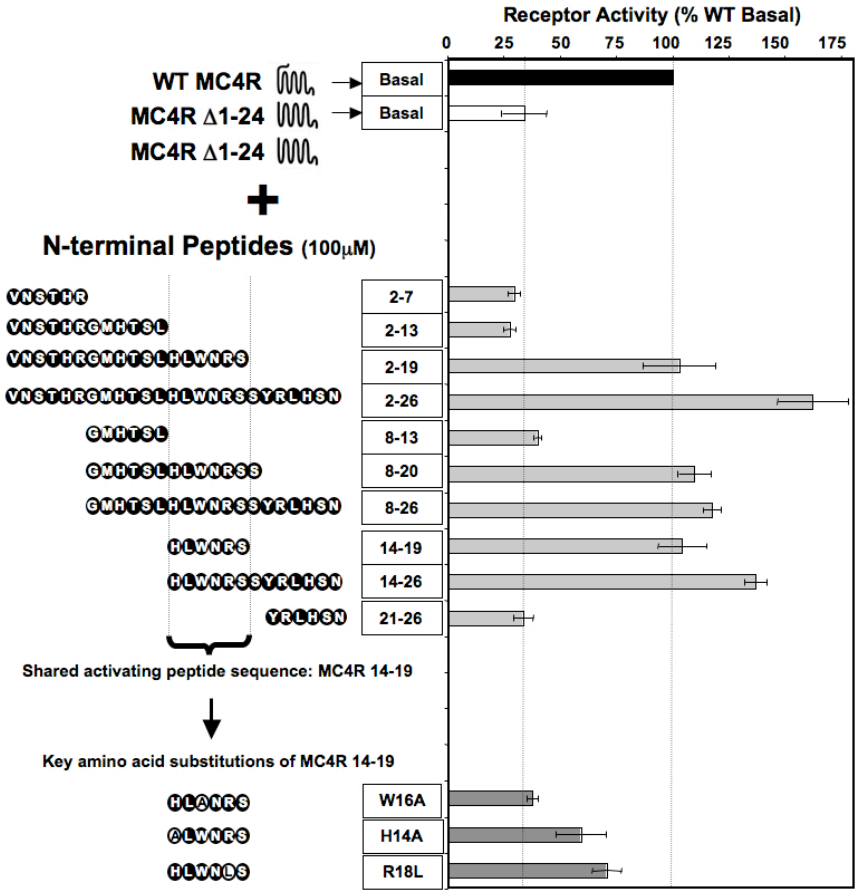

Figure 1.5: Determination of the minimal activating sequence and the essential amino acids of MC4R2-26 for basal activation. Small overlapping segments of MC4R2-26 peptide and the single amino acid substitution of the minimal activating peptide are displayed on the left panel of the figure. The mutated residues are indicated with black font on white background whereas the original sequence is indicated with white font on black background. The bar graph represents the WT basal activity (black), MC4R Δ1-24 basal activity (white), and the stimulation of MC4R Δ1-24 by the corresponding peptide on the left (grey). Error bars represent standard error for the triplicate.

```
human          -MVNSTHRGMHTSLHLWNRSYRLHSNASESLGKGYS- 36
chimp          -MVNSTHRGMHTSLHLWNRSYRLHSNASESLGKGYS- 36
mouse          -MNSTHHHGMYTSLHLWNRSYGLHGNASESLGKGHP- 36
Rat            -MNSTHHHGMYTSLHLWNRSHGLHGNASESLGKGHS- 36
cat            RMNSTHHHGMHTSLHFWNRSTYGPHSNASESPGKGYS- 37
horse          -MDSTHRHGMHTSLHFWNRSTYGLHSNASESLGKGYS- 36
dog            RMNSTLQHGMHTSLHFWNRSTYGQHGNATESLGKGYP- 37
cow            -MNSTQPLGMHTSLHSWNRSAHGMPTNVSESLAKGYS- 36
chicken        -MNFTQHRGTLQPLHFWNHS-NGLHRGASEPSAKGHSS 36
                *   :   *    .** **:*      ..:*. .**:.
```

Figure 1.6: Multiple alignments of the MC4R N-terminal sequences of multiple species. 100% conserved residues are marked by star (*). 13th through 19th amino acids are bracketed between vertical dashed lines.

Core transmembrane residues involved in N-terminus mediated activation

We reasoned that mutations in amino acids solely implicated in the N-terminal mediated activity of MC4R would impair the constitutive activity of the receptor but not the activation of the receptor by αMSH. We first surveyed naturally-occurring obesity-causing mutations studied in the laboratory of Christian Vaisse for such a biochemical phenotype (Figure 1.1, white on black). Out of 71 mutations examined, 8 had decreased basal activity and a conserved response to αMSH. Five of these mutations were in the N-terminal domain of the receptor (R7H, R18H, R18C, R18L, T11A), and three were in the intracellular domains of the receptor (V95I, A154D, G231S) (*15*), but none was located in the solvent-accessible region of the receptor.

Because of the positively charged nature of the N-terminal domain, we systematically screened all the remaining negatively charged solvent-accessible residues for such a biochemical phenotype by Alanine scanning mutagenesis (Figure 1.1, among black on grey). Substitution of these acidic amino acids did not alter the basal or αMSH activation of the receptor (Figure 1.7a).

Since mutational analysis of the N-terminal domain suggested a possible role for an aromatic residue mediating its activity, we also tested all remaining accessible aromatic and basic residues in a similar manner (Figure 1.1, among black on grey). Of 17 residues tested, mutagenesis of 9 (W174A, Y187A, F201A, F202A, W258A, F261A, F262A, H264A, and F284A) led to significantly reduced basal activity compared to the WT receptor (Figure 1.7b and 1.7c). Of these mutants, W174A, Y187A, F202A, F261A, H264A, F284A

Figure 1.7: The basal activity of the previously unstudied acidic, basic and aromatic residues accessible from the extracellular domain. A) Acidic residues. B) Basic residues C) Aromatic residues. Dashed line and the black bars represent the WT basal activity. MC4R mutations' basal activity (grey bars). Mock DNA (white bars). Error bars represent standard error for the triplicate.

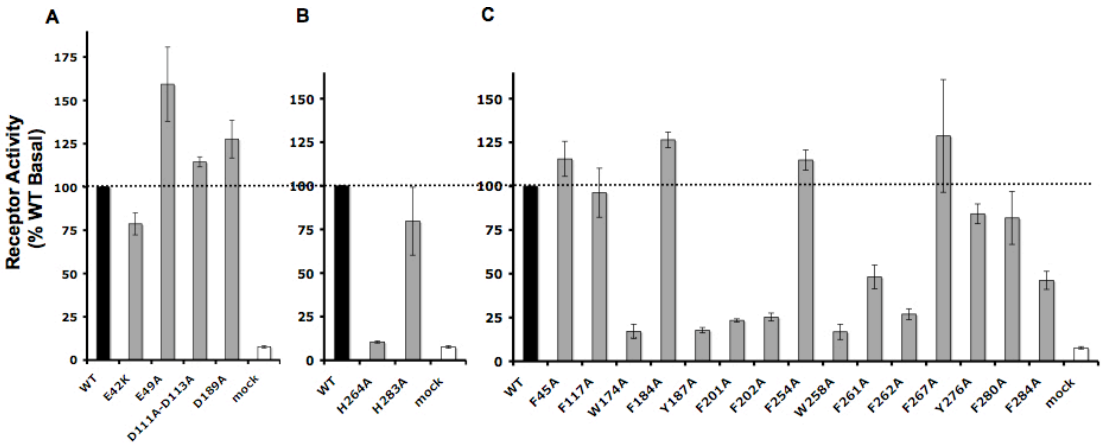

had a significantly altered response to αMSH (data not shown) but three mutant receptors (F201A, W258A, F262A) displayed a normal response to the agonist αMSH making them identical to MC4R Δ1-24 for their functional profile, and thus candidates for activation by the N-terminal domain (Figure 1.8a). We next tested whether any of the 3 residues exclusively altering the constitutive activity of the receptor were implicated in its activation by the N-terminal domain. When introduced into MC4R Δ1-24, mutations of the residues F201, W258, and F262 to alanine impaired activation of the receptors by exogenously added N-terminal peptide, confirming their specific involvement in the partial agonism of the N-terminal domain of the receptor (Figure 1.8b).

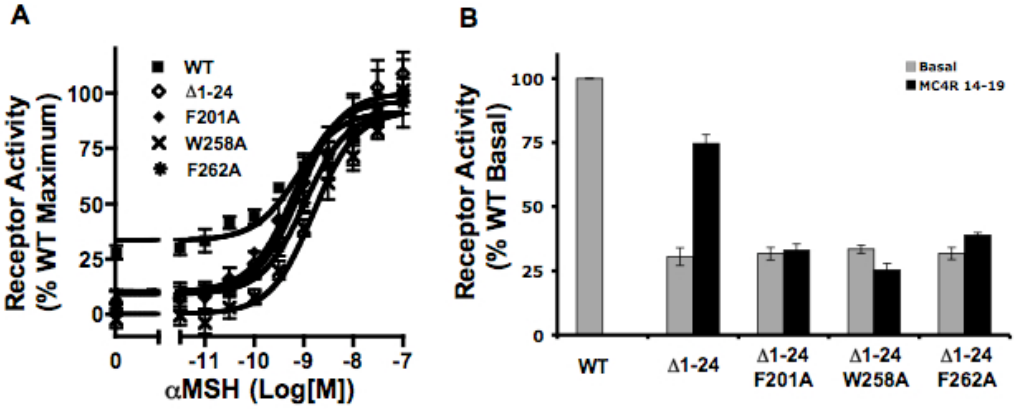

Figure 1.8: Activation profile of low basal MC4R mutants with WT-like αMSH response. A) F201A, W258A, F262A mutations αMSH dose response. B) The activation of MC4R Δ1-24 mutants by MC4R14-19 peptide. Error bars represent standard error for the triplicate.

Structural determinants of N-terminal domain mediated activation of the MC4R

As distinct sets of residues in the TM domain appear to be involved in interactions with the N-terminus and with exogenous ligands, we sought to establish the relative location of these molecular actors. In the absence of a structure for the MC4R, such a structural framework can be obtained from a homology-based model, since the crystal structures of related receptors are available. We built a homology model of the TM domain of the MC4R based on the recently obtained crystal structure of the β2-Adrenergic receptor (β2 AR) (*16*, *17*). Helix ends were estimated from the structure of the β2AR and no structural modifications were performed on the backbone.

As shown on Figure 1.9, most amino acids involved specifically in activation by the hormone, including the well characterized negatively charged residues E100, D122 and D126 (*18*), are clustered at the extracellular portion of TM2 and TM3. In sharp contrast, residues involved solely in the activation by the N-terminus are located at the interface between TMV and

TMVI, forming a spatially distinct cluster from residues involved in α-MSH activation. Interestingly, this cluster correspond to W286$^{6.48}$ and F290$^{6.52}$ in the β2AR, in which it comprises the "rotamer toggle switch", a conserved molecular switch that has been proposed to be involved in activation of the amine and opsin receptor families (*19*).

It should also be noted that while the cytoplasmic end of the TMV of the MC4R shares common motifs with that of the β2 adrenergic receptor, the upper half (towards the extra-cellular region) is significantly divergent, and does not include the normally conserved P5.50. This suggests that the helical bulge observed in the β2AR and in rhodopsin is likely to be absent in the melanocortin receptors which would thus bring F202 towards the center of the bundle and F201 towards TMVI, explaining the similar functional profiles of the MC4R mutants F201A and F202A.

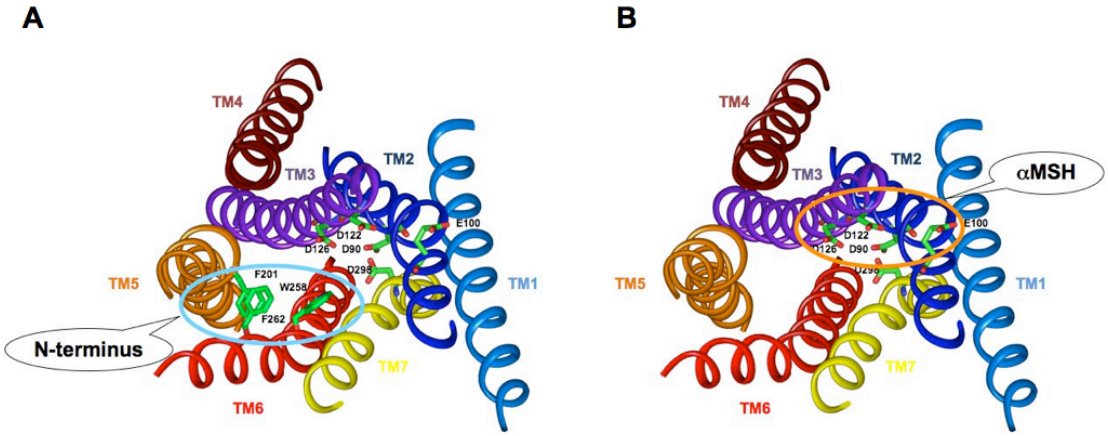

Figure 1.9: 3D Molecular model viewed from the top extracellular surface of MC4R. Ligand specific activation sites are displayed. A) F201, W258, and F262 as activation site downstream of N-terminal domain. B) E100, D122, and D126 as the αMSH specific activation site. MC4R 3D TM alignment is done by taking B_2-AR crystal structure as a model.

Discussion

A peptide mimicking the N-terminus of the MC4R restores constitutive activity of a truncated receptor. Most GPCRs have some level of basal activity (*20*). The evidence presented here clearly establishes a role for the N-terminus for stimulation of this GPCR. This is not the first report of N-terminal modulation of activity, leading us to speculate the N-terminus of other GPCRs may play a crucial part in this form of activity (figure 1.10).

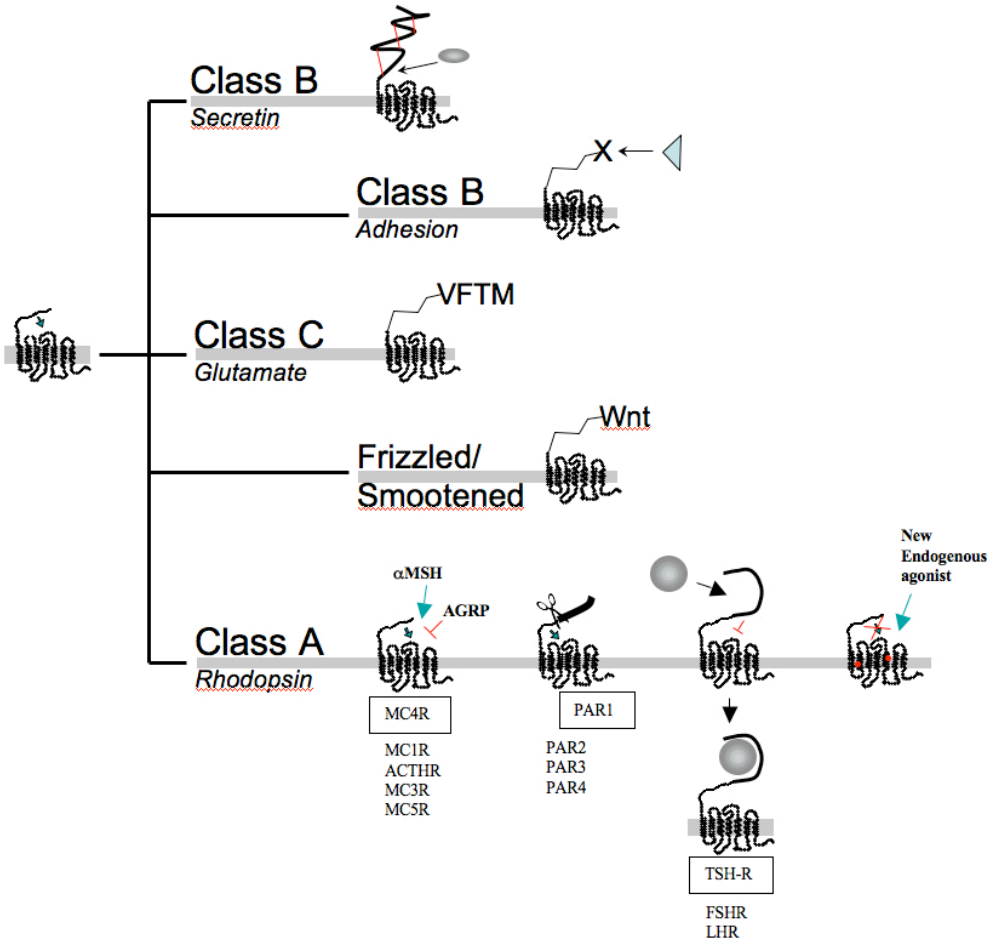

Figure 1.10: Evolutionary model of the role of the N-terminal domain in GPCRs. Class A GPCR activation and N-terminal modifications are shown on the right panel. N-terminal domains of GPCRs are not structural representations; they depict their functional role. Secretin receptor family - red lines represent the cystein network. Adhesion receptor family - "X" represents multiple diverse N-terminal motifs. Glutamate receptor - Venus Flytrap motif (VFTM). Frizzled/Smoothened receptor family - Wnt motif.

Another consequence of the framework proposed above and specifically of our observation that the N-terminal/AGRP interaction can independently modulate the activity at the MC4R is the suggestion that physiological negative regulation by inverse agonist might be the unique mode of regulation at GPCRs. Indeed, despite extensive efforts in the search for physiological agonists, a large number of GPCRs remain orphan or have proposed physiological ligands with pharmacological characteristics that are not compatible with a physiological role. The high constitutive activity of a number of these orphan receptors could indicate that inverse agonism is the only physiological modulation at these receptors and would explain the failure of deorphanizing studies using high throughput assays limited to detecting agonism (figure 1.11a and 1.11c). Whether the interaction of an activating N-terminal domain and a physiological inverse agonist will be the basis for activity modulation at these GPCRs remains to be tested but GPR61 is a recent example of a GPCR with a high constitutive activity, which is also mediated by the agonistic effect of its own N-terminal domain (*21*).

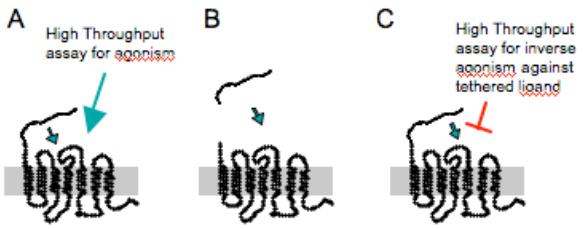

Figure 1.11: Orphan receptors with N-terminus mediated high constitutive activity. A) The current method of deorphanizing GPCRs. B) Proposed method to test N-terminal mediated activation. C) How constitutively active orphan receptors should be studied.

References

1. Ervin, R. B. (2009) Prevalence of Metabolic Syndrome Among Adults 20 Years of Age and Over, by Sex, Age, Race and Ethnicity, and Body Mass Index: United States, 2003–2006 http://www.cdc.gov/nchs/data/nhsr/nhsr013.pdf.
2. Huszar, D., Lynch, C. A., Fairchild-Huntress, V., Dunmore, J. H., Fang, Q., Berkemeier, L. R., Gu, W., Kesterson, R. A., Boston, B. A., Cone, R. D., Smith, F. J., Campfield, L. A., Burn, P., and Lee, F. (1997) Targeted disruption of the melanocortin-4 receptor results in obesity in mice, *Cell 88*, 131-141.
3. Farooqi, I. S., and O'Rahilly, S. (2008) Mutations in ligands and receptors of the leptin-melanocortin pathway that lead to obesity, *Nat Clin Pract Endocrinol Metab 4*, 569-577.
4. Cone, R. D. (2006) Studies on the physiological functions of the melanocortin system, *Endocr Rev 27*, 736-749.
5. Srinivasan, S., Lubrano-Berthelier, C., Govaerts, C., Picard, F., Santiago, P., Conklin, B. R., and Vaisse, C. (2004) Constitutive activity of the melanocortin-4 receptor is maintained by its N-terminal domain and plays a role in energy homeostasis in humans, *J Clin Invest 114*, 1158-1164.
6. Lubrano-Berthelier, C., Cavazos, M., Dubern, B., Shapiro, A., Stunff, C. L., Zhang, S., Picart, F., Govaerts, C., Froguel, P., Bougneres, P., Clement, K., and Vaisse, C. (2003) Molecular genetics of human obesity-associated MC4R mutations, *Ann N Y Acad Sci 994*, 49-57.
7. Lubrano-Berthelier, C., Durand, E., Dubern, B., Shapiro, A., Dazin, P., Weill, J., Ferron, C., Froguel, P., and Vaisse, C. (2003) Intracellular retention is a common characteristic of childhood obesity-associated MC4R mutations, *Hum Mol Genet 12*, 145-153.
8. Vaisse, C., Clement, K., Durand, E., Hercberg, S., Guy-Grand, B., and Froguel, P. (2000) Melanocortin-4 receptor mutations are a frequent and heterogeneous cause of morbid obesity, *J Clin Invest 106*, 253-262.
9. Lubrano-Berthelier, C., Le Stunff, C., Bougneres, P., and Vaisse, C. (2004) A homozygous null mutation delineates the role of the melanocortin-4 receptor in humans, *J Clin Endocrinol Metab 89*, 2028-2032.
10. Ballesteros, J. A., and Weinstein, H. (1995) Integrated methods for the construction of three-dimensional models and computational probing of structure-function relations in G protein-coupled receptors, *Methods in Neurosciences 25*, 366-428.
11. Coughlin, S. R. (1999) How the protease thrombin talks to cells, *Proc Natl Acad Sci U S A 96*, 11023-11027.
12. Scarborough, R. M., Naughton, M. A., Teng, W., Hung, D. T., Rose, J., Vu, T. K., Wheaton, V. I., Turck, C. W., and Coughlin, S. R. (1992) Tethered ligand agonist peptides. Structural requirements for thrombin receptor activation reveal mechanism of proteolytic unmasking of agonist function, *J Biol Chem 267*, 13146-13149.

13. Nijenhuis, W. A., Oosterom, J., and Adan, R. A. (2001) AgRP(83-132) acts as an inverse agonist on the human-melanocortin-4 receptor, *Mol Endocrinol 15*, 164-171.
14. Peter, J. C., Nicholson, J. R., Heydet, D., Lecourt, A. C., Hoebeke, J., and Hofbauer, K. G. (2007) Antibodies against the melanocortin-4 receptor act as inverse agonists in vitro and in vivo, *Am J Physiol Regul Integr Comp Physiol 292*, R2151-2158.
15. Xiang, Z., Litherland, S. A., Sorensen, N. B., Proneth, B., Wood, M. S., Shaw, A. M., Millard, W. J., and Haskell-Luevano, C. (2006) Pharmacological characterization of 40 human melanocortin-4 receptor polymorphisms with the endogenous proopiomelanocortin-derived agonists and the agouti-related protein (AGRP) antagonist, *Biochemistry 45*, 7277-7288.
16. Cherezov, V., Rosenbaum, D. M., Hanson, M. A., Rasmussen, S. G., Thian, F. S., Kobilka, T. S., Choi, H. J., Kuhn, P., Weis, W. I., Kobilka, B. K., and Stevens, R. C. (2007) High-resolution crystal structure of an engineered human beta2-adrenergic G protein-coupled receptor, *Science 318*, 1258-1265.
17. Rasmussen, S. G., Choi, H. J., Rosenbaum, D. M., Kobilka, T. S., Thian, F. S., Edwards, P. C., Burghammer, M., Ratnala, V. R., Sanishvili, R., Fischetti, R. F., Schertler, G. F., Weis, W. I., and Kobilka, B. K. (2007) Crystal structure of the human beta2 adrenergic G-protein-coupled receptor, *Nature 450*, 383-387.
18. Yang, Y. K., Fong, T. M., Dickinson, C. J., Mao, C., Li, J. Y., Tota, M. R., Mosley, R., Van Der Ploeg, L. H., and Gantz, I. (2000) Molecular determinants of ligand binding to the human melanocortin-4 receptor, *Biochemistry 39*, 14900-14911.
19. Kobilka, B. K., and Deupi, X. (2007) Conformational complexity of G-protein-coupled receptors, *Trends Pharmacol Sci 28*, 397-406.
20. Rosenbaum, D. M., Rasmussen, S. G., and Kobilka, B. K. (2009) The structure and function of G-protein-coupled receptors, *Nature 459*, 356-363.
21. Toyooka, M., Tujii, T., and Takeda, S. (2009) The N-terminal domain of GPR61, an orphan G-protein-coupled receptor, is essential for its constitutive activity, *J Neurosci Res 87*, 1329-1333.

Chapter 2

Species Specific Synthesis of Agouti Related Protein

(Much of the text and figures of this chapter appeared originally as "Phosphodiesterase inhibitor-dependent inverse agonism of agouti-related protein on melanocortin 4 receptor in sea bass (Dicentrarchus labrax)" published in *Am J Physiol Regul Integr Comp Physiol*. 2009 May;296(5):R1293-306. This work was done in the laboratory of Jose-Miguel Cerda-Reverter and is reprinted with his and *AJP* permissions.)

The melanocortin system is not limited to mammals and, likewise, neither are the endogenous antagonists, Agouti Related Protein (AgRP) and Agouti Signaling Protein (ASIP). In the animal kingdom fish (*1*) and birds (*2*) have been shown to possess all the necessary components. Of particular interest is a species of teleost fish known as zebrafish (*3*). The entire zebrafish genome has been sequenced and made publicly available (http://www.ncbi.nlm.nih.gov/projects/genome/guide/zebrafish/). Peptide synthesis is a quick way to assemble bioactive polypeptide chains from sequence data (*4*).

Figure 2.1 shows the postulated open reading frame of AgRP from the zebrafish genome predicted computationally with GNOMON (*5*). The C-terminal, cysteine rich domain from human AgRP is sufficient for inhibiting the melanocortin 4 receptor (MC4R) response to melanocyte stimulating hormone (MSH) (*6*). The MC4R is positively coupled to adenylyl cyclase. The zebrafish C-terminus is 51% identical compared to human with 9/10 cysteines spatially conserved. We hypothesized that synthetic zfAgRP 83-127 would adequately down regulate zebrafish MC4R.

It can take up to 3 years for a single researcher to get an entirely new expression system going, in contrast, it took just two weeks to synthesize 2 mg of oxidized zfAgRP Ac-83-127-NH_2. While the yield is not impressive, it represents sufficient peptide for hundreds of pharmacological experiments.

Translated zebrafish AgRP ORF

MMLNTVIFGW FLVNVVVMAS HPHLRRRENS FILTSDTDSL PEMEHLEINS AEEKILEDLE
AYDEDLGKAV HLQRRGTRSP SRCIPHQQSC LGHHLPCCNP CDTCYCRFFK AFCYCRSMDN
TCKNEYA

zfAgRP 83-127

CIPHQQSCLGHHLPCCNPCDTCYCRFFKAFCYCRSMDNT---CKNEYA
CVRLHESCLGQQVPCCDPCATCYCRFFNAFCYCRKLGTAMNPCSRT

human AgRP 87-132

Figure 2.1. The primary amino acid sequence of zebrafish AgRP translated directly from the zebrafish genome. Synthesized region shown in blue text. An alignment with the C-terminal cysteine rich region of human AgRP is shown for comparison, conserved amino acids shown in red.

Zebrafish embryos have the dual advantage of being translucent and developing in just 72 hours (*7*). Initially zfAgRP was synthesized as part of a collaboration with Youngsup Song in the laboratory of Roger Cone at Oregon Health Sciences University. The zebrafish pineal gland secretes a protein called AgRP2. Unlike the mammalian pineal gland, in fish this gland has a more pivotal role in development (*8*). My colleague, Michael Madonna, and I chemically synthesized zfAgRP2 Ac-Y-93-136-NH_2. ZfAgRP2 is a nanomolar antagonist of the zebrafish melanocortin 1 receptor ((MC1R) unpublished results). As a control I synthesized zfAgRP. Figure 2.2 demonstrates zfAgRP antagonizes zebrafish MC1, 3, and 4R at the nanomolar level. Sea bass is also a teleost fish, but its genome remains unsequenced. Jose-Miguel Cerda-Reverter is an endocrinologist at Instituto de Acuicultura de Torre de la Sal in

Spain whose research is concentrated on sea bass. We reasoned that zebrafish and sea bass are closely enough related evolutionarily that their AgRP biochemistry would be indistinguishable.

In addition to being a competitive antagonist at the MC4R AgRP is also an inverse agonist, reducing the basal activity of adenylyl cyclase in the absence of agonist (*9*). The product of adenylyl cyclase, cAMP, is a phosphodiester. The phosphodiesterase inhibitor, isobutylmethylxanthine (IBMX), prolongs the cytoplasmic lifetime of cAMP. The inverse agonist activity of zfAgRP on the sea bass MC4R was entirely dependent on the presence of IBMX.

Methods

Peptide synthesis, purification, and folding.

Zebrafish AGRP (Ac-83-127-NH2) was synthesized using Fmoc synthesis on an Applied Biosystems (Foster City, CA) 433A peptide Synthesizer on a 0.25-mmol scale. The synthesis was monitored using the SynthAssist version 2.0 software package. The peptide was assembled on a Rink-amide-MBHA resin, and preactivated Fmoc-Cys(trt)-OPfp was used. All amino acids and resins were purchased through NovaBiochem (San Diego, CA). 2-(1H-benzotriazole-1-yl)-1,1,3,3-tetramethyluronium hexafluorophosphate (HBTU) was obtained from Advanced Chemtech (Louisville, KY). Fmoc deprotection was achieved using a 1% hexamethyleneimine and 1% 1,8-diazabicyclo[4.5.0]-undec-7-ene solution in dimethylformamide (DMF). Deprotection was monitored by conductivity and

continued until the conductivity level returned to the baseline, and then synthesis resumed. Deprotection time ranged from 2.5 to 7 min. Coupling used four equivalents of Fmoc-amino acid in HBTU/diisopropylethylamine (DIEA) for all amino acids with the exception of preactivated cysteine. A threefold excess of Fmoc-Cys(Trt)-OPfp was dissolved in 1.5 ml of 0.5 M HOAt/DMF with no DIEA for coupling. The peptides were NH2-terminal acetylated by reacting with 0.5 M acetic anhydride in DMF for 5 min. Fully synthesized peptide resin was split into three reaction vessels, washed with dichloromethane, and dried. A solution of 8 ml of trifluoracetic acid (TFA) containing 200 μl each of triisopropylsilane/1,2-ethanedithiol/liquefied phenol (TIS/EDT/phenol, as scavengers) was added to each reaction vessel of dry peptide resin for 1.5 h. The resin was filtered and washed with 1 ml of TFA, and the combined filtrate and wash was then added to 90 ml of cold, dry diethyl ether for precipitation. The precipitate was collected by centrifugation, and the ether was discarded. The pellet was dissolved in 40 ml of 1:1 H_2O:acetonitrile (0.1% TFA) and then lyophilized.

The crude peptide was purified by reversed-phase (RP)-HPLC on C4 Vydac (Hesperia, CA) preparative columns. Fractions were collected and analyzed by electrospray ionization-mass spectrometry (ESI-MS) on a Micromass (Wythenshawe, UK) ZMD mass spectrometer to confirm the correct molecular weight. Fractions containing the peptide as a major constituent were combined and lyophilized.

Air oxidative folding of zAgRP was accomplished by dissolving the unfolded peptide into folding buffer (2.0 M guanidine HCl/0.1 M Tris, 3 mM

GSH, and 0.4 mM GSSG, pH 8, at a peptide concentration of 0.1 mg/ml) and stirring for 14 h. Folding was monitored by RP-HPLC on a C18 analytical column, which revealed a single peak for the folded material that shifted to an earlier retention time than the fully reduced peptide, and ESI-MS indicated a difference of 10 atomic mass units (amu). The folded product was purified by RP-HPLC on a C18 preparative column, and its identity was confirmed as the fully oxidized product by ESI-MS (AGRP Ac-83-127-NH2: 5,287.1 calculated average amu isotopes, 5,288 amu observed). Reinjecting a small sample of the purified peptide on an analytical RP-HPLC column assessed purity of the peptide. Quantitative analysis of the peptide concentration was carried out by amino acid analysis at the molecular structure facility at the University of California, Davis.

Zebrafish pharmacological experiments

Generation of stable transfectants.

HEK-293 cells were used for generating cell lines stably expressing melanocortin receptors. Transfection was performed according to the manufacturer's instruction. In brief, the day before transfection, HEK-293 cells were plated at about 80 - 100% confluency in 100 mm dishes, without antibiotic. About 20 mg of DNA was used for transfection using 40 ml of either lipofectamine, or lipofectamine2000 (Invitrogen) in Optimem medium (Invitrogen). 5 hrs after transfection, 20% FBS / DMEM medium was supplied. 24 hour after transfection, transfectants were split into 2 or 3 100 mm dishes in 10% FBS DMEM and incubated another 24 hour. Medium was replaced with medium containing 1000 mg/ml concentration of G418. Fresh

G418 medium was supplied every 3 - 4 days. 2 - 3 weeks later, when there were enough cells or colonies grown, the whole population of individual transfectants were split, pooled and selected by G418 medium again.

β-galactosidase assay

Zebrafish melanocortin receptor activity was measured using a cAMP-dependent β-galactosidase assay (*10*). Briefly, HEK-293 cell transfectants expressing zebrafish melanocortin receptors or control HEK-293 cells were transiently transfected with a CRE-β-galactosidase expression vector. Next day, cells were plated on 96 well plates with 5 X 10^4 cells per well. 24 hours later after plating, cells were incubated with serially diluted concentrations of α-MSH in the presence or absence of zAgRP in a 50 μl volume of 0.1 mM IBMX, 0.01 % BSA in DMEM at 37 °C for 6 hours. After one wash with PBS, cells were lysed in 50 μl of lysis buffer (250 mM Tris-Cl, ph8.0, 0.1% Triton X-100), and frozen at –80 °C overnight. Plates were thawed for 20 minutes at room temperature, and the following solutions were applied sequentially: 40 ml of 0.5% BSA in PBS, then 150 μl of β-galactosidase substrate (60 mM sodium phosphate, 1 mM $MgCl_2$, 10 mM KCl, 5 mM β-mercaptoethanol, 2 mg/ml ONPG). Plates were incubated at 37 °C without light for 1-3 hours. Color development was measured at 405 nm with a Benchmark Plus plate spectrophotometer (Biorad).

Sea Bass Pharmacological Experiments

Molecular Cloning of Sea Bass MC4R

Genomic DNA isolated from blood was used as template for touchdown PCR reactions with Taq DNA polymerase (Invitrogen) and

degenerate primers designed against conserved regions of the known MC4R sequences. The following reaction conditions were used: 0.2 mM dNTP, 0.4 mM FwFish and RevFish primers, 1 X Taq DNA polymerase buffer, 1.5 mM $MgCl_2$ and 0.5 units Taq DNA polymerase. The 5´ primer (FwFish) was a 20-mer with the sequence: 5´ TAYATCACCATMTTYTACGC 3´. The 3' primer (RevFish) had the sequence 5´ TSAGVGTGATGGCKCCCTT 3´ (Fig.1). PCR products of about 300 base pair (bp) were isolated from low melting point (LMP) Nusieve GTG agarose gel (FMC) ligated into pGEM-T easy vector (Promega) and subsequently transformed into XLI-Blue E. coli. One clone containing an insert of expected size was sequenced. To resolve 3' end of sea bass MC4R cDNA, 3' RACE-PCR was performed. For 3' RACE PCR cDNA was synthesized using dT-adapter primer (5' CAGTCGAGTCGACATCGA $(T)_{17}$3'). Two rounds of PCR amplified the 3' end with adapter (5' CAGTCGAGTCGACATCGA 3') and sbMC4R_3´RACE_1 (5' GTTGGTCATCAGCAGCAT 3') primers and then adapter primer and sbMC4R_3´RACE_1 (5' GCATCCTGTTTATCATCTAC 3', Fig. 1). After LMP purification a 532-bp fragment was subcloned into pGEM-T easy vector and sequenced. The 5´region was cloned using the Genome Walker Kit (Clontech) and following manufacturer's instruction. Specific primers for genome walking were sbMC4R_5Walker_1 primer (5' GCAATGCTGCGATGCGCTTCATGTGCA 3') for the first PCR and sbMC4R_5Walker_2 primer (5' GTCCAGATGCTGCTGATGACCAACATTGC 3´) for the nested PCR (Fig.1). A 547-bp fragment was subcloned into pGEM-T easy vector and sequenced.

Finally, the full coding region was amplified by PCR, using genomic DNA as template and the primers Hind-MC4R-Forward (5' TATAAGCTTATGAACACCACAGAGGCTC 3') and XhoI-MC4R-Reverse (5' TATCTCGAGGAGTCGTAGCTGCTGCTC 3', Fig.1). A 1036-bp DNA fragment was subcloned into pGEM-T easy vector and sequenced on both strands. The nucleotide sequence of sea bass MC4R has been deposited with EMBL Nucleotide Sequence Database under accession numbers FM253127.

Cell culture and transfection

If not specifically indicated, HEK cells were transfected using a modified calcium phosphate transfection method (Chen and Okayama, 1987) and grown in DMEM (Invitrogen) containing 10% foetal bovine serum (Invitrogen), penicillin (100 units/ml) and streptomycin (100 mg/ml) in a humidified atmosphere of 5% CO_2 at 37ºC.

Galactosidase enzyme assay

Galactosidase enzyme assays were performed as previously described (Chen et al., 1995). Briefly the medium was removed and 50 μl of lysis buffer containing 250 mM Tris-HCl pH=8 and 0.1 % Triton X-100 were added. After one round of freezing (-80 ºC) and thawing, ten microlitres of the lysate were preserved for protein assays. Forty microliters of phosphate saline buffer containing 0.5 % BSA and 60 μl of substrate buffer (1mM MgCl2, 10mM KCl, 5mM β-mercaptoethanol and 200 mg/ml *o*-nitrophenyl-b-D-galactopyranoside, ONPG) were added to the remaining lysate volume. The plate was incubated at 37 ºC for 5h and the absorbance was read at 405 nm in

a 96-well plate reader (Tecan). Measurements were normalized by the protein content determined using the BCA protein assay kit (Pierce).

Pharmacological experiments

A HEK-293 cell clone, stably expressing β-galactosidase under the control of vasoactive intestinal peptide promoter placed downstream of tandem repetitions of cAMP responsive elements (CRE, Chen et al., 1995), was generated by co-transfecting (50:1) pCRE/β-galactosidase plasmid (kindly supplied by Dr. R Cone, Vanderbilt University Medical Center) and tgCMV/HyTK plasmid, which harbours a hygromycin resistance gene (Wellbrock et al., 1998). Cells were selected in medium containing 400 mg/ml of hygromycin B (Invitrogen). β-galactosidase activity was tested after incubating resistant clones in 96-well plates (15.000 cells/well) with assay medium (DMEM medium + 0.1mg/ml bovine serum albumin, BSA + 0.1 mM isobutylmethylxanthine, IBMX) containing 10^{-6} M forskolin during 6 hours. The clone showing highest response to forskolin (Clon-Q) was selected for subsequent experiments. The full coding region of the sea bass MC4R was released from pGEM-T easy vector (see above) and subcloned into pcDNA3 (Invitrogen). Double stable clones expressing β-galactosidase and sea bass MC4R were made by transfecting Clon-Q with the latter construct using G-418 selection (800 mg/ml). Clones were tested by incubating cells with MTII 10^{-6} M in the assay medium. The clone Q/9 was selected for the characterization of the activation profiles in response to several melanocortins (α-MSH, diacetyl-MSH, desacetyl-MSH, human ACTH, monkey β-MSH, zfAGRP, SHU9119 and HS024) in the absence of

IBMX. The effect of zfAGRP on basal and MTII-stimulated MC4R activity was studied in both the presence and absence of the phosphodiesterase inhibitor. MC4R activation assays were performed in quadruplicate wells and repeated at least three independent times.

Results

The HPLC of the crude product from one third of the synthesis is shown in figure 2.3A. The ether precipitated pellet was dissolved in 50:50 ACN:water (0.1% w/v TFA) and lyophilized. Lyophilized, crude peptide (approximately 200 mg) was suspended in 25 mL 6M GuHCl 0.1% TFA and c4 RP-HPLC (22 x 250 mm, 10 mL/min) purified. ESI-MS detected 3 fractions with 5298 amu as the predominant component (Fig. 2.4A); these were combined and lyophilized. The chromatogram from injecting a small amount of 1 of these fractions on analytical HPLC is demonstrated by Figure 2.3B. This yielded 18.8 mg of reduced zfAgRP Ac-83-127-NH_2.

The purified, reduced and lyophilized peptide was dissolved in 33 mL 6M GuHCl 0.1M Tris 100 mg reduced glutathione 30 mg oxidized glutathione pH 8 and then diluted with 67 mL 0.1M Tris pH 8. The solution stirred overnight in air, pH lowered with acetic acid, filtered, and preparative HPLC purified. Mass spectrometry demonstrated the majority product mass of 5288 amu (Fig. 2.4B). Figure 2.3C shows the HPLC of the overnight oxidation before purification and the product is displayed in Figure 2.3D. Quantitative amino acid analysis results revealed 2.0 ± 0.3 mg oxidized zfAgRP Ac-83-127-NH_2.

Binding and activation of sea bass MC4R by melanocortin analogs

For pharmacological and functional characterization of the sea bass MC4R, the coding region was ligated into pcDNA3 and stably expressed in HEK 293 cells already producing β-galactosidase under the control of cAMP responsive elements. Saturation experiments displayed a single saturable site for ^{125}NDP-MSH (fig. 2.5A) and showed that the sea bass receptor binds this agonist in a manner similar to that of the human, zebrafish, and goldfish MC4R (*11*). The sea bass MC4R is not activated by potential melanocortin antagonists such as SHU9119, HS024 or zfAGRP. However Sea bass MC4R is positively coupled to the cAMP-signaling pathway in response to diacetyl-MSH with a half-maximal effective concentration (EC50) of 0.094 nM. Sea bass MC4R activation by α-MSH and monkey β-MSH showed an EC50 of 0.822 nM and 3.333 nM, respectively, whereas effective concentration increased to 18.8 nM and 15.13 nM when cells were incubated with human ACTH or desacetyl-MSH (Fig 2.5). Sea bass MC4R was also activated by the

non-selective melanocortin agonist MTII (EC50= 0.31 nM). However, MTII-stimulated cAMP intracellular accumulation decreased by co-incubation with 1 μM of HS024 (EC50=17 nM) , SHU9119 (EC50=120 nM) and zfAGRP (EC50=85 nM; Fig. 2.6). When a phosphodiesterase inhibitor (IBMX) was added to the medium, the response of the reporter gene to the MTII incubation increased (EC50=0.01 nM, Fig. 2.7). However, the incubation of sbMC4R-expressing HEK cells with zfAGRP in the presence of IBMX sharply decreased the basal activity of the receptor as an inverse agonist would (EC50= 1.14 nM). Under these conditions, zfAGRP also decreased MTII-stimulated cAMP production (EC50=9.9 nM) as an endogenous antagonist would.

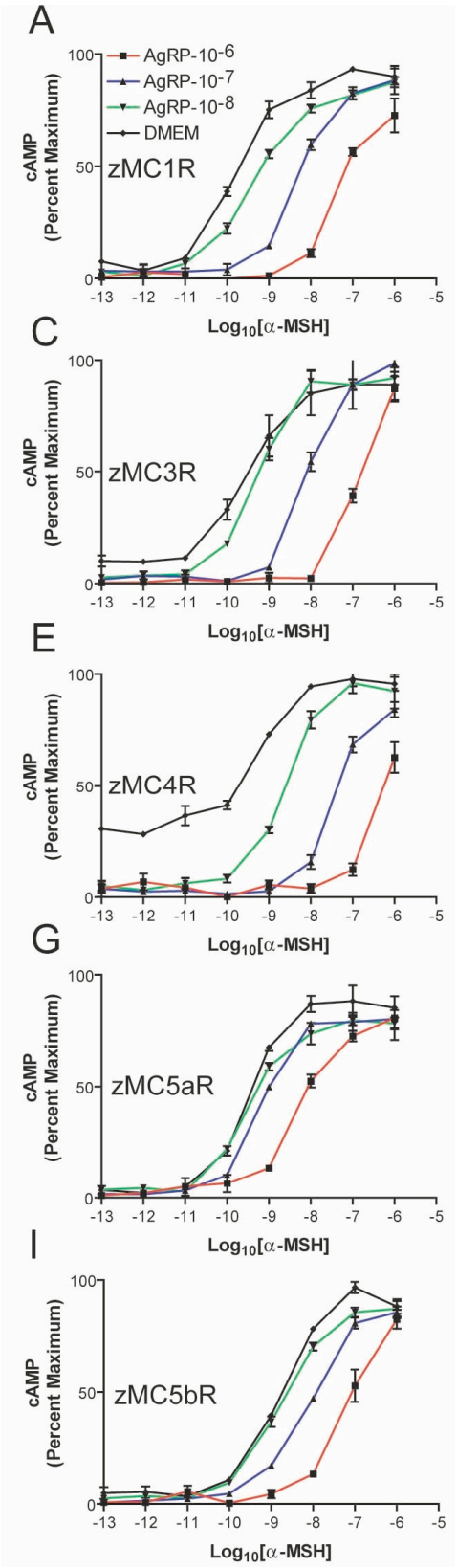

Figure 2.2. Zebrafish AgRP activity at the zebrafish melanocortin receptors. 10-6=1 μM, 10-7=100 nM, 10-8=10 nM, DMEM = dubelco modified eagles medium or no zfAgRP. Increasing concentrations of zfAgRP Ac-83-127-NH_2 effect the EC_{50} of α-MSH. Copyright Youngsup Song 2007.

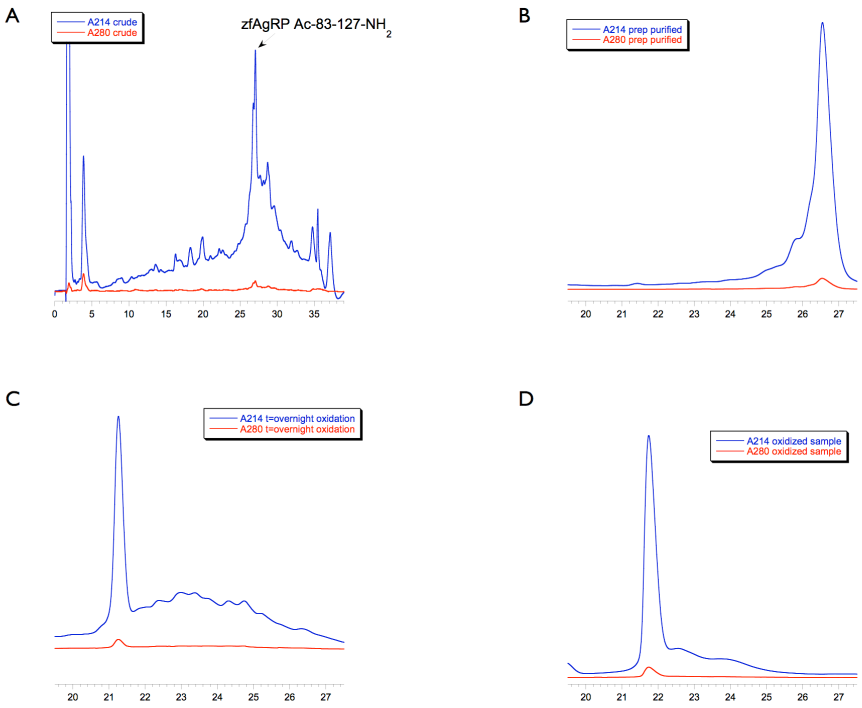

Figure 2.3. Zebrafish AgRP production. Analytical c4 RP-HPLC of the various stages :A) crude, B) purified reduced, C) overnight oxidation, and D) purified oxidized

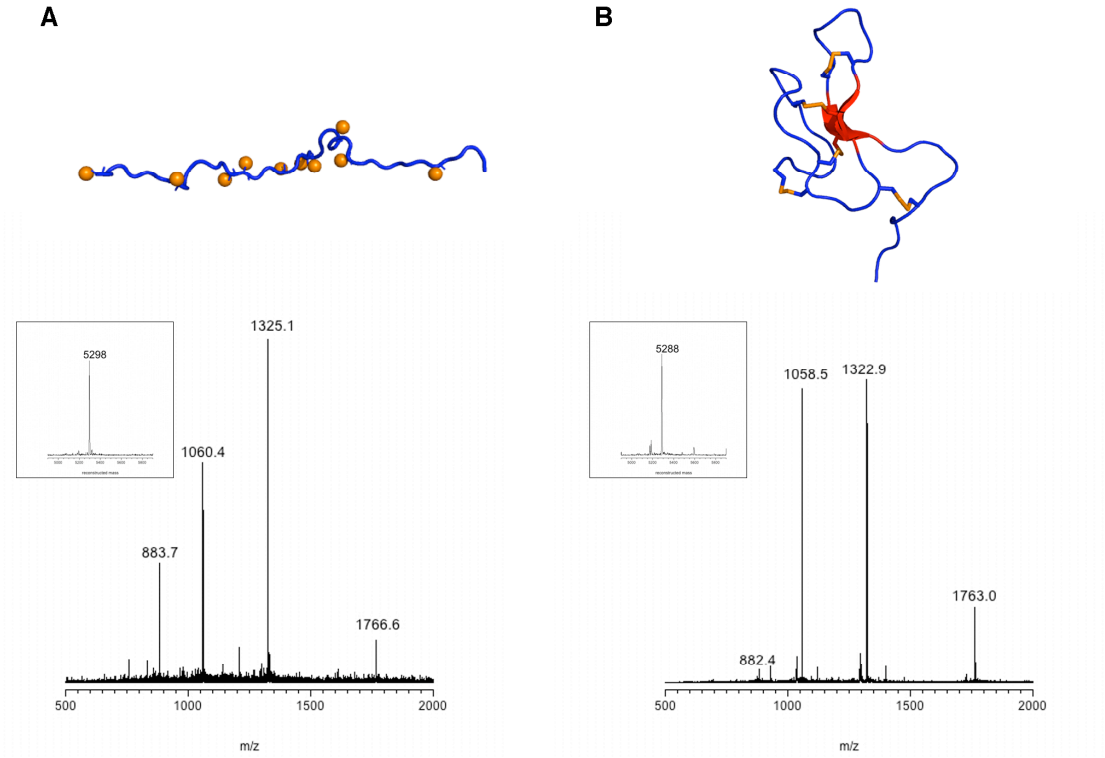

Figure 2.4. A) ESI-MS of reduced zfAgRP Ac-83-127, the protein is shown as a linear chain, cysteine sulfurs are shown in orange, and represented as spacefilled atoms B) ESI-MS of oxidized zfAgRP Ac-83-127, the folded protein was homology modeled based on the published human AgRP Ac-87-132 NMR structure (PDB ID 1HYK) with the software package Modeller 9v5, cystine sulfurs are shown in orange. (Sali, A.; Blundell, T. L., Comparative protein modelling by satisfaction of spatial restraints. *J Mol Biol* **1993,** 234, (3), 779-815.)

Fig. 2.5. *A*: saturation curves were obtained with ^{125}I-[Nle4, D-Phe7] α-MSH, showing specific binding (■) and binding in the presence of 10 μM cold [Nle4,D-Phe7]α-MSH (△). Lines represent the computer-modeled best fit of the data,assuming that ligands bound to one site. *B*: pharmacological properties of melanocortin agonists and antagonists (human ACTH, monkey β-MSH, α-MSH, desacetyl-MSH, diacetyl-MSH, zfAGRP, SHU9119, and HS024) at human embryonic kidney (HEK)-293 cells stably expressing both sea bass MC4R and a cAMP-responsive β-galactosidase reporter gene in the absence of phosphodiesterase inhibitors (IBMX). GAL, β-galactosidase activity. Data were normalized to protein levels and are expressed as percentages of the basal levels. Experiments were performed using quadruplicate data points and repeated at least 3 independent times. Used with permission.

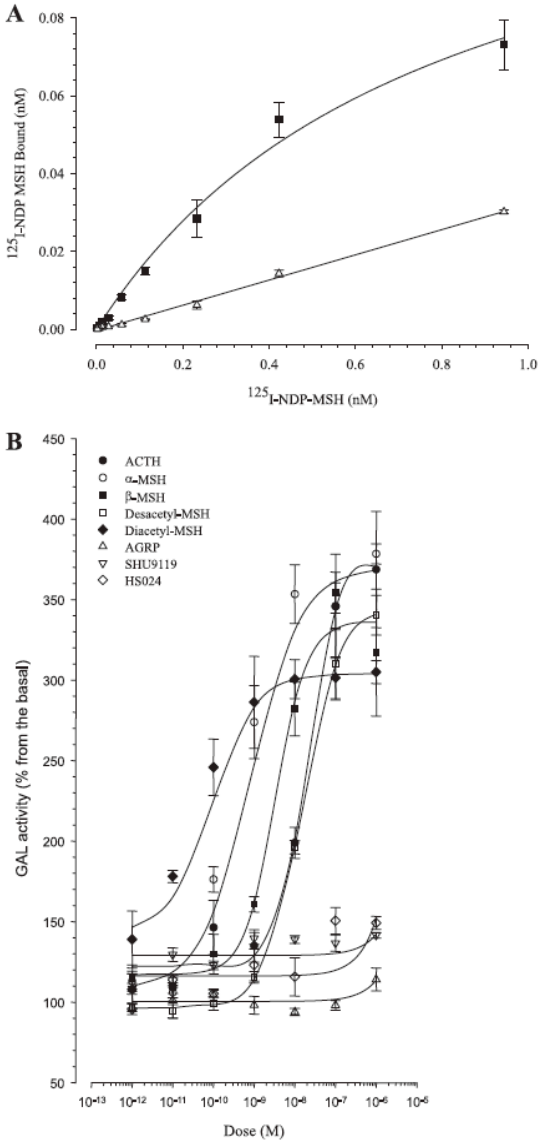

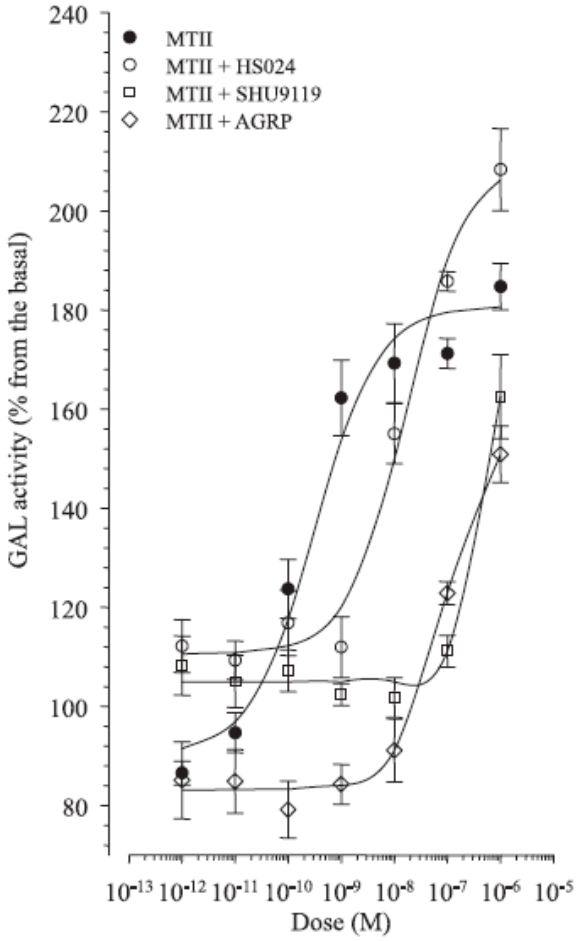

Fig. 2.6. Effects of synthetic (SHU9119 and HS024) and endogenous antagonist (AGRP, agouti-related protein) on MCR agonist MTII-stimulated galactosidase activity in HEK-293 cells stably expressing both sea bass MC4R and a cAMP-responsive β-galactosidase reporter gene in the absence of phosphodiesterase inhibitors (IBMX). Data were normalized to protein levels and are expressed as percentages of the basal levels. Experiments were performed using quadruplicate data points and repeated at least 3 independent times. Used with permission.

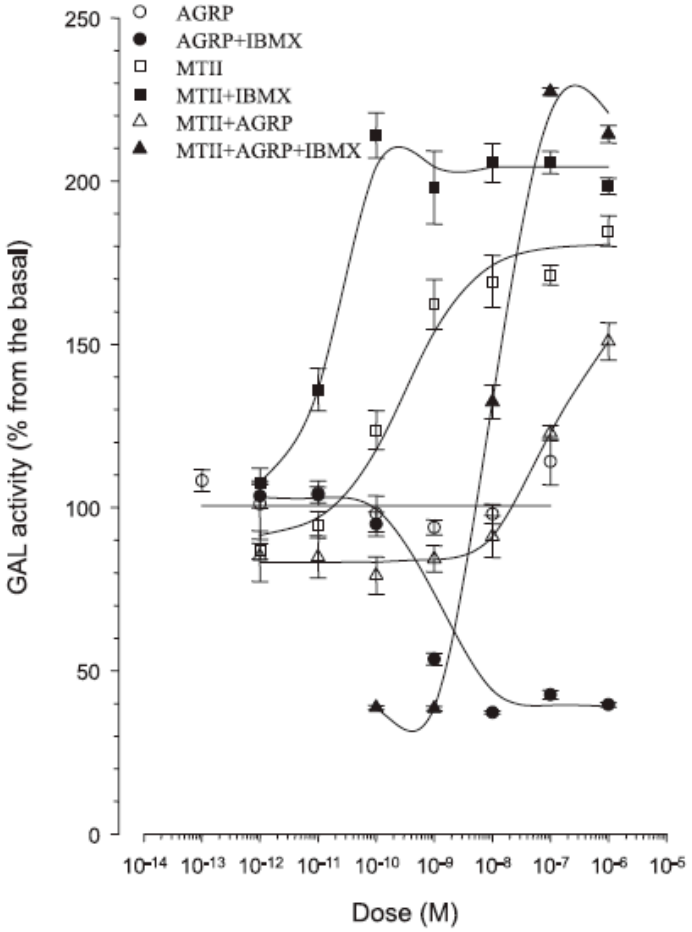

Fig. 2.7. Effects of phosphodiesterase inhibitors (IBMX) on pharmacological properties of agonist (MTII) and antagonist (AGRP) in HEK-293 cells stably expressing both sea bass MC4R and a cAMP-responsive β-galactosidase reporter gene. Data were normalized to protein levels and are expressed as percentages of the basal levels. IBMX alone induced an increase in the β-galactosidase activity of 131 ± 8.57% compared with the basal enzyme activity in the absence of IBMX. Experiments were performed using quadruplicate data points and repeated at least 3 independent times. Used with permission.

Discussion

Many thousands of biologically active peptides and proteins have been chemically synthesized (*12*). This chapter demonstrates zebrafish species specific synthesis of AgRP from a genomic DNA sequence. Assuming that GNOMON correctly calculated the primary amino acids. The C-terminus of AgRP is contained in one exon (*13*), it is difficult to imagine how GNOMON could be mistaken. The DNA sequence does not always directly correspond to mRNA sequence, however, depending on adenosine deaminase action on the transcribed mRNA (*14*).

The present study shows that AGRP acts as an inverse agonist at sea bass MC4R. However, the inverse agonism, but not the competitive antagonism, is dependent on the presence of a phosphodiesterase inhibitor in the culture medium. None of the synthetic (HS024 and SHU9119) or endogenous (AGRP) MC4R antagonists had any effect on sea bass MC4R-mediated galactosidase activity but all three peptides acted as competitive antagonists at the sea bass receptor activity in the absence of IBMX. Both SHU9119 and AGRP were more efficient than HS024 when MTII-stimulated galactosidase activity decreased. The data show that all three antagonists are suitable for physiological studies in sea bass. As expected, when IBMX was added to the incubation medium, the EC50 value of the MTII-induced galactosidase activity decreased. Therefore, the use of IBMX increases the sensitivity of the assays to evaluate the activation of positively cAMP-coupled receptors. Under the above conditions, AGRP competitively antagonized the effects of MTII on sea bass MC4R activity in a similar manner to that

observed without IBMX but severely decreased the basal activity of the sea bass MC4R, just as an inverse agonist would. These results were corroborated by incubating cells with MTII and AGRP in the presence of IBMX. At the lowest does of MTII (10^{-10}-10^{-9} M) the addition of 10^{-7} M AGRP maintained the sea bass MC4R activity at around 30 % of the basal level. The competitive antagonism of AGRP on fish MC4R has already been reported (Song and Cone, 2007) but the agonism is newly reported here. However, we have demonstrated that the AGRP inverse agonism is dependent on treatment of the cells with IBMX. To the best of our knowledge, all assays reporting AGRP effects on melanocortin receptors have pre-treated cells with IBMX. Only one study has reported the effect of phosphodiesterase inhibitor on α-MSH-induced receptor activation, showing IBMX-dependent differences in the intracellulalr signalling (*15*). These authors defended the view that the measurement of cAMP after pre-treating the cells with IBMX does not truly reflect the melanocortin receptor signalling. Therefore, we thought initially that the inverse agonism of AGRP on melanocortin receptors (MCR1 and MCR4) could be an artifact of the IBMX used in the incubation medium. IBMX modifies the intracellular levels of cAMP by affecting their degradation but also interfere with their binding to the target enzyme, cAMP-dependent protein kinase A (PKA). Therefore, IBMX increases the basal activity of PKA and inhibits the activation promoted by cAMP (*16*). However, we developed the same experiment using HEK cells stably overexpressing sea bass MC5R and no effects of AGRP by itself or reducing MTII-induced galactosidase activation (competitive antagonism) were observed with or without IBMX

treatment (unpublished results, Sánchez E, Rubio VC and Cerdá-Reverter JM). These results demonstrate that the AGRP agonism is specific of the MC4R and strongly depends on the phosphodiesterase inhibition in vitro. A possible explanation for these results would involve an AGRP-induced conformational change of the MC4R, leading to the activation of the intracellular phosphodiesterase system. This activation would reduce the cAMP intracellular levels imposed by the constitutive activity of the MC4R, thus decreasing the activation of the PKA. The overexpression in vitro of the MC4R, but not MC5R, could dramatically increase adenylyl cyclase activity because of its constitutive nature. Therefore, this over-activation of adenylyl cyclase could induce high levels of phosphodiesterase activity and the effects of AGRP in vitro could be observed only after previous inhibition of the phosphodiesterase. Alternatively, phosphodiesterase has also been shown to interact with arrestins to regulate the branching of signalling from G-coupled receptors (*17*). Phosphodiesterases bind arrestins and are recruited to the occupied receptors, limiting the cAMP accumulation in localized domains. The phosphodiesterase binding to arrestins has been also proposed to control the PKA-phosphorylation of the β-adrenergic receptor regulating the efficiency of the receptor switch from Gs protein to Gi. This exchange could decrease the rate of cAMP generation because Gi activation inhibits adenilyl cyclase and couples the receptor to Gi-linked pathways (*18*). Interestingly, it has been reported that AGRP induces arrestin-mediated endocytosis of the human MC4R (*19*) which exhibits a constitutive traffic in hypothalamic neurons (*20*). Intracellular signaling pathways through which melanocortin

receptors exert their effects are not well understood. Activated melanocortin receptor binds to Gs and this leads to stimulation of adenilyl cyclase while increased concentrations of intracellular cAMP activate PKA. Active PKA initiates the transcription of new genes by phosphorylating and activating cAMP-responsive element binding protein (CREB). However, other intracellular signalling pathways, including mitogenic activated protein (MAP) kinase (*21*), inositol/Ca2+ (*22*), and probably adenosine monophosphate activated-protein kinase (AMPK) pathways (*23*) have also been reported to be involved in MC4R intracellular signaling. A very recent paper has demonstrated that the disruption of regulatory subunit RIIβ of PKA in agouti lethal yellow mice partially reverses obesity, possibly by increasing kinase activity (*24*). This suggests that the agouti-induced metabolic syndrome is mediated by downregulation of the PKA, probably mediated by reduction of cAMP levels.

Our results demonstrate that the competitive antagonism of AGRP is not dependent on the presence of IBMX, suggesting that both AGRP agonism and antagonism in sea bass MC4R are mediated through different intracellular signalling pathways with differential sensitivities to phosphodiesterase inhibitors. More experiments involving the intracellular signalling pathways of the MC4R must be made to corroborate this hypothesis, which opens up new targets for the treatment of melanocortin-induced metabolic syndrome.

The AGRP-mediated decrease of basal galactosidase activity in HEK cells expressing sea bass MC4R suggests that the receptor is constitutively

activated. The constitutive activity of the mammalian MC4R has already been demonstrated in vitro and in vivo. It has been proposed that the N-terminal domain functions as a tethered intramolecular ligand preserving the constitutive activity of the receptor (*25*). This constitutive activity of the MC4R is supposed to impose an inhibitory tone on food intake that is regulated by AGRP binding (*26*). Therefore mutations of arginine 18 within the N-terminal domain that do not impair the binding of agonist but drastically reduce the constitutive activity leads to obesity in humans. Interestingly, sea bass MC4R exhibits an arginine residue N-terminally flanked by an asparagine residue in a similar position to that observed in human. We do not know if the putative constitutive activity of the sea bass MC4R can operate in vivo but the physiological data reported here support the idea. Progressive fasting does not increase hypothalamic POMC expression in the sea bass as previously observed in the goldfish (*27*) and zebrafish (Song et al., 2003), suggesting a limited production of agonist during negative energy balance states. In the latter species, fasting dramatically induces hypothalamic AGRP expression (*28*), suggesting a downregulation of MC4R signaling in the absence of a decrease of agonist production, through AGRP binding.

In conclusion, we demonstrate that AGRP can work as a competitive antagonist of melanocortin peptides or as inverse agonist on sea bass MC4R. However, the inverse agonism, but not the competitive antagonism, depends on inhibition of the intracellular phosphodiesterase system, which suggests

that both systems operate through different intracellular pathways in the regulation of CREB protein activation.

References

1. Song, Y., Golling, G., Thacker, T. L., and Cone, R. D. (2003) Agouti-related protein (AGRP) is conserved and regulated by metabolic state in the zebrafish, Danio rerio, *Endocrine 22*, 257-265.
2. Ling, M. K., and Schioth, H. B. (2005) Subtype-specific pharmacological properties of the melanocortin receptors in chicken, *Ann N Y Acad Sci 1040*, 378-380.
3. Song, Y., and Cone, R. D. (2007) Creation of a genetic model of obesity in a teleost, *FASEB J 21*, 2042-2049.
4. Siani, M. A., Thompson, D. A., Canne, L. E., Wilken, J., Figliozzi, G. M., Kent, S. B. H., and Simon, R. J. (1999) Rapid modular total chemical synthesis of chemokines based on genome sequence data, *Peptides: Frontiers of Peptide Science, Proceedings of the American Peptide Symposium, 15th, Nashville, June 14-19, 1997*, 643-644.
5. unknown. Gnomon, the NCBI eukaryotic gene prediction tool., in *http://www.ncbi.nlm.nih.gov/genome/guide/gnomon.shtml*.
6. Yang, Y. K., Thompson, D. A., Dickinson, C. J., Wilken, J., Barsh, G. S., Kent, S. B., and Gantz, I. (1999) Characterization of Agouti-related protein binding to melanocortin receptors, *Mol Endocrinol 13*, 148-155.
7. Kimmel, C. B., Ballard, W. W., Kimmel, S. R., Ullmann, B., and Schilling, T. F. (1995) Stages of embryonic development of the zebrafish, *Dev Dyn 203*, 253-310.
8. Ziv, L., Levkovitz, S., Toyama, R., Falcon, J., and Gothilf, Y. (2005) Functional development of the zebrafish pineal gland: light-induced expression of period2 is required for onset of the circadian clock, *J Neuroendocrinol 17*, 314-320.
9. Chai, B. X., Neubig, R. R., Millhauser, G. L., Thompson, D. A., Jackson, P. J., Barsh, G. S., Dickinson, C. J., Li, J. Y., Lai, Y. M., and Gantz, I. (2003) Inverse agonist activity of agouti and agouti-related protein, *Peptides 24*, 603-609.
10. Chen, W., Shields, T. S., Stork, P. J., and Cone, R. D. (1995) A colorimetric assay for measuring activation of Gs- and Gq-coupled signaling pathways, *Anal Biochem 226*, 349-354.

11. Cerda-Reverter, J. M., Ling, M. K., Schioth, H. B., and Peter, R. E. (2003) Molecular cloning, characterization and brain mapping of the melanocortin 5 receptor in the goldfish, *J Neurochem 87*, 1354-1367.
12. Wilken, J., and Kent, S. B. (1998) Chemical protein synthesis, *Curr Opin Biotechnol 9*, 412-426.
13. Brown, A. M., Mayfield, D. K., Volaufova, J., and Argyropoulos, G. (2001) The gene structure and minimal promoter of the human agouti related protein, *Gene 277*, 231-238.
14. Jin, Y., Zhang, W., and Li, Q. (2009) Origins and evolution of ADAR-mediated RNA editing, *IUBMB Life 61*, 572-578.
15. Guo, L., Munzberg, H., Stuart, R. C., Nillni, E. A., and Bjorbaek, C. (2004) N-acetylation of hypothalamic alpha-melanocyte-stimulating hormone and regulation by leptin, *Proc Natl Acad Sci U S A 101*, 11797-11802.
16. Tomes, C., Rossi, S., and Moreno, S. (1993) Isobutylmethylxanthine and other classical cyclic nucleotide phosphodiesterase inhibitors affect cAMP-dependent protein kinase activity, *Cell Signal 5*, 615-621.
17. Conti, M., and Beavo, J. (2007) Biochemistry and physiology of cyclic nucleotide phosphodiesterases: essential components in cyclic nucleotide signaling, *Annu Rev Biochem 76*, 481-511.
18. Baillie, G. S., Sood, A., McPhee, I., Gall, I., Perry, S. J., Lefkowitz, R. J., and Houslay, M. D. (2003) beta-Arrestin-mediated PDE4 cAMP phosphodiesterase recruitment regulates beta-adrenoceptor switching from Gs to Gi, *Proc Natl Acad Sci U S A 100*, 940-945.
19. Breit, A., Wolff, K., Kalwa, H., Jarry, H., Buch, T., and Gudermann, T. (2006) The natural inverse agonist agouti-related protein induces arrestin-mediated endocytosis of melanocortin-3 and -4 receptors, *J Biol Chem 281*, 37447-37456.
20. Mohammad, S., Baldini, G., Granell, S., Narducci, P., and Martelli, A. M. (2007) Constitutive traffic of melanocortin-4 receptor in Neuro2A cells and immortalized hypothalamic neurons, *J Biol Chem 282*, 4963-4974.
21. Patten, C. S., Daniels, D., Suzuki, A., Fluharty, S. J., and Yee, D. K. (2007) Structural and signaling requirements of the human melanocortin 4 receptor for MAP kinase activation, *Regul Pept 142*, 111-122.
22. Newman, E. A., Chai, B. X., Zhang, W., Li, J. Y., Ammori, J. B., and Mulholland, M. W. (2006) Activation of the melanocortin-4 receptor mobilizes intracellular free calcium in immortalized hypothalamic neurons, *J Surg Res 132*, 201-207.
23. Minokoshi, Y., Alquier, T., Furukawa, N., Kim, Y. B., Lee, A., Xue, B., Mu, J., Foufelle, F., Ferre, P., Birnbaum, M. J., Stuck, B. J., and Kahn, B. B. (2004) AMP-kinase regulates food intake by responding to hormonal and nutrient signals in the hypothalamus, *Nature 428*, 569-574.

24. Czyzyk, T. A., Sikorski, M. A., Yang, L., and McKnight, G. S. (2008) Disruption of the RIIbeta subunit of PKA reverses the obesity syndrome of Agouti lethal yellow mice, *Proc Natl Acad Sci U S A 105*, 276-281.
25. Srinivasan, S., Lubrano-Berthelier, C., Govaerts, C., Picard, F., Santiago, P., Conklin, B. R., and Vaisse, C. (2004) Constitutive activity of the melanocortin-4 receptor is maintained by its N-terminal domain and plays a role in energy homeostasis in humans, *J Clin Invest 114*, 1158-1164.
26. Cone, R. D. (2006) Studies on the physiological functions of the melanocortin system, *Endocr Rev 27*, 736-749.
27. Cerda-Reverter, J. M., Schioth, H. B., and Peter, R. E. (2003) The central melanocortin system regulates food intake in goldfish, *Regul Pept 115*, 101-113.
28. Cerda-Reverter, J. M., and Peter, R. E. (2003) Endogenous melanocortin antagonist in fish: structure, brain mapping, and regulation by fasting of the goldfish agouti-related protein gene, *Endocrinology 144*, 4552-4561.

Chapter 3

Bacterial Expression of Murine Agouti Signaling Protein

(Chapter 3 and chapter 4 are quite similar, chapter 3 describes methods which I believe are sufficiently complex to warrant a stand alone chapter, chapter 4 is written in manuscript format.)

A description of experiments highlighting the protein expression of Agouti Signaling Protein (ASIP) follows, both successes and failures. First off, a source of the cDNA must be identified. The laboratory of Greg Barsh provided the DNA of murine ASIP cloned into the bluescript vector. The cDNA can be chemically synthesized and the codons optimized for expression, however this is costly. The bluescript vector has both SalI and BamHI restriction endonuclease cleavage sites flanking the cloning region. If no insert is present, enzymatic cleavage should produce a piece of DNA 45 base pairs in length. Figure 3.1 clearly shows a band between 500 and 750 bp

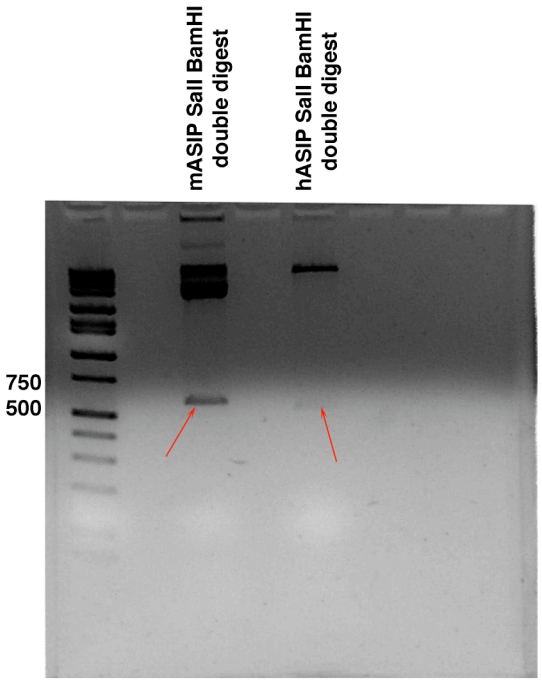

Figure 3.1. 1.5 % agarose gel of plasmid DNA digested with the SalI and BamHI restriction endonucleases.

for double digested DNA. Plasmid DNA obtained from the Barsh lab was transformed into DH5α cells (Saltikov lab UCSC), plated onto ampicillin agar,

a winning colony grown in 100 mL LBA at 37 °C overnight, and plasmid DNA collected with a Qiagen (Valencia, CA USA) midi-prep kit. New England Biolabs (Ipswich, MA USA) instructions were followed for enzymatic digest. Cleaved DNA was run on a 1.5% agarose gel containing .01 % 10 mg/mL aqueous ethidium bromide and photographed using a UV light source. No further attempts were made to verify the DNA sequence.

Traditional DNA cloning makes use of restriction endonucleases that generate sticky ends on the insert, complimentary sticky ends on the vector, and DNA ligase joining the insert to the vector creating a circular plasmid (*1*). The pET 19b vector from Novagen (San Diego, CA USA) contains NdeI and BamHI restriction sites. The cDNA encodes for the entire 131 amino acid sequence as well as a eukaryotic promoter, approximately 550 bp. PCR of the secreted ASIP (109 aa) with forward and reverse primers, including NdeI and BamHI cleavage sites respectively, should produce a 339 bp fragment. The Fermentas (Burlington, Ontario Canada) pyrostart master mix contains the Taq polymerase, dNTPs, $MgCl_2$, and PCR buffer having the advantage of just adding template, primers, and H_2O. Midi-prep purified plasmid DNA, forward primer (NdeI) with the sequence 5'-ACCGTCCACCATAATGAAAGCACTCGAG-3' (P1), reverse primer (BamHI) with the sequence 5'-GGATCCTCAGCAGTTGGGGTTGAG-3' (P4), water, and pyrostart master mix were combined according to the manufacturer's protocol. PCR products were run on a 1.5% agarose gel (figure 3.2) containing .01 % 10 mg/mL aqueous ethidium bromide and photographed using a UV light source.

Figure 3.2. (Top) Amino acid sequence of ASIP, eukarytokic promoter and cleaved

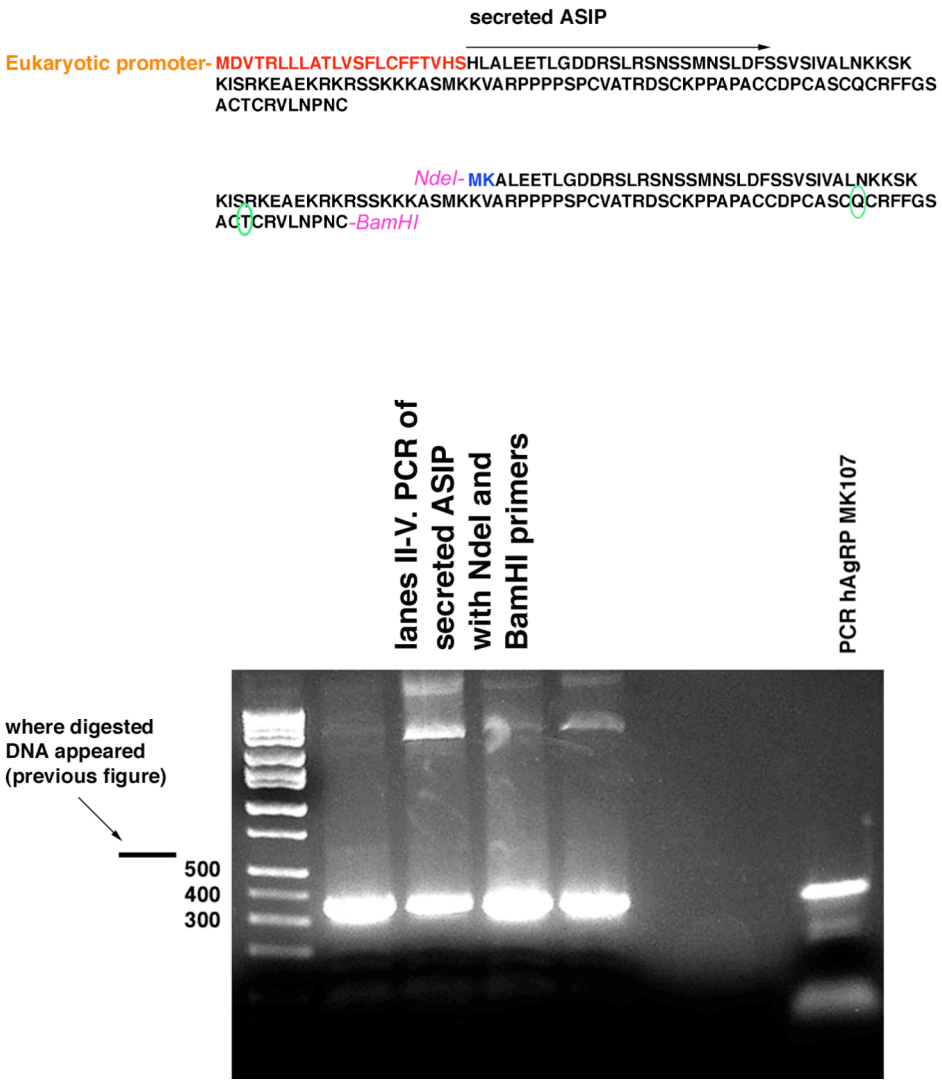

signal sequence (ASIP 1-22) contribute to the larger sized fragment cut from the bluescript vector. (Bottom) 1.5% agarose DNA gel of PCR products from P1 and P4 primers, lane 8 PCR of AgRP as positive control.

Bands containing the proper size fragment were excised with a razor blade and purified with the illustra PCR and gel band cleanup kit from GE Healthcare (Buckinghamshire UK). Peptide oxidative folding was greatly enhanced by tyrosine substitution at key positions in the final two β-strands

(2). We hypothesized mutation of homologous residues in the full length mouse protein would produce identical results. There are basically two methods of generating a controlled mutation: 1) methylate parent DNA, PCR amplify DNA with mutant primers, and digest methylated parent DNA or 2) split parent DNA into two fragments by PCR with mutant primers, and recombine parent DNA, again with PCR (figure 3).

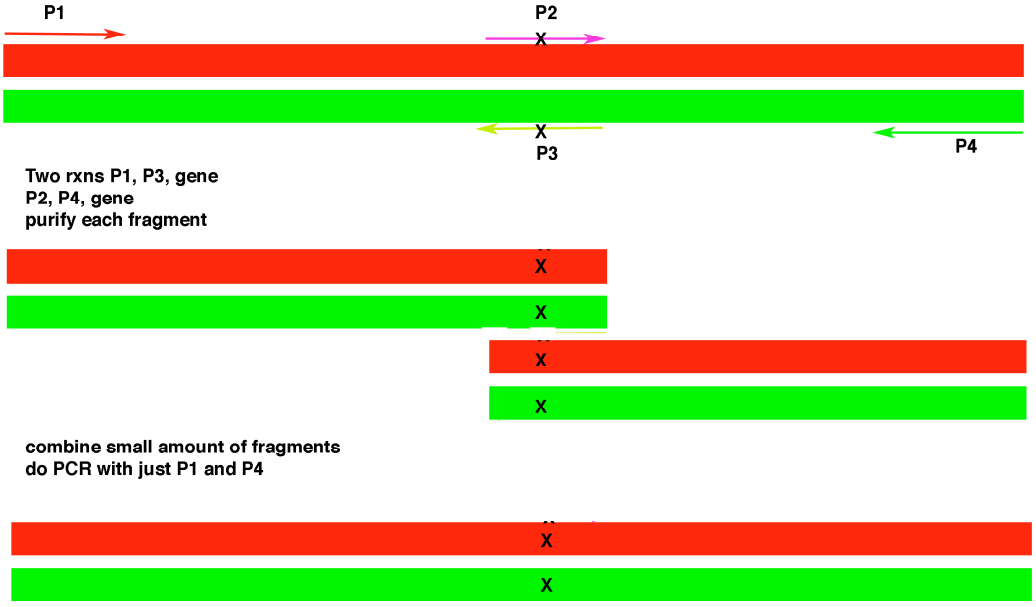

Figure 3.3. Scheme which generated point mutations

The second mechanism was chosen because the first technique normally requires the gene of interest to be present in a plasmid. As seen in figure 3.4, glutamine 114 and threonine 123 were mutated to tyrosine. For the mutation of glutamine forward primer having the sequence 5'-TGCGCCTCCTGCtAtTGCCGTTTCTTC-3' (P2) and reverse primer, 5'-GAAGAAACGGCAaTaGCAGGAGGCGCA-3' (P3), were used in separate

PCR reactions with P1 and P4 together utilizing wild type secreted ASIP template DNA and pyrostart master mix. The glutamine to tyrosine

MKALEETLGDDRSLRSNSSMNSLDFSSVSIVALNKKSK
KISRKEAEKRKRSSKKKASMKKVARPPPPSPCVATRDSCKPPAPACCDPCASCQCRFFGS
ACTCRVLNPNC

MKALEETLGDDRSLRSNSSMNSLDFSSVSIVALNKKSK
KISRKEAEKRKRSSKKKASMKKVARPPPPSPCVATRDSCKPPAPACCDPCASCYCRFFGS
ACYCRVLNPNC

Figure 3.4. Primary sequence of ASIPYY.

substitution, and likewise the threonine mutation, generated a long and short fragment of DNA. The long fragment, > 300 bp, possessed affinity for gfx spin columns, therefore the illustra kit was used to purify this piece, however the short fragment, < 100 bp, did not bind to the gfx stationary phase. Electroelution was employed to purify the shorter section. Briefly, bands encompassing the short piece were cut from a DNA agarose gel, clamped in 10-14KDa cutoff dialysis tubing containing 1 mL TBE, placed back in the electrophoresis apparatus, run at 100V for 10-15 minutes, TBE removed, and DNA precipitated with 100% ethanol. The purified segments were recombined and PCR amplified using only P1 and P4 primers. Experimental results as well as DNA sequencing analysis are shown in figure 3.5, threonine to tyrosine exchange outcome was nearly identical (data not shown). Primers used for threonine mutation had the sequences, forward 5'-GGCAGCGCCTGCtaCTGTCGAGTACTC-3' and reverse 5'-GAGTACTCGACAGtaGCAGGCGCTGCC-3'.

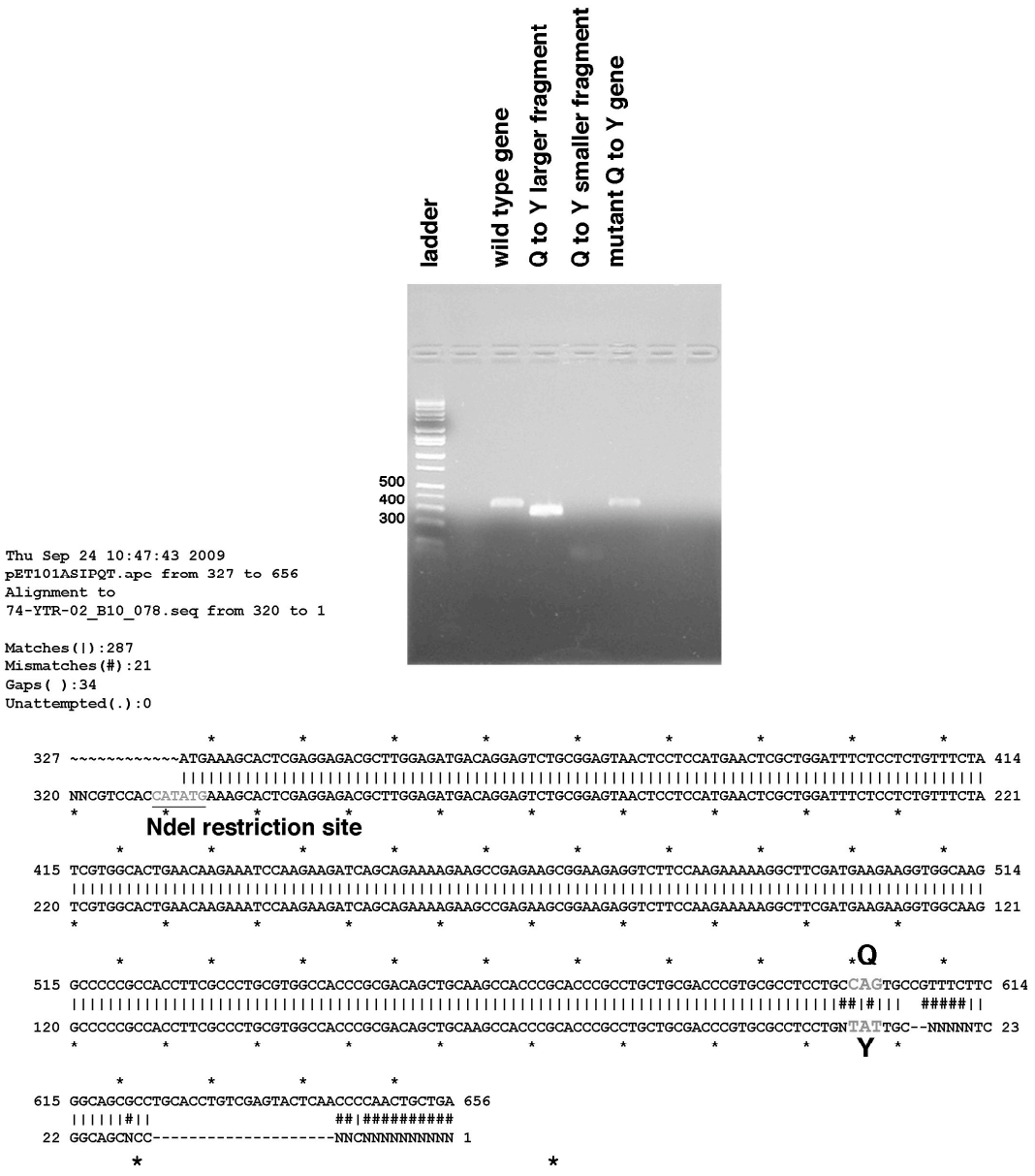

Figure 3.5 (Top) 1.2% DNA agarose gel of starting material, fragments, and recombined gene arising from mechanism outlined in 3.3 for the Q114Y mutation. (Bottom) DNA sequencing results, wild type ASIP aligned with Q114Y sequence.

With mutated DNA in hand attempts at ligation into the pET19b vector were made. Vector and insert DNA were doubly digested with the BamHI and NdeI restriction enzymes, gel purified, combined, T4 DNA ligase

added, the mixture incubated on the benchtop for 2 hours, transformed into DH5α cells, and plated on LB agar containing ampicillin. However, no winning colonies grew, this method was discarded.

The Millhauser lab has successfully ligated the prion protein DNA from various species into the pET-101 vector using topoisomerase. Invitrogen (Carlsbad, CA USA) markets a pET-101 sequence with topoisomerase already fused to the DNA called pET-101/D-TOPO. Blunt end PCR of the insert having 5'-CACCATG(Gene)-3' as the initial sequence is combined with pET-101/D-TOPO, the topoisomerase reaction creates phosphodiester bonds between insert and vector directionally, as the vector has a 3'-GTGG-5' overhang which base pairs with the insert. This bypasses the need for restriction enzymes and DNA ligase, but requires blunt end PCR product. The pyrostart master mix Taq polymerase adds an additional adenosine to the 3' end of DNA therefore Pfx50 polymerase was used. Fresh PCR was performed using 5'-CACCATGAAAGCACTCGAGGAG-3' (TOPO) as forward primer and the BamHI reverse primer. The product added to pET-101/D-TOPO in adherence to invitrogen's directions, transformed into TOP10 cells, and plated on LB agar containing ampicillin. A winning colony was grown at 37 ºC in 100 mL LBA overnight and DNA harvested with a Macherey-Nagel (Germany) nucleobond midi-prep kit.

Purified plasmid DNA sequence was verified by sequencing and transformed into BL21 (DE3) *e. coli* cells. A pilot expression grown at 37 ºC with 0, 1, 2 and 3 hour induction time points were lysed and spun down. The supernatant and pellet were analyzed on a coomassie blue stained 18% SDS-

PAGE gel (data not shown). Promising bands around 12 kDa were observed but no overexpression was detected. When the protein of interest is not over produced adding a hexahistidine tag greatly facilitates purification. The his tag has affinity for Nickel (II); the entire lysate can be incubated with nickel chelated sepharose, weakly bound molecules washed off, and cloned protein eluted. The pET-101 vector has the DNA for a histidine tag after the v5 epitope for western blot detection (figure 3.6). This will add 32 amino acids to whatever insert is cloned, ASIP is only 109 residues, a 25% increase in size was deemed unacceptable and an enterokinase cleavage site was added. Template DNA, TOPO primer and 5'-AGCTTTATCATCATCATCGCAGTTGGGGTTGAG-3' reverse primer were PCR amplified with the Pfx50 polymerase. The primary sequence DDDDKA was appended to the ASIP C-terminus producing NH_2-ASIPYY-DDDDKA-v5-6H-OH (ASIPYYv56H). Following the protocol described above insert was ligated into the vector, transformed, and sequenced.

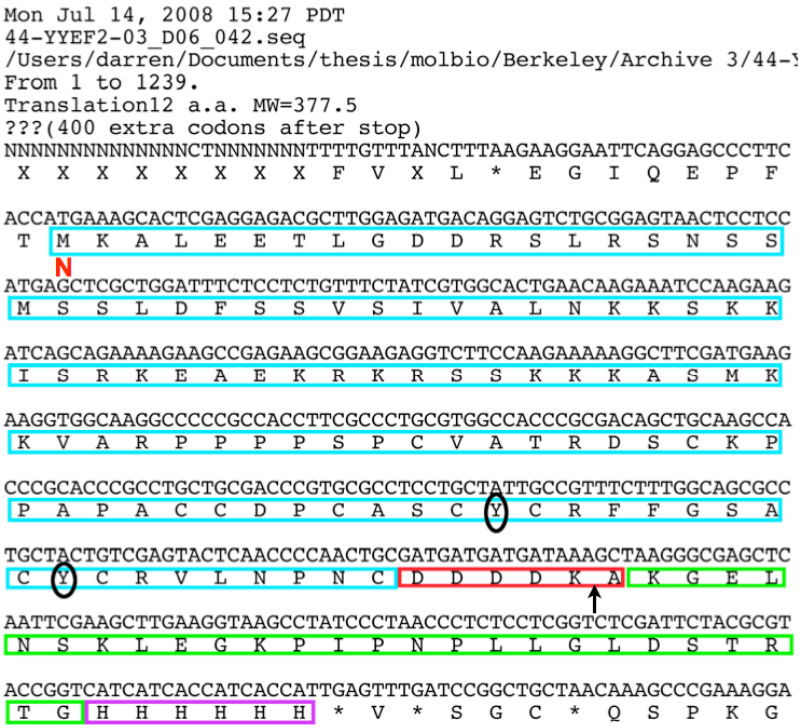

Figure 3.6 Full sequence of ASIPYYv56H. Red N indicates asparagine 43, arrow indicates enterokinase cleavage site, purple box highlights six his tag, and the green box demarcates the v5 epitope.

DNA sequencing results found asparagine 43 was mutated to serine. This substitution was not drastic enough to warrant beginning again. Researchers should be aware PCR with the Pfx50 polymerase is not free from error. BL21 (DE3) cells transformed with ASIPYYv56H plasmid DNA were grown in 1.5 L LBA until OD_{600nm}=0.6, 1 mM IPTG added, induced overnight, and spun down at 3500 rpm for 30 minutes. 5 g cells were lysed by resuspension in 80 mL 10% glycerol 0.1% Triton X 500 mM NaCl 20 mM Tris pH 7.4, freezing in liquid nitrogen, thawing in water, and sonicating for 1 minute. Soluble and insoluble fractions separated by centrifugation at 9000 rpm 4 ºC for 30 minutes, supernatant discarded, and pellet stored in -20 ºC

freezer until further use. The pellet dissolved in 60 mL .1 M Tris .1 M Acetate 10 mM reduced glutathione 8 M amberlite treated Urea pH 8, rocked for 1 hour, and lysate cleared by centrifugation at 9000 rpm 10 ºC for 30 minutes. This cleared lysate was loaded onto 20 mL bed volume nickel chelated sepharose column equilibrated with .1 M Tris .1 M Acetate 8 M Urea pH 8 (IMAC A) with a peristaltic pump (0.5 mL/min), washed with IMAC A, and eluted with .1 M Tris .1 M Acetate 8 M Urea pH 4. Fractions containing protein were purified by c4 RP-HPLC and analyzed by ESI-MS. A small amount of ASIPYYv56H was identified, the yield was substantially improved by the use of 2-mercaptoethanol as reducing agent (figure 3.7) instead of glutathione.

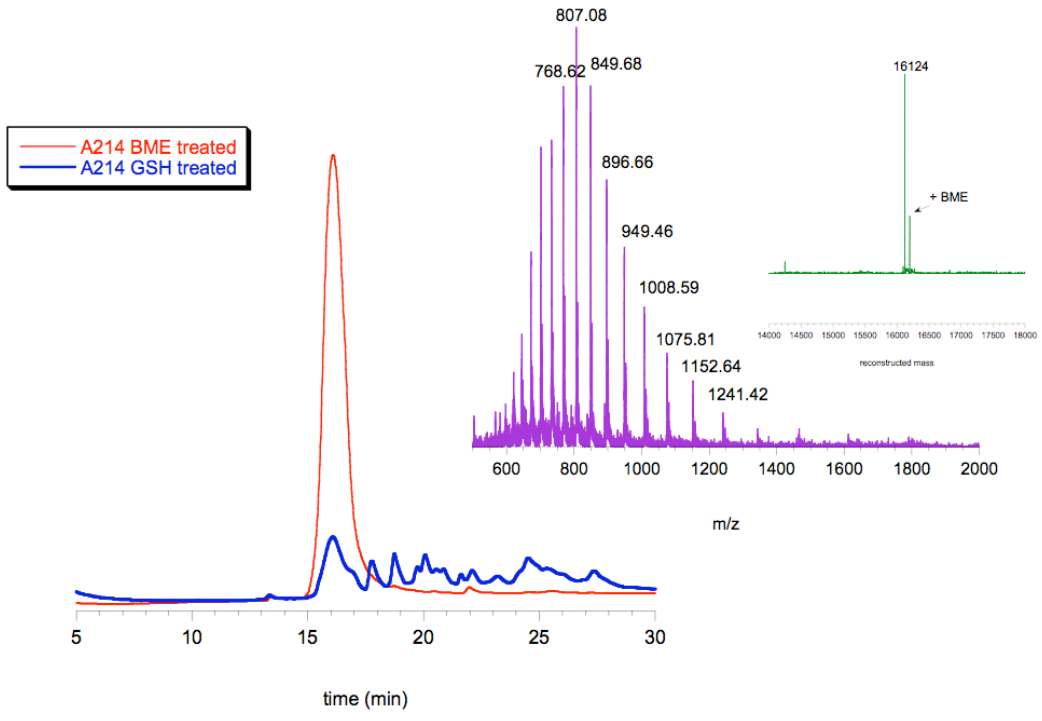

Figure 3.7. HPLC and ESI-MS of ASIPYYv56H.

Despite what is commonly advertised enzymatic proteolysis is hardly ever specific (*3*). Recombinant bovine enterokinase (.2 units of activity in 21 μL) was purchased from Sigma (St. Louis, MO USA) and 180 μL 20 mM Tris 200 mM NaCl 2 mM $CaCl_2$ 50% glycerol pH 7.4 added, the enzyme was stored at -20 ^{o}C. To approximately 200 μg lyophilized ASIPYYv56H added 200 μL 500 mM Tris 2 mM $CaCl_2$ pH 7.5, 4 μL enzyme solution, incubated 24 hours on benchtop, and products analyzed by c4 analytical HPLC and ESI-MS (data not shown). Although NH_2-Ala-v56H-OH was seen as expected, ASIPYY-DDDDK was not, at least five proteins with molecular weight above 9 kDa were detected, none of which were simple amide bond cleavage products. SDS-PAGE analysis (figure 3.8) showed the existence of 5 bands, including starting material, and a promising band below 15 kDa, but ESI-MS detected 10,829 Da as the major cleavage product (12514 Da expected).

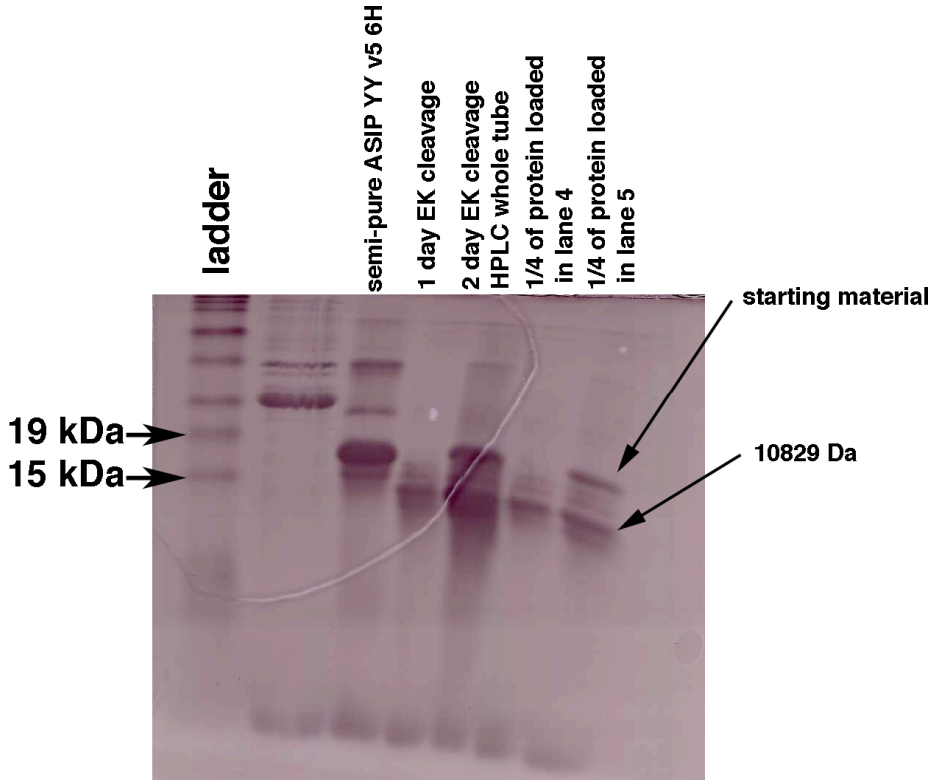

Figure 3.8 SDS-PAGE analysis of cleavage products from ASIPYYv56H treatment with enterokinase.

Obviously a C-terminal his tag proved unsuccessful, invitrogen sells Topoisomerase vectors that have DNA for N-terminal his tags, namely pET-100/D-TOPO and pET-151/D-TOPO, and enzymatic cleavage sites, enterokinase and TEV protease respectively. Given how ineffective enzymatic proteolysis was in my hands I thought it more prudent to clone a six his tag directly to the N-terminus of murine ASIP (figure 3.9).

Figure 3.9. A cartoon comparison between ASIPYYv56H and M6HASIPYY.

Two rounds of PCR with pyrostart master mix were performed. PCR with 5′-CACCATCATCATATGAAAGCACTC-3′ as forward primer and the BamHI reverse primer added 4 histidines to ASIP DNA, this was DNA gel purified and used in the subsequent reaction, PCR with 5′-CACCATGCATCATCACCATCATCAT-3′ as forward primer and the BamHI reverse primer appended the topoisomerase directional ligation sequence, an initiating methionine, and two more histidines creating M6HASIPYY. Blunt end PCR with the Pfx50 polymerase was carried out, DNA gel band purified, and ligated into the pET-101 vector as above. A new random point mutation was observed from DNA sequencing, alanine 54 to threonine (figure 3.10).

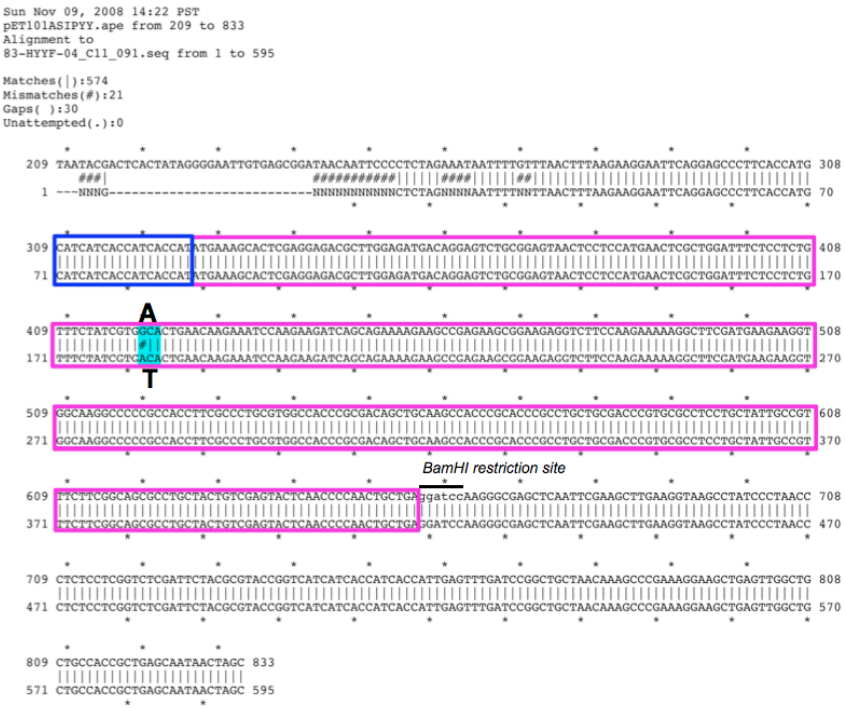

Figure 3.10. DNA sequencing result for M6HASIPYY highlighting the alanine 54 threonine mutation.

This substitution is conservative and in the N-terminus and was thought not to have a large impact on protein function. Identical procedure as for ASIPYYv56H was followed for expression, lysis, and purification. RP-HPLC of fractions eluting from the nickel chelated sepharose column major component was consistent with protein truncated at residue 87 (figure 3.11A). After raising the pH to 8 and dithiothreitol reduction a miniscule amount of M6HASIPYY A54T was detected (figure 3.11B). The source of this shorter species was not ascertained, but several control experiments revealed what it was not. PCR of purified plasmid DNA identified only the whole gene was present (figure 3.12), eliminating abbreviated ligation of insert. Cell lysis with

a bacterial protease inhibitor cocktail (Sigma) did not significantly decrease the production of the fragment (data not shown), abolishing post lysis proteolytic cleavage as a contributing factor.

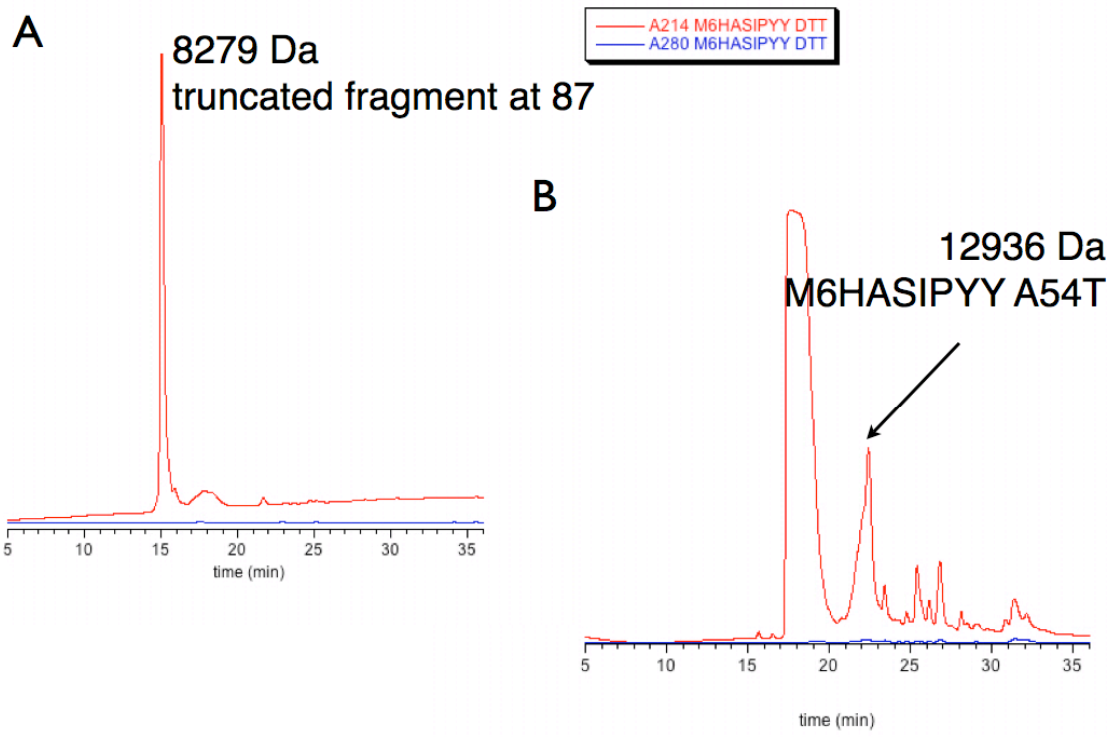

Figure 3.11. HPLC trace of IMAC column elution A) before reduction and B) after reduction. Loaded 14 times as much protein in B) as A).

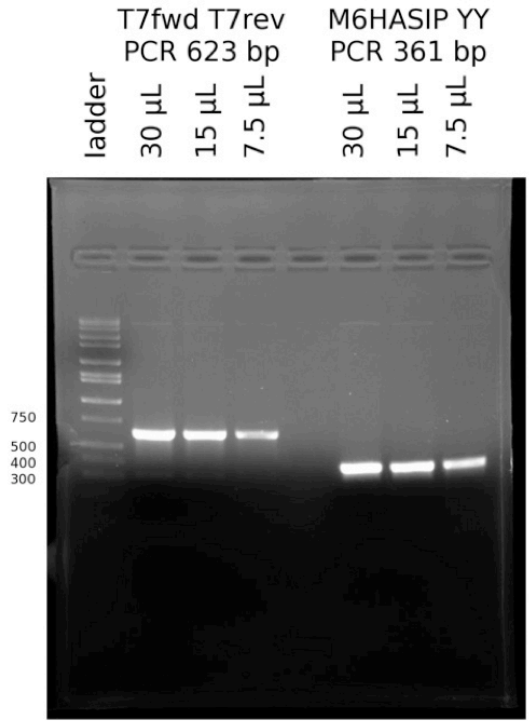

Figure 3.12. 1.2% agarose gel analysis of PCR products from pET 101 plasmid containing M6HASIP YY gene.

A novel purification protocol was developed. BL21 cells containing M6HASIPYY A54T plasmid were grown until OD_{600nm}=0.6 in 1.5L LBA at 24 ºC, induced with 1 mM IPTG for 2 hours, and spun down. 100 mL of 6M GuHCl 500 mM NaCl 100 mM Tris pH 8 was added to pelleted cells, frozen and thawed 3 times, sonicated for 2 minutes, and placed on an orbital rocker for 1 hour. Lysate cleared by centrifigution at 9000 rpm for 30 minutes at 10 ºC and 50 mL supernatant loaded onto 10 mL Nickel beads equilibrated with 6M GuHCl 100 mM Tris pH 8, washed with 6M GuHCl 100 mM Tris 25 mM imidizole pH 8, and his tagged proteins eluted with 6M GuHCl 100 mM Tris 500 mM imidizole pH 8. Entire elution fraction, approximately 10 mL,

reduced with 2-mercaptoethanol (i.e. made 20% v/v with BME and incubated at 42 °C for 30 minutes), pH lowered by addition of 1 mL acetic acid, and injected onto a c4 RP-HPLC column and eluted with increasing acetonitrile concentrations (figure 3.13). A fraction containing the N-terminal fragment was still observed, although substantially less in comparison to the target protein.

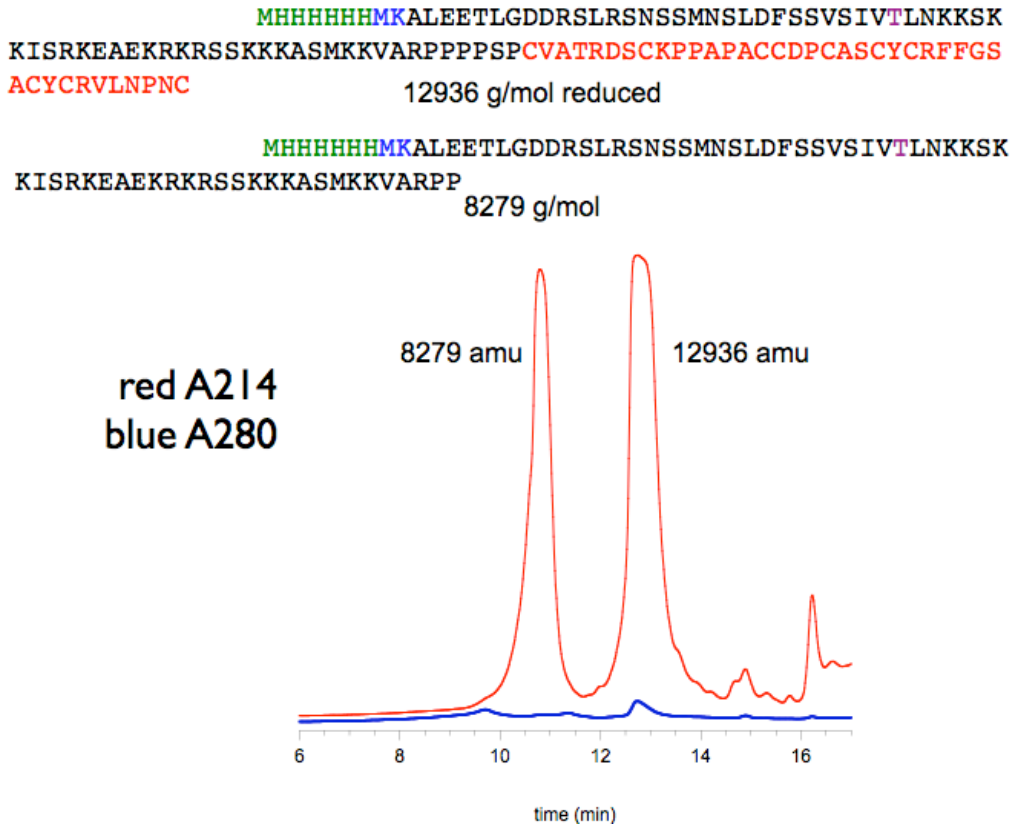

Figure 3.13. HPLC chromatogram of improved full length M6HASIPYY yield.

The reduced protein is not the folded, bio-active molecule. Oxidation/folding was achieved by dissolving reduced protein in buffer containing 6 mM reduced glutathione 0.6 mM oxidized glutathione 2M GuHCl .1 M Tris pH 8. Analytical c18 RP-HPLC (figure 3.14) of time equal zero oxidation experiment identified a peak at 24 minutes corresponding to

fully reduced M6HASIPYY A54T (12936 amu). Two hours later, using the same HPLC conditions, the peak at 24 minutes diminished and a new peak appeared at 20.8 minutes corresponding to fully oxidized M6HASIPYY A54T (12926 amu). Oxidation was judged complete overnight as peak position and intensity did not change from days 2-4. Scale up oxidation generated 387 ± 76 μg folded M6HASIPYY A54T.

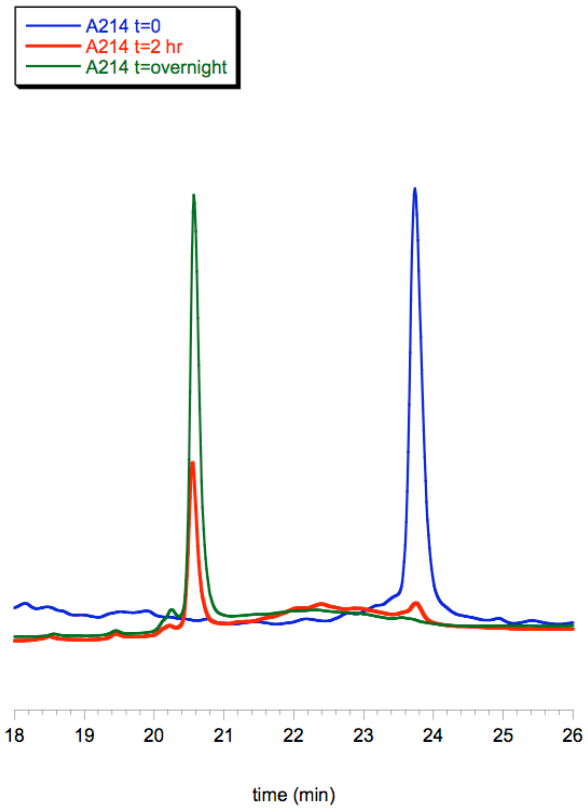

Figure 3.14. Folding of M6HASIPYY.

While not deleterious to oxidation, and likely having little impact on function, the threonine mutation at position 54 was reverted to alanine. Since the gene was ligated into a plasmid mutation mechanism 1 (see above) was employed and the invitrogen gene tailor kit purchased. In adherence to the invitrogen manual, plasmid DNA was methylated, PCR amplified using

forward primer 5′-TCCTCTGTTTCTATCGTGgCACTGAACAAGA-3′, 5′-CACGATAGAAACAGAGGAGAAATCCAGC-3′ reverse primer and high fidelity platinum Taq (invitrogen) DNA polymerase (figure 3.15),

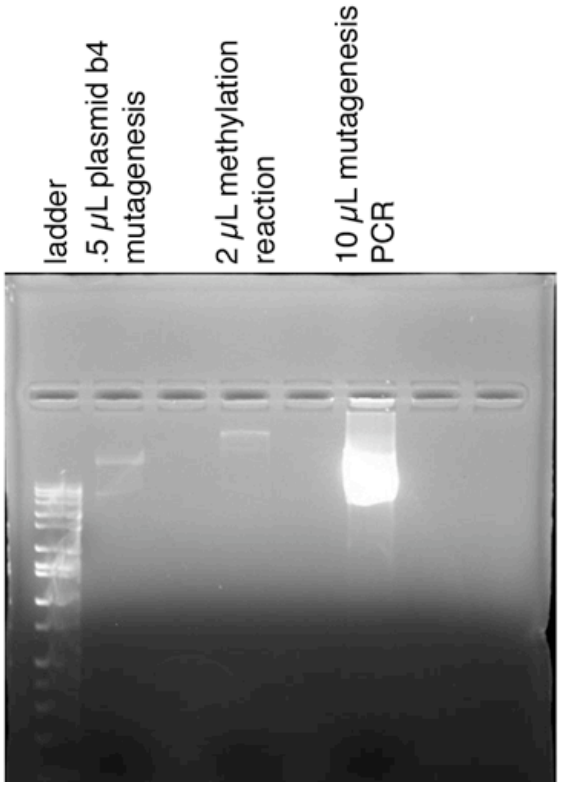

Figure 3.15. Representative 1.2% agarose gel of genetailor mutagenesis reaction. Loaded 1/5 the amount of methylated plasmid DNA in lane 6 as lane 4. If no amplification had occurred then lane 6 would show a very faint band.

and transformed into DH5α cells (Millhauser lab UCSC). A winning colony was grown in 100 mL LBA at 37 °C overnight, DNA purified with a midi-prep kit, and sequenced. Sequencing results confirmed mutation and reversal back to wild type N-terminal amino acid sequence. Expression and folding of M6HASIP YY yielded 4 tubes containing 528 ± 27 μg each, amount determined by amino acid analysis (Table 3.I), of highly homogeneous full length protein (figure 3.16).

	B #aa in seq	C nmol total aa	C/B nmol per aa		
Ala	10	8.103	0.810	ave. nmol (C/B)	0.794
Asx	10	8.270	0.827	std dev	0.042
Arg	9	7.618	0.846		
Phe	3	2.519	0.840		
Pro	10	7.752	0.775		
Ser	17	12.553	0.738		
Thr	2	1.608	0.804		
Tyr	2	1.518	0.759		
Ile	2	1.442	0.721		
Lys	14	11.917	0.851		
Leu	6	4.826	0.804		
His	6	4.719	0.787		
Val	5	3.794	0.759		
~~Glx~~	~~4~~	~~4.013~~	~~1.003~~		
~~Gly~~	~~2~~	~~2.312~~	~~1.156~~		
~~Met~~	~~4~~	~~1.203~~	~~0.301~~		

Nle (Std)	1.936
normalized ave	0.82
mw pep (g/mol)	12895
dilute aaa	5
microgram aaa	52.88
dilute sample	10
microgram sample	528.8482201

Table 3.I Amino Acid Analysis of folded M6HASIPYY. Glutathione contains both glycine and glutamic acid, those were thrown out and did not contribute to the average. The result for methionine was artificially low and discarded.

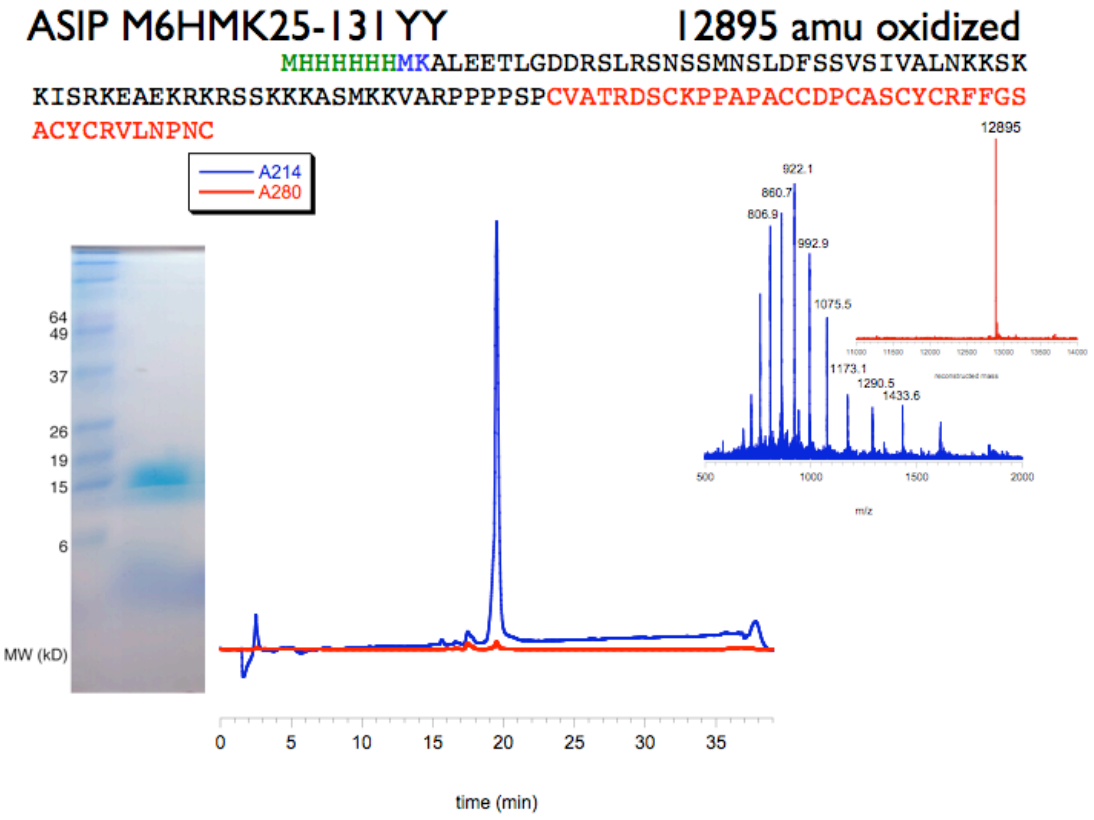

Figure3.16. Homogeneous M6HASIPYY

Verification of the positive folding effect of the tyrosine substitution required M6HASIPYY mutation back to wild type M6HASIPQT. Again, the invitrogen gene tailor kit afforded the appropriate point mutation. For tyrosine back to glutamine forward primer was 5′-GACCCGTGCGCCTCCTGCcAgTGCCGTTTCT-3′ and reverse primer was 5′-GCAGGAGGCGCACGGGTCGCAGCAGGCG-3′. The PCR required the addition of 5 μL enhancer (invitrogen Cat. No. 11495-017). Transformed DH5a cells were grown in 5 mL LBA at 37 ^{o}C overnight and plasmid DNA collected with a qiagen mini-prep kit. For tyrosine back to threonine forward primer was 5′-TTCTTCGGCAGCGCCTGCacCTGTCGAGTAC-3′ while reverse primer was 5′-GCAGGCGCTGCCGAAGAAACGGCACTGG-3′. DNA sequencing results are shown in figure 3.17. Duplicate protocol was

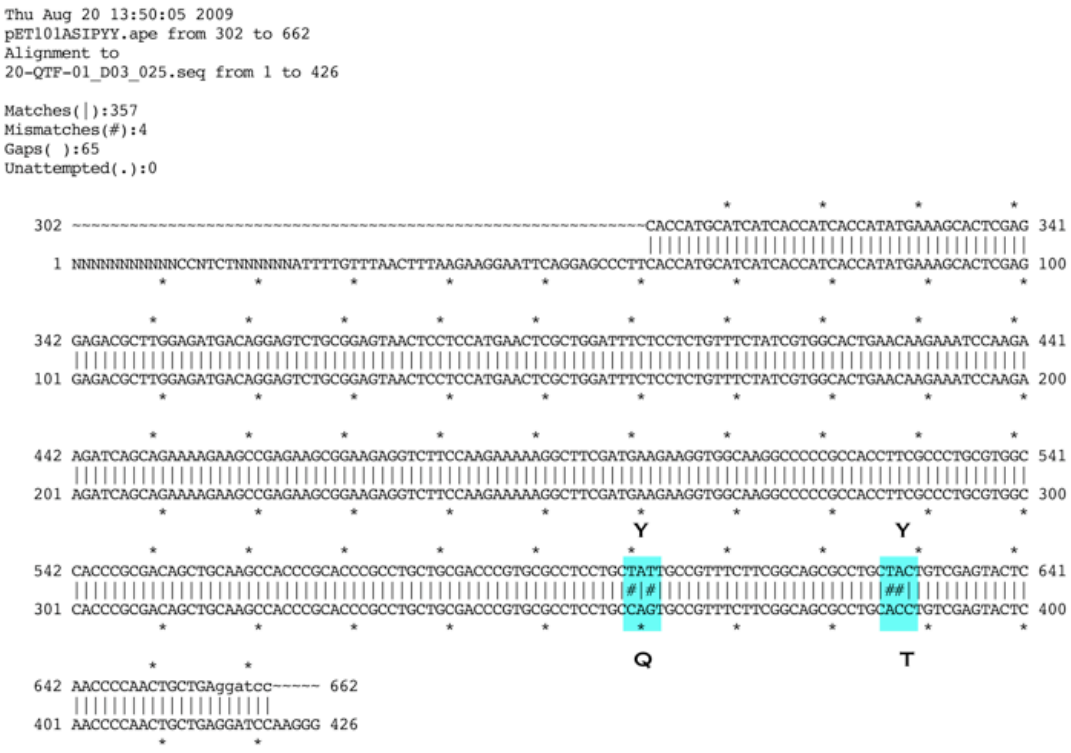

Figure 3.17 DNA sequencing results verifying mutation of M6HASIPYY back to M6HASIPQT.

followed in the expression and purification of M6HASIPQT, except 1 M GuHCl was used in the oxidation. Qualitatively, M6HASIPYY displays enhanced folding characteristics compared to M6HASIPQT (figure 3.18).

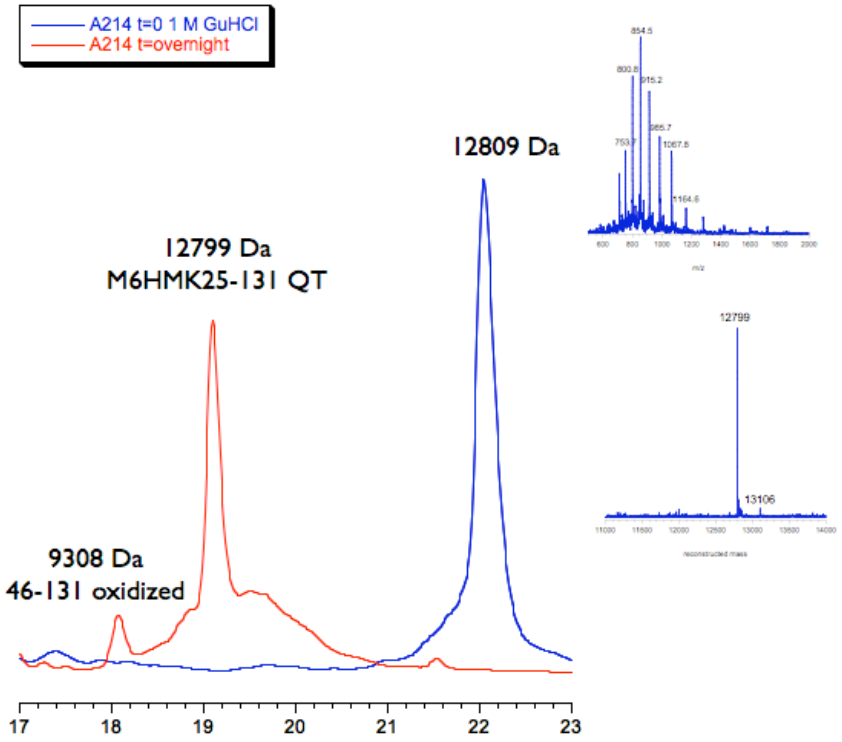

Figure 3.18 Folding of M6HASIPQT.

1. Sambrook, J., and Russell, D. W. (2001) *Molecular cloning : a laboratory manual*, 3rd ed., Cold Spring Harbor, N.Y. : Cold Spring Harbor Laboratory Press.
2. McNulty, J. C., Jackson, P. J., Thompson, D. A., Chai, B., Gantz, I., Barsh, G. S., Dawson, P. E., and Millhauser, G. L. (2005) Structures of the agouti signaling protein, *J Mol Biol 346*, 1059-1070.
3. Huang, H., et al. (2003) Cloning and Fusion Expression of Bovine Enterokinase Light Chain Gene in *Escherichia Coli*, *Hereditas(Beijing) 25*, 6.

Chapter 4

A Robust Technique for Agouti Signaling Protein Production

Introduction

The genetics of mammalian coat color origin have provided much insight into a myriad of biological processes. Signal transduction, body weight regulation, DNA transcription, and linkage analysis have all benefited significantly from insights gained in this field. Some strains of inbred agouti mice display a pleitropic phenotype including an all yellow coat, hyperphagia, pronounced obesity, and increased linear growth. These mice are called lethal yellow mice (genotype A^y/a), owing to their yellow coat and the embryonic lethality of homozygotes(*1*). In the early 1990's the A^y/a genotype was explained as a genetic fusion between the agouti signaling protein (ASIP) and a ubiquitously expressed RNA binding protein(*2*). The ASIP cDNA was cloned and expressed in insect cells by two independent groups in the mid to late '90's, the Barsh group at Stanford and the Wilkison group at Glaxo. This recombinant purified protein was characterized as antagonizing the Melanocortin 1 Receptor (MC1R) response to alpha melanocyte stimulating hormone (α-MSH). The activation of MC1R in mice regulates a switch between melanin pigment colors explaining the yellow coat of mice universally producing ASIP in the A^y/a genotype. A homologous receptor from the hypothalamus, the Melanocortin 4 Receptor (MC4R), is also activated by α-MSH and antagonized by ASIP. This receptor produces a satiety signal blocked by ASIP elucidating the lethal yellow mouse mechanism of hyperphagia and obesity(*3*).

ASIP is found primarily in skin not the hypothalamus, a search of the Expressed Sequence Tags database revealed the similar Agouti Related

Protein (AgRP) mRNA is expressed in the hypothalamic arcuate nucleus and antagonizes MC4R but not MC1R(*4*). The research focus shifted to AgRP leaving many unanswered biochemical questions about the true nature of ASIP's remarkable function. Gryphon Sciences successfully chemically synthesized a number of AgRP analogues, including human AgRP 87-132 and mouse AgRP 21-131(*5*). AgRP and ASIP are secreted paracrine hormones, so although in mice they are 131 amino acids long, 132 in humans, when translated, there is a sequence to signal these proteins be secreted from the cell, this signal is proteolytically cleaved creating a protein of 109 amino acids for murine ASIP and 111 amino acids for murine AgRP. Both proteins have a cysteine free N-terminal domain and a cysteine rich C-terminal domain. AgRP is further processed along the regulated secretory pathway to a peptide composed of the cysteine rich domain(*6*). ASIP also undergoes an additional post-translation modification, namely N glycosylation of a single asparagine residue, N39, however there is much evidence mature ASIP is the full 109 amino acids.

Using a modified air-oxidation protocol adopted from the laboratory of Ian Clarke-Lewis both AgRP 87-132 and 21-131 formed the correct disulfide pairs *in vitro*. Chemically synthesized AgRP 87-132 antagonized MC4R with nanomolar potency. Digestion of recombinant ASIP 23-131 with the Lys C endoprotease generated ASIP 83-131 inhibiting agonist binding to MC1R at nanomolar strength(*7*). The C-terminal cysteine rich domain in both proteins elicits a response at the receptor level, but evolution has evidently preserved the N-terminus of ASIP.

AgRP 87-132 is soluble as evidenced by the homonuclear NMR structure(*8*), the cysteine rich domain of ASIP 93-132, in contrast, is not soluble at high enough concentrations to make air oxidation feasible. ASIP 80-132 dissolves in the air oxidation buffer yet approximately less than 10% of the native cystines are formed *in vitro*. This hurtle is ameliorated by tyrosine substitution at key positions in ASIP, giving rise to a peptide known as ASIP YY. Although the homonuclear NMR structure was solved using ASIP YY generated by native chemical ligation of two peptide segments(*9*), the peptide is tractable by standard single chain solid phase peptide synthesis. The 109 amino acid coupling cycles necessary to make a mature ASIP protein by standard single chain peptide synthesis make this method untenable. A recombinant method of full length ASIP production was developed. *E. coli* was chosen as the host, bacterial protein expression is relatively inexpensive and a mature science. The identical two tyrosines that led to efficient oxidation in the peptide were mutated creating full length ASIP YY.

In 1998 a group at Amgen published a manuscript detailing the bacterial expression of a variant of full length AgRP(*10*). This protein they termed MKd5-AgRP, M for the initiating methionine, K for a lysine they cloned in, and d5 because the first AgRP residue was 26, producing AgRP MK26-132. The Millhauser lab reproduced much of this work (ibid) only with a polyhistidine tag at the N-terminus for affinity purification and expression in minimal media for isotope edited NMR. In the spirit of these studies ASIP MK25-131 YY was cloned into the pET101 vector with an N-terminal six His tag and expressed in *e. coli* BL21 cells. Asparagine 39 is not

glycosylated as bacteria do not generate this post translational modification. ASIP 23-131 purified from the media of baculovirus infected insect cells is glycosylated, presumably at Asn 39(*11*). Though there is no proof this glycosylation resembles that found in mammals, in fact, quite to the contrary, insect glycoproteins are often immunogenic in mammals(*12*). There is one report of mutagenesis coupled with transgenesis where mutation of Asn 39 to Asp results in partial ASIP activity, with the caveat that the authors did not assess protein integrity(*13*). Glycosylation may be paramount to *in vivo* activity.

When exogenous murine ASIP is added to the cell culture media of melan-A cells a large number of genes are modulated(*14*). ASIP is known to act at MC1R, these genes could be coupled to MC1R, or there could be an as yet unknown mechanism of genetic manipulation. The microarray study referenced used protein from insect cell media. Researchers identified a band on SDS-PAGE of 16 kDa as being ASIP 1-131. This is highly improbable, as to get to insect cell media the protein has to have a signal sequence, which would subsequently get cleaved, it is likely ASIP 23-131 with N39 glycosylation. Emphasizing the necessity for a well characterized preparation.

Methods

The full mouse ASIP 1-131 cDNA cloned into a bluescript vector was a generous gift from Greg Barsh. PCR allowed the creation of a histidine tagged variant of the ASIP open reading frame, ASIP M6HMK25-131 YY (FL-ASIP YY). The PCR product was ligated into the pET-101 vector using the

pET-101/D-TOPO kit from invitrogen. Wild type DNA, ASIP M6HMK25-131 QT (FL-ASIP), was created using the invitrogen GeneTailor kit. The presence of the insert was confirmed with PCR. DNA was sequenced at the UC Berkeley DNA Sequencing Facility prior to expression. These vectors were transformed into *E. coli* BL21 Star (DE3) chemically competent cells, cells were grown in LB Miller broth containing 100 μg/mL ampicillin at 37ºC until OD_{600}=.6, and induced with 1 mM IPTG for 2 hours. Induced cells were centrifuged at 4000 rpm at 4ºC for 30 minutes.

Pelleted cells were resuspended in 6M GuHCl .5 M NaCl .1 M Tris pH 7.8, frozen in liquid nitrogen, thawed in room temperature water, and sonicated for 2 minutes. The lysate was centrifuged at 9000 rpm for 30 minutes and the supernatant loaded onto nickel chelated sepharose (GE Healthcare), washed with 6M GuHCl .1 M Tris 25 mM imidazole pH 7.8, and histidine tagged proteins eluted with 6M GuHCl .1 M Tris 500 mM imidazole pH 7.8. β-mercaptoethanol was added to elution fractions until 20% v/v, incubated at 42 ºC for 30 minutes, filtered through a .2 μm filter, purified by c4 RP-HPLC (vydac) with water/acetonitrile (0.1 % w/v TFA) gradients, and lyophilized. Protein used in oxidation/folding trials was suspended in 6M GuHCl .1 M Tris 100 mM DTT pH 8 and subjected to an additional c4 RP-HPLC purification. Fractions were collected and analyzed by electrospray ionization-mass spectrometry (ESI-MS) on a Micromass (Wythenshawe, UK) ZMD mass spectrometer to confirm the correct molecular weight.

Oxidation/folding trials were initiated by dissolving freshly weighed out oxidized (3.4 mg) and reduced (16.6 mg) glutathione and reduced protein

(≈ 500 μg) in 6 M GuHCl .1 M Tris pH 8 the diluted with Tris buffered water (pH 8) to the desired guanidine concentration and a final total volume of 9 mL. For time equal zero points protein solution was added to 30 mg DTT, volume brought to 1 mL with 6 M GuHCl .1 M Tris pH 8, and injected onto analytical c18 RP-HPLC (vydac).

Purified, reduced YY protein was oxidized in a solution of 2M GuHCl .1M Tris 6 mM reduced glutathione .6 mM oxidized glutathione pH 8 and stirred overnight. Protein concentration was estimated using absorbance at 280 nm at .05 mg/mL. Oxidation was confirmed by the loss of ten mass units on ESI-MS and the formation of an earlier eluting HPLC peak. Final protein purification was accomplished by c18 RP-HPLC and pure fractions lyophilized. Quantitative analysis of the protein concentration was carried out by amino acid analysis at the molecular structure facility at the University of California, Davis.

Cyanogen Bromide was purchased from Sigma. Pure oxidized FL-ASIP YY, approximately 100 μg, was dissolved in 160 μL neat formic acid, 30 μL H2O was added, 3 mg of CNBr, covered with aluminum foil, and rocked overnight. The next day the entire reaction mixture was diluted into 12 mL H2O, covered with aluminum foil, and lyophilized. The dry, cleaved protein was resuspended in 2 mL 95% water 5% ACN 0.1% (w/v) TFA and purified by c18 RP-HPLC.

Binding assays and statistics were performed as previously described in Candille, S et al. Science. **2007** Nov 30;318(5855):1418-23.

Results

Initial attempts to cleave the His tag with an Enterokinase cleavage site were wholly unsuccessful, therefore this scheme was abandoned and the His tag was cloned to directly precede the N-terminus. The C-terminus is the known MCR binding domain, it is reasonable to assume a His tag 69 amino acids from this domain would not interrupt this interaction.

An N-terminal fragment, composed of ASIP M6HMK25-87 (figure 4.1), was present after IMAC column elution. This was proven by mutation of

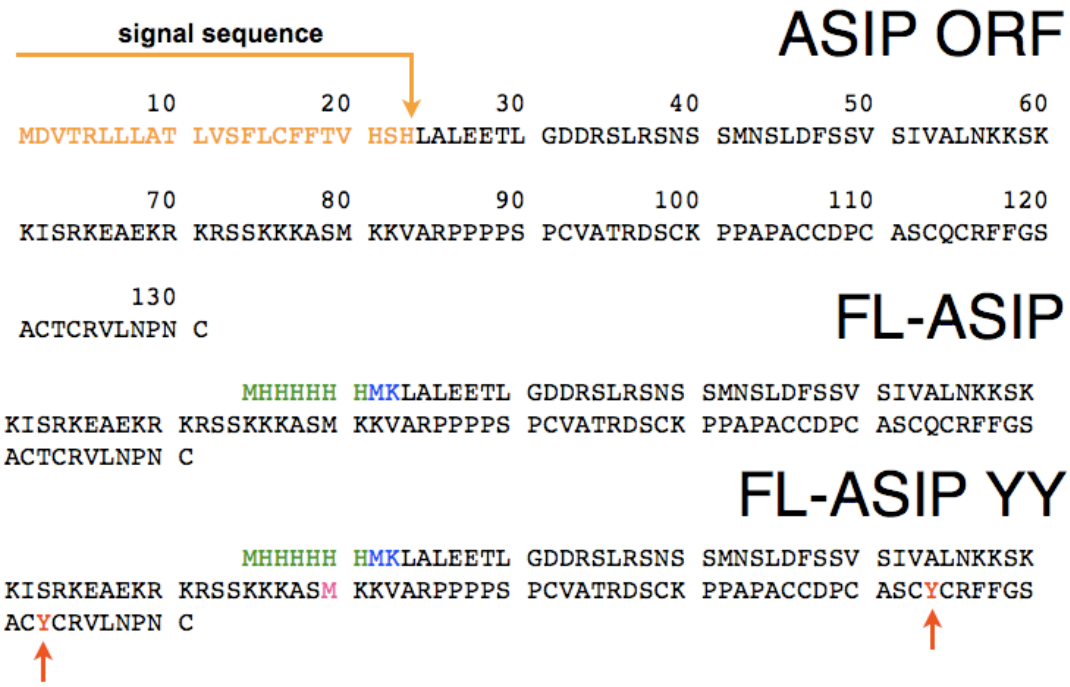

Figure 4.1. Primary amino acid sequences of proteins used in this study. Red arrows indicate tyrosine substitution.

alanine 54 to threonine and a gain of 30 mass units by ESI-MS in the fragment and protein. Although induction at lower temperatures reduced the amount of the fragment, the decrease was not significant (data not shown) and 37 ºC induction used. Under non-reducing conditions the major peak

Figure 4.2 A) HPLC of IMAC column elution (non-reducing) B) reducing

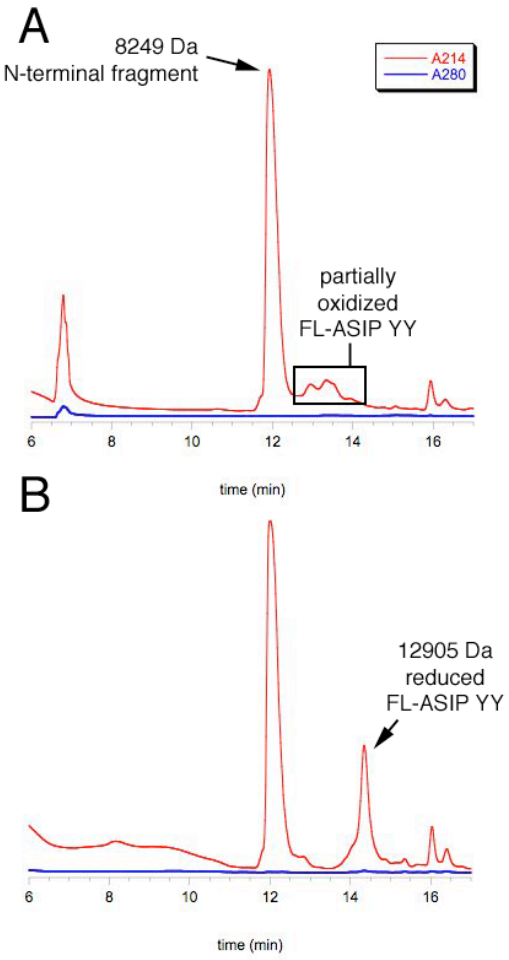

from IMAC column elution was 8249 Da (figure 4.2A) consistent with the fragment. The intracellular environment of *e. coli* is slightly oxidizing and since ASIP forms 5 disulfide bonds there are 945 possible constitutional isomers, *a priori* these should all behave slightly different on RP-HPLC. Only after reduction (figure 4.2B) does ASIP coalesce into a single peak.

Scale-up produced multiple milligrams of reduced full length ASIP, however, the reduced form is not biologically relevant. Oxidation of wild type FL-ASIP formed multiple minor peaks on RP-HPLC (figure 4.3), even

after 16 hours, and one major, symmetric peak. Of the three Guanidine concentrations tried, 0.5 M, 1 M, and 2 M, 1 M consistently yielded the largest major peak. After 8 days the chromatogram did not change dramatically (data not shown). The major, symmetric peak is probably correctly disulfide paired, as the reconstructed ESI-MS gave a mass in agreement with the formation of 5 disulfide bonds and presumably the wild-type protein folds *in vivo*.

Figure 4.3 HPLC trace of FL-ASIP wild type. Reduced in blue, oxidized in red. Inset shows ESI-MS of oxidized species.

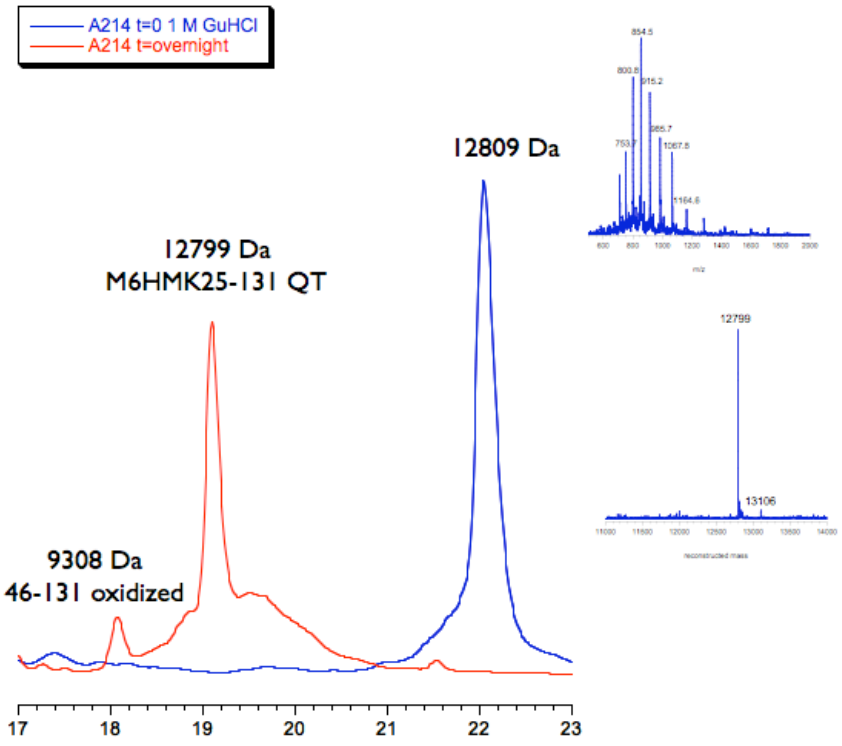

Sixteen hours of FL-ASIP YY oxidation produced a single, perfectly symmetric, earlier eluting RP-HPLC peak (figure 4.4). ESI-MS of this peak reconstructed to a mass of 12895 Da, exactly 10 mass units less than the

reduced protein. For bioactivity tests the DELFIA assay was employed. FL-ASIP YY showed 50 nM Ki for the human MC1R (figure 4.5a). Although this is approximately the Ki shown in other studies, it was cause for concern, control peptide possessed Ki considerably less.

Figure 4.3 HPLC trace of FL-ASIP YY. Reduced in blue, oxidized in red. Inset shows ESI-MS of oxidized species.

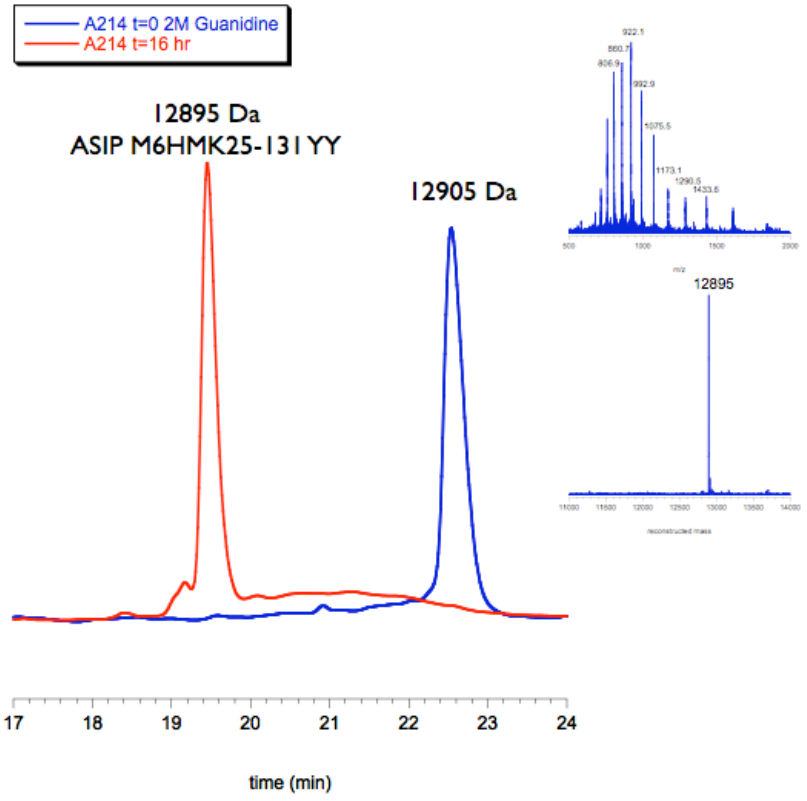

FL-ASIP YY has four methionine residues. The chemical cleavage reagent cyanogen bromide is known to cleave C-terminally to methionine (*15*). Reaction at residue 80 should yield a peptide composed of residues 81-131. Disulfide bonds are stable at low pH. Oxidized FL-ASIP YY was dissolved in 80% formic acid and cyanogen bromide reacted in the dark 16 hours, diluted with water, lyophilized, and then RP-HPLC purified. ESI-MS

detected multiple species with 1-3 formylations, no further attempts were made to remove these formylations. ASIP YY 81-131 + formyl displaced

Figure 4.5 Binding curves for A) FL-ASIP YY and B) ASIP 81-131 YY.

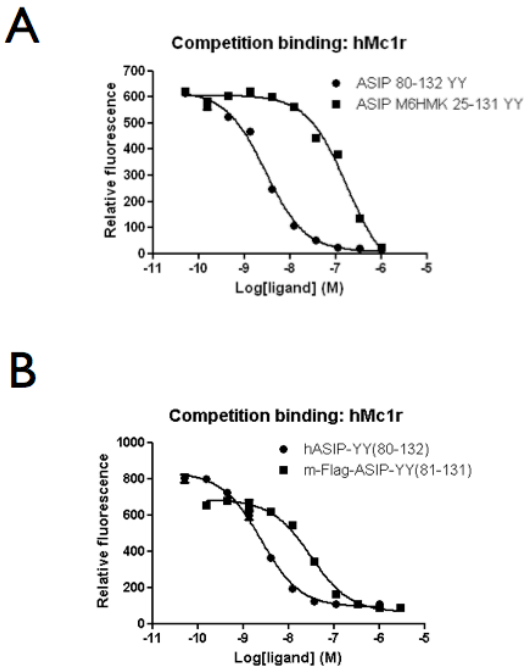

Europium labeled MSH with 8.96 nM Ki (figure 4.5b).

Discussion

To truly dissect the biochemistry of a protein one must have access to milligrams of a homogeneous preparation. Pharmacological experiments typically require small amounts of protein, owing to high receptor affinity, and the pharmacology of ASIP is well established (*16*). ASIP 80-132 can be

manufactured at the several milligram level by solid phase peptide synthesis, but this is difficult, expensive, and uses harsh chemicals. Production of FL-ASIP by standard single chain peptide synthesis is impossible, at least in our hands. The method presented here is cost effective and uses few severe chemicals.

The presence of formyl groups on ASIP 81-131 YY could contribute to the 9 nM Ki, removal of these formylations might bring Ki down to 1 nM, but the goal of this research was not to make a peptide. Since no disulfide reshuffling can occur in formic acid, the cystine pattern of the protein will remain in the peptide. The peptide has the bioactive conformation as evidenced by its ability to displace MSH. The weak affinity of protein must be due to the absence of N-glycosylation or presence of the His tag.

The seminal work of Anfinsen proved unequivocally amino acid sequence determines structure. Micro-evolution has operated for millions of years on the ASIP sequence. Does wild type ASIP not fold? Was Anfinsen wrong? It is more likely we haven't sampled the right oxidation/folding condition. There is the remote possibility that lack of glycosylation inhibits proper oxidation.

Once a protocol is established it is relatively facile to perform site directed mutagenesis. Future directions of research should include mutations of methionines 42 and 80 to alanine and cyanogen bromide cleavage to make ASIP K25-131 YY, eliminating the six His tag, and optimization of protein production. Oxidized FL-ASIP YY does not need to be RP-HPLC purified,

conceivably IMAC purification could be utilized, and oxidized protein eluted with a low pH acetate buffer.

1. Barsh, G. (1999) From Agouti to Pomc--100 years of fat blonde mice, *Nat Med 5*, 984-985.
2. Duhl, D. M., Stevens, M. E., Vrieling, H., Saxon, P. J., Miller, M. W., Epstein, C. J., and Barsh, G. S. (1994) Pleiotropic effects of the mouse lethal yellow (Ay) mutation explained by deletion of a maternally expressed gene and the simultaneous production of agouti fusion RNAs, *Development 120*, 1695-1708.
3. Fan, W., Boston, B. A., Kesterson, R. A., Hruby, V. J., and Cone, R. D. (1997) Role of melanocortinergic neurons in feeding and the agouti obesity syndrome, *Nature 385*, 165-168.
4. Ollmann, M. M., Wilson, B. D., Yang, Y. K., Kerns, J. A., Chen, Y., Gantz, I., and Barsh, G. S. (1997) Antagonism of central melanocortin receptors in vitro and in vivo by agouti-related protein, *Science 278*, 135-138.
5. Yang, Y. K., Thompson, D. A., Dickinson, C. J., Wilken, J., Barsh, G. S., Kent, S. B., and Gantz, I. (1999) Characterization of Agouti-related protein binding to melanocortin receptors, *Mol Endocrinol 13*, 148-155.
6. Jackson, P. J., Douglas, N. R., Chai, B., Binkley, J., Sidow, A., Barsh, G. S., and Millhauser, G. L. (2006) Structural and molecular evolutionary analysis of Agouti and Agouti-related proteins, *Chem Biol 13*, 1297-1305.
7. Kiefer, L. L., Ittoop, O. R., Bunce, K., Truesdale, A. T., Willard, D. H., Nichols, J. S., Blanchard, S. G., Mountjoy, K., Chen, W. J., and Wilkison, W. O. (1997) Mutations in the carboxyl terminus of the agouti protein decrease agouti inhibition of ligand binding to the melanocortin receptors, *Biochemistry 36*, 2084-2090.
8. McNulty, J. C., Thompson, D. A., Bolin, K. A., Wilken, J., Barsh, G. S., and Millhauser, G. L. (2001) High-resolution NMR structure of the chemically-synthesized melanocortin receptor binding domain AGRP(87-132) of the agouti-related protein, *Biochemistry 40*, 15520-15527.
9. McNulty, J. C., Jackson, P. J., Thompson, D. A., Chai, B., Gantz, I., Barsh, G. S., Dawson, P. E., and Millhauser, G. L. (2005) Structures of the agouti signaling protein, *J Mol Biol 346*, 1059-1070.
10. Rosenfeld, R. D., Zeni, L., Welcher, A. A., Narhi, L. O., Hale, C., Marasco, J., Delaney, J., Gleason, T., Philo, J. S., Katta, V., Hui, J., Baumgartner, J., Graham, M., Stark, K. L., and Karbon, W. (1998) Biochemical, biophysical, and pharmacological characterization of bacterially expressed human agouti-related protein, *Biochemistry 37*, 16041-16052.

11. Ollmann, M. M., Lamoreux, M. L., Wilson, B. D., and Barsh, G. S. (1998) Interaction of Agouti protein with the melanocortin 1 receptor in vitro and in vivo, *Genes Dev 12*, 316-330.
12. Altmann, F., Staudacher, E., Wilson, I. B., and Marz, L. (1999) Insect cells as hosts for the expression of recombinant glycoproteins, *Glycoconj J 16*, 109-123.
13. Perry, W. L., Nakamura, T., Swing, D. A., Secrest, L., Eagleson, B., Hustad, C. M., Copeland, N. G., and Jenkins, N. A. (1996) Coupled site-directed mutagenesis/transgenesis identifies important functional domains of the mouse agouti protein, *Genetics 144*, 255-264.
14. Le Pape, E., Passeron, T., Giubellino, A., Valencia, J. C., Wolber, R., and Hearing, V. J. (2009) Microarray analysis sheds light on the dedifferentiating role of agouti signal protein in murine melanocytes via the Mc1r, *Proc Natl Acad Sci U S A 106*, 1802-1807.
15. Gross, E. (1967) Cyanogen bromide reaction [with peptides], *Methods in Enzymology 11*, 238-255.
16. Yang, Y. K., Ollmann, M. M., Wilson, B. D., Dickinson, C., Yamada, T., Barsh, G. S., and Gantz, I. (1997) Effects of recombinant agouti-signaling protein on melanocortin action, *Mol Endocrinol 11*, 274-280.

Chapter 5

Peptoid Mimics of Agouti Related Protein

(The text and figures presented here are primarily from the manuscript "Peptoid mimics of agouti related protein" published in Bioorg Med Chem Lett 2003 April 17, 13(8):1409-1413 and is reprinted with permission.)

Introduction

The Agouti Related Protein (AGRP) is a secreted signaling molecule of 112 amino acids and is expressed in the hypothalamic arcuate nucleus (*1*). AGRP stimulates feeding behavior in mammals and functions, in part, by blocking α-melanocyte stimulating hormone (α-MSH) at the hypothalamic melanocortin-3 and melanocortin-4 receptors (MC3R and MC4R) (*2*). Targeted disruption of MC4R in the mouse hypothalamus leads to obesity (*3*) and transgenic mice over expressing AGRP are also obese. Ablation of the MC3R coding sequence from the mouse genome results in metabolic malfunctions suggesting that this receptor operates in concert with MC4R to control energy balance (*4*). Intracerebroventricular (ICV) injection of melanocortin receptor agonists reduces food intake, while injection of antagonists such as AGRP increases food consumption in lean mice (*5, 6*). Several studies implicate MC4R mutations in human morbid obesity (*7*).

The C-terminal domain of AGRP, residues 87-132, forms the principal MCR binding domain. Alanine scanning of the homologous agouti protein revealed contiguous residues Arg-Phe-Phe, within this domain, as crucial for high affinity binding (*8*). In AGRP, binding was eliminated by replacement of amino acids 111-114 (RFFN) with alanine (*9*) and AGRP (87-132, R111A) fails to antagonize NDP-MSH (a potent α-MSH analogue) stimulated cAMP production at MC4R (*10*). In addition, a number of anionic residues in MC4R significantly modulate AGRP's affinity. A pair of aspartate residues separated by a helical turn on predicted transmembrane helix 3 is implicated in the hMC4R/AGRP interaction and a glutamate on helix 2 in mMC4R also

contributes to AGRP affinity (*11, 12*). It is thought that these anionic residues help anchor AGRP by interaction with R111. Together, these findings implicate the sequence 111-113 – the RFF triplet – as an active MC4R pharmacophore in AGRP.

AGRP's C-terminal domain contains an inhibitor cystine knot (ICK) motif (residues 87 – 120) that is responsible for high affinity MCR antagonism (*13*). The RFF triplet is presented in the turn region of a β-haripin formed by residues 107-120 within this ICK domain. Analysis of the AGRP 87-132 NMR structure shows that RFF side chains are fully solvent exposed, and project out of the protein with similar orientations (*14*). The backbone torsion angles for Phe 113 lie in the αR region of ramachandran space, while those of Phe 112 are extended. A cyclic peptide corresponding to AGRP (110-117), cyclo[CRFFNAFC], antagonizes MC4R, albeit with 1 - 2 logs less potency than that of AGRP(87-132) or AGRP(87-120). Interestingly, the linear analogue SRFFNAFS has no detectable MC4R affinity. These finding suggest that activity of the RFF triplet requires that its backbone take on a turn configuration.

Successful molecular mimicry depends upon constraining the mimic's structure enough to allow conformational adaptation to the target's molecular shape. N-substituted glycines (peptoids) offer a unique backbone, which can be used in molecular design. The peptoid backbone and side chain rotamers are partially constrained by the steric bulk of the N-alkyl substituent (*15*). Peptoid chemical diversity is virtually unlimited and easily exploited by combinatorial solid phase synthesis (*16*). The peptoid amide bond, unlike the

L-peptide amide bond, is resistant to protease cleavage (*17*). Peptoids make fewer intramolecular H-bonds than the corresponding peptide, possibly contributing to enhanced lipophilicity (*18*).

The progressive decrease in size, from a 12 kDa protein to a 5 kDa C-terminal domain to a 4 kDa ICK motif to a 1 kDa cyclic peptide, while still maintaining MC4R functionality, motivates the search for an even smaller AGRP like ligand. Other non-peptide ligands have been discovered. An agonist based on NDP-MSH is active in a mouse MC1R assay at 42.5 μM (*19*) and ligands, characterized by binding studies, have been identified in a large peptoid combinatorial library and in peptidic N-alkylamino acid derivatives (*20*, *21*).

Methods

Materials

Fmoc-Rink amide MBHA resin and Fmoc-Aib-OH were from Novabiochem (San Diego, CA), primary amines, 3,5-dimethylpyrazole carboxamidine nitrate, and Bromoacetic acid were from Aldrich (Milwaukee, WI), DMF was from Burdick and Jackson (McGaw Park, IL), all materials were at least ACS grade and used without further purification. α-MSH, Nle4-α-MSH and NDP-MSH were purchased from Peninsula Laboratories (Belmont, CA). AGRP (86-132) was purchased from Peptides International (Louisville, KY). ASIP [90-132(L89Y]) was purchased from Gryphon Sciences (S. San Francisco, CA). cAMP and binding assays were performed on whole HEK-293 cells stably transfected with the human (h) melanocortin receptor subtypes hMC1R, hMC3R, and hMC4R.

N-(3-Guanidinopropyl)glycine-N-Phenethylglycine-N-benzylAib-NH2 (1)

0.5 g Fmoc-Rink amide MBHA resin was deprotected with 2 x 5 min 20% piperidine/DMF. The free amine was acylated with 2 mmol Fmoc-Aib-OH and DIC in DMF for 30 min, deprotected as before, the resulting amine was alkylated with a 1:1:3 Benzylbromide:DIEA:DMF solution for 1 hr. Acylation of secondary amines was accomplished by DIC and Bromoacetic acid for 1.5 hr. A 20% solution of Phenethylamine in DMSO was added and left overnight (typical yield < 50%). The secondary amine acylated with bromoacetic acid/DIC for 30 min. Diaminopropane was added as a 2M solution in DMSO for 1 hr, followed by guanidinylation by 3,5-dimethylpyrazole carboxamidine nitrate (4 mmol 20% DIEA/DMF 50 ºC 1.5 hrs). The reaction vessel was DMF washed after every synthetic step. Reactions were at 35 ºC unless otherwise noted. MH+ calculated: 510.7 (ave. isotopes) found: 511.3.

Typical Peptoid Synthesis

0.3 g Fmoc-Rink amide MBHA resin was deprotected with 2 x 5 min 20% piperidine/DMF. Step I: The amine was acylated with excess Bromoacetic acid/DIC for 30 min. Step II: 2M solutions of primary amines in DMSO were added for 1-2 hrs. Steps I and II repeated two additional times, followed by guanidinylation of 3-aminopropyl side chains as before. The reaction vessel

was DMF washed after every synthetic step. The library was synthesized by the split pool mix method.

Typical Resin Cleavage

To 0.2 g DCM washed and dried peptoid resin a 2 mL 95:2.5:2.5 TFA:H2O:Triisopropylsilane solution was added for 30 min, filtered, filtrate collected, and filtrate evaporated to dryness. The cleaved peptoid was resuspended in 1 mL 1:1 ACN/H2O solution then HPLC purified.

HPLC, mass spec, CD

All compounds were purified using c18 RP-HPLC columns using water (0.1% w/v TFA)/ACN (0.1% w/v TFA) gradients. Analytical HPLC verified sample purity (see supporting information). Compound molecular weight was confirmed on a VG-Quattro II ESI-MS. Circular Dichroism measurements were taken with an Aviv 60 DS spectrometer using 0.1 cm path length rectangular quartz cuvettes. Compounds were suspended in 0.010 M sodium phosphate pH 7 at 200-400 μM, filtered, and scanned from 300-191 nm at 25 ^{o}C. No significant changes in spectral shape were observed from 100-400 μM 2.

Distance Geometry

SMILES for the compounds were generated manually such that the molecular graph for each novel chemical structure was represented as a text string. The SMILES31 containing defined atoms, bonds, and stereochemistry

were converted to 2000 random, low-energy 3D conformations using distance geometry techniques by Rubicon (Daylight Chemical Information Systems, Irvine, CA), then subjected to 200 steps of conjugate gradient minimization using the MM2* force field (Macromodel/Batchmin, Columbia University, New York, NY).

cAMP assays

cAMP assays were performed using a competitive binding assay (Amersham Pharmacia Biotech, cAMP assay kit TRK 432). Cells were grown to confluence in 24-well tissue culture plates. HEK-293 cells were maintained in Dulbecco's modified Eagles medium containing 4.5 g/100 ml glucose, 10% fetal calf serum, 1 mM sodium pyruvate. Media contained 100 units/ml penicillin and streptomycin and 1 mg/ml of geneticin. For assays, the media was removed and cells were washed twice with phosphate buffered saline. For determining ligand effects on basal cAMP, cells were incubated for 1 h with ligands in 0.3 ml EBSS with 10-5 M isobutylmethylxanthine at 37˚C. The reaction was stopped by adding ice-cold 100% ethanol (500 μl/well). The cells in each well were pipetted and scraped and transferred to a 1.5 ml tube and centrifuged for 10 min at 1900 x g. The supernatant was evaporated in a 55˚C water bath with prepurified nitrogen gas. cAMP content was measured by competitive binding assay according to the assay instructions.

Binding assays

125I-Nle4-α-MSH, 125I-NDP-MSH, 125I-AGRP (86-132), and 125I-ASIP [90-132(L89Y] were prepared by simple oxidative methods as previously described using chloramine-T and Na125I followed by HPLC purification over a C18 column2. 12 h prior to the experiments 0.3 million cells were plated on 24 well plates. Before initiating the binding experiments cells were washed twice with MEM medium. Cells were then incubated with different concentrations of unlabeled ligand containing 0.2% BSA and either 1 x 105 cpm of 125I-Nle4-α-MSH (100,000 cpm = 0.45 nM Nle4-α-MSH), 125I-NDP-MSH (100,000 cpm = 0.496 nM NDP-MSH), 125I-AGRP (86-132) (100,000 cpm = 0.76 nM AGRP (86-132)) or 125I-ASIP [90-132(L89Y] (100,000 = 0.58 nM ASIP [90-132(L89Y)]). After 1 h incubation the cells were again washed twice with MEM medium and the experiment terminated by lysing the cells with 0.1 N NaOH, 1% Triton X-100. Radioactivity present in the lysate was quantified using an analytical gamma counter. Nonspecific binding was determined by measuring the amount of 125I-label remaining bound in the presence of 10-5 M unlabeled ligand and specific binding was obtained by subtracting nonspecific bound radioactivity from total bound radioactivity. Untransfected HEK-293 cells did not display specific binding to any of the radioligands used.

Data analysis

Data was analyzed using Graphpad Prism (Graphpad Software, San Diego, CA). All values for cAMP assays and binding experiments are means +/ - the S.E.M. The cAMP assays were performed three times with quadruplicate wells on different days. The binding studies were performed two or three

times with 2-4 wells per point on different days. Statistical significance was calculated with student's t-test at 95% confidence interval.

Results and Discussion

Two peptoid-like scaffolds, each containing a steric restraint, were developed. One of these scaffolds exhibited antagonist function at MC4R. Using this scaffold, we then rationally designed a seven-member library and, within this library, identified an antagonist that displaced both agonist and antagonist at MC4R with micromolar IC50 values. These findings enhance the understanding of structure activity relationships involved in MCR antagonism, and may yield insight into the molecular determinants of melanocortin receptor signaling and drugs aimed at treating disorders related to energy balance.

A turn is the simplest element of secondary structure. In its most basic form, a turn is defined by the torsion angles of two contiguous amino acids. AGRP residues 111-113 lie at the beginning of a hairpin turn. In solution, the critical residues of NDP-MSH, a high affinity MC4R agonist (22), also form a β_turn. It is therefore reasonable to design a scaffold with a structural turn restraint in order to mimic the RFF triplet. Scaffolds I and II (Figure 5.1) were designed to incorporate such a restraint. In scaffold I, the two backbone methyl groups of an Aib residue at the i+2 backbone position sterically restrain the local conformation. Indeed, conformational sampling using distance geometry techniques followed by MM2* force field calculations and minimization indicated the significant reduction in degrees of backbone rotational freedom in 1 results in a high population of a turn conformer.

Compound 1 did demonstrate weak displacement of the radiolabeled agonist 125I-[Nle4]-α-MSH at MC4R (data not shown). However, synthetic difficulties with scaffold I impeded construction of multiple compounds; consequently, this design was abandoned.

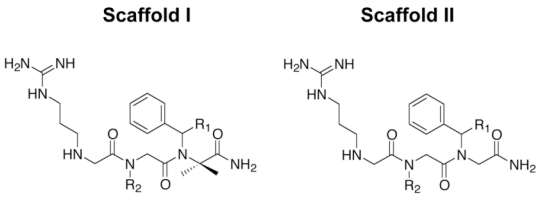

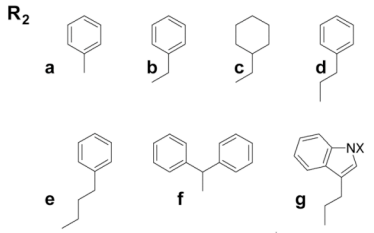

Compound #	R_1	R_2	Scaffold #
1	H	d	I
2	(R)-methyl	b	II
3	H	b	II
4	(S)-methyl	b	II
5	(R)-methyl	f	II
library	(R)-methyl	a-g	II

Figure 5.1. Two-dimensional drawings of compounds used in this study.

It has been established elsewhere that chiral N-substituted glycines form helical conformers in solution (*23*), a helix can be thought of as repetitive turns. A methyl group at the R1 position confers a chiral center in the benzylamide and thus introduces helical phi angles. The specific R and S stereoisomers confer a left hand helical pitch with positive circular dichroism

(CD) signal and right hand helical pitch with negative CD signal, respectively (*24*).

Scaffold II tripeptoids, were synthesized individually as R and S isomers corresponding to compounds 2 and 4, respectively. Compound 3, lacking a chiral center, was also prepared. CD spectra for these three constructs are shown in Figure 5.2a. Spectra for 2 and 4 are characteristic of peptoid helices and differ by a change of sign consistent with molecules of opposite stereochemistry. Compound 3 lacks a stereo center and, as expected, is not CD active.

Figure 5.2. a) Far-UV CD (25 ºC 10 mM phosphate pH 7) of 200 μM 2, 3, and 4. b) Dose response curves for α-MSH stimulated cAMP production at hMC4R in the absence (▩) and presence of 50 μM 2 (▲), 3 (◆), and 4 (▼).

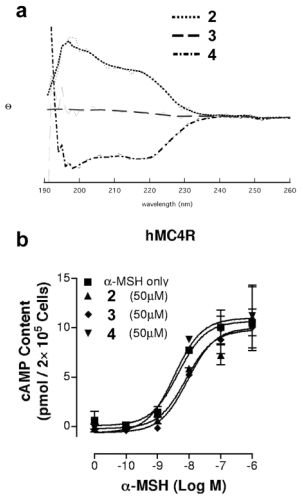

Conformational minimizations were performed on compound 2. As with 1, the resulting low energy structures displayed significant overlap with a turn conformation for 2.

Compounds 2, 3 and 4 were tested for their ability to inhibit α-MSH stimulated cAMP production in hMC4R-transfected cells. The rightward shift in cAMP activity shown in Figure 5.2b demonstrates that 2 and 3 have weak antagonist properties. In contrast, 4 has no effect on activity of hMC4R at 50 μM.

The marginal success with compound 2 motivated the synthesis of a library in which the i (3-Guanidinopropylamine) and i+2 (R-α-Methylbenzylamide) side chain and backbone were kept constant and the i+1 side chain (R2) was varied. The specific choices for the R2 side chains, based on variations of phenylalanine or tryptophan, are shown in Figure 1. Unpurified compounds, direct from TFA cleavage, gave a 13.3 μM IC50 assuming an aggregate theoretical molecular weight of 7 x 490 g/mol = 3430 g/mol (Table 5.1). Fractions A – H, from HPLC purification, had IC50 of 6.6 μM for [Nle4]-α-MSH and also displaced radiolabeled AGRP (86-132) with an IC50 of 27 μM. Table 5.1 shows that pooled fractions A – D weakly displace 125I-[Nle4]-α-MSH while pooled fractions E – H exhibit significant activity with an IC50 of 9 μM (theoretical molecular weight 3.5 x 490 g/mol = 1715 g/mol). Individual cAMP activity assays demonstrated fractions G and H inhibited hMC4R a-MSH cAMP production at 10 μM, with fraction H having greater inhibition than fraction G.

Table 5.1. hMC4R IC_{50} (μM)

cold ligand	^{125}I-Radiolabeled ligand [Nle4]-α-MSH	NDP-MSH	AGRP (86-132)
1	> 100	-	-
2	> 100	-	> 100
3	> 100	-	> 100
4	NA[a]	-	NA[a]
5	3.1 ± 0.9	2.1 ± 0.4	1.9 ± 0.2
crude library	13.3	-	-
fract. A-H	6.6	-	27
fract. A-D	> 100	-	-
fract. E-H	9	-	-
[Nle4]--MSH	0.016 ± 0.007	0.019[b]	0.015 ± 0.001
AGRP	0.001 ± 0.0002	0.011[b, c]	0.003 ± 0.0009
NDP-MSH	0.001 ± 0.0003	0.0013[b]	0.0038[b, d]
$_C$110-117	-	0.621[b]	-

[a]NA = No Activity [b]from ref 2, 9, 13 [c]AGRP 87-132 displace 125I-NDP-MSH
[d]NDP-MSH displace 125I-AGRP 87-132.

ESI-MS of fraction H showed a major component of 558 g/mol consistent with the MH+ of compound 5 (Figure 5.1). This molecule was synthesized separately, product confirmed by ESI-MS, and purified by HPLC. Although the peptoid showed no significant hMC4R cAMP inhibition at 100 nM, there is significant inhibition at 1.0 μM (Figure 5.3). In addition, 5 is an improved antagonist over fraction H at 10 μM. Partial agonist activity is seen with 10 μM peptoid at hMC1R. At high dosage 5 is also a partial agonist at hMC4R (data not shown). No significant antagonist activity is detected for 5 at hMC1R or hMC3R at 10 μM concentration (Figure 5.3).

Dose displacement curve indicated remarkably similar IC50 values for 5 when assayed against all three radiolabeled ligands. Fifty percent displacement by 5 at hMC4R was at 3.1 μM for 125I-[Nle4]-α-MSH, 2.1 μM for 125I-NDP-MSH, and 1.9 μM for 125I-AGRP (86-132). Table 5.2 shows these IC50's for 5 at hMC4R, as well as hMC1R and MC3R.

Table 5.2. IC50 (μM) of 5 displacing agonist and antagonist ligands at human melanocortin receptors.

	^{125}I-[Nle4] α-MSH	**^{125}I-AGRP (86-132)**	**^{125}I ASIP Y[90-132]**
hMC1R	9.1 ± 0.3	-	25 ± 4
hMC3R	48 ± 4	> 50	-
hMC4R	3.1 ± 0.9	1.9 ± 0.2	-

5 gives a 9.1 μM IC50 for 125I-[Nle4]-α-MSH displacement and 25 μM IC50 for displacement of 125I-hAgouti (ASIP (90-132, L89Y)). The pharmacology of 5 at hMC3R is consistent with a lack of activity with 48 μM IC50 for radiolabeled [Nle4]-α-MSH, and IC50 > 50 μM for AGRP (86-132). We explored two strategies for incorporating a turn into a peptoid backbone. Of these, one scaffold where a single chiral center was placed on a fixed side chain, was found to be synthetically convenient. Molecular geometry calculations and CD confirmed that backbone stereochemistry was indeed influenced by this single stereoactive center. A ligand displacement assay found that 2 was active whereas its enantiomer 4 was not. Interestingly, a non-chiral version, compound 3, was also active according to this assay. Using 2 as a starting point, a restricted library was developed and lead to the

identification of compound 5 as an MC4R antagonist with activity in the low micromolar range.

Several recent studies have used similar strategies for the development of MCR agonists. For example, Haskell-Luevano et al. recently used a heterocycle scaffold based on a β-turn motif to produce a 951 membered library. Within this library, an MC1R agonist with an EC50 of 42 μM was identified. Using an N-alkylaminoacid design, Mutulis et al. identified several compounds with low μM binding activity; however, agonist vs. antagonist function was not explored. The library based on the chiral peptoid scaffold developed here was significantly smaller than that of these previous studies yet quickly lead to the identification of compound 5 with μM activity.

Figure 5.3. cAMP activity at the hMC1, 3, and 4R for 10 nM α-MSH alone, with various concentrations of 5, and with 10 μM fraction H at hMC4R. * = significantly different from 10 nM α-MSH $P < 0.001$. ** = significantly different from control $P < 0.001$ (95% confidence interval).

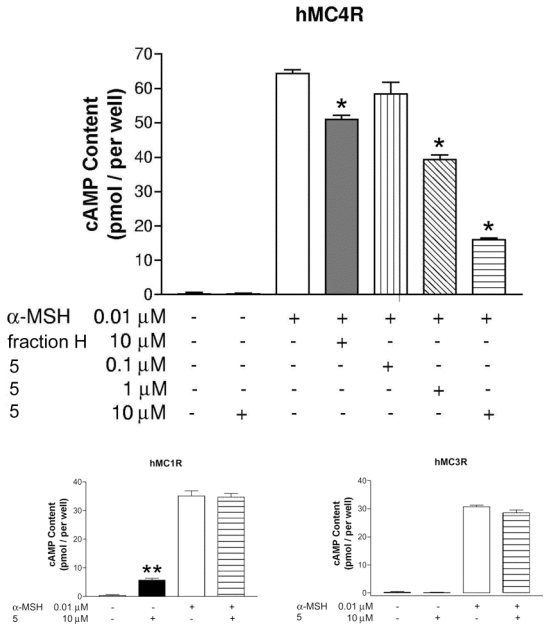

Molecules with AGRP-like function may play an important role in treating disorders related to negative energy balance. An AGRP polymorphism has been linked to anorexia nervosa and it has been suggested that MC4R targeted antagonists may serve as appropriate therapeutics (*25*). Cachexia is the wasting condition often associated with cancer and AIDS. Recent work on mice, in an anorexic state induced by tumor growth, has demonstrated that administration of AGRP stimulated feeding and helped reduce loss of lean body mass (*26*). The tunable molecular scaffold developed here may serve as an ideal starting point for the development of molecules for treating these and related conditions.

Here we demonstrated, using simple rational techniques, the development of a low micromolar antagonist mimicking AGRP activity at the hMC4R. The low molecular weight, protease resistance, enhanced lipophilicity, and synthetic accessibility of this template make it ideal for further structure function studies in regards to antagonism, agonism and inverse agonism. This molecule is the first rationally designed functional mimic of AGRP 111-113, supporting the established view of the RFF triplet as an active hMC4R pharmacophore in AGRP.

Acknoweldgements

Supported by NIDDK grants DK58606 (G.L.M.), DK54032 (I.G.), and by the University of Michigan Gastrointestinal Peptide Research Center (NIH Grant

P30DK34933). The authors are grateful to Justin Bursch for valuable synthesis assistance and Dr. Ying-kui Yang for preliminary pharmacological experiments. DT also thanks Drs. Reyna Simon and Lynne Canne for helpful discussions.

References

1. Ollmann, M. M., Wilson, B. D., Yang, Y. K., Kerns, J. A., Chen, Y., Gantz, I., and Barsh, G. S. (1997) Antagonism of central melanocortin receptors in vitro and in vivo by agouti-related protein, *Science 278*, 135-138.
2. Yang, Y. K., Thompson, D. A., Dickinson, C. J., Wilken, J., Barsh, G. S., Kent, S. B., and Gantz, I. (1999) Characterization of Agouti-related protein binding to melanocortin receptors, *Mol Endocrinol 13*, 148-155.
3. Huszar, D., Lynch, C. A., Fairchild-Huntress, V., Dunmore, J. H., Fang, Q., Berkemeier, L. R., Gu, W., Kesterson, R. A., Boston, B. A., Cone, R. D., Smith, F. J., Campfield, L. A., Burn, P., and Lee, F. (1997) Targeted disruption of the melanocortin-4 receptor results in obesity in mice, *Cell 88*, 131-141.
4. Butler, A. A., Kesterson, R. A., Khong, K., Cullen, M. J., Pelleymounter, M. A., Dekoning, J., Baetscher, M., and Cone, R. D. (2000) A unique metabolic syndrome causes obesity in the melanocortin-3 receptor-deficient mouse, *Endocrinology 141*, 3518-3521.
5. Fan, W., Boston, B. A., Kesterson, R. A., Hruby, V. J., and Cone, R. D. (1997) Role of melanocortinergic neurons in feeding and the agouti obesity syndrome, *Nature 385*, 165-168.
6. Rossi, M., Kim, M. S., Morgan, D. G., Small, C. J., Edwards, C. M., Sunter, D., Abusnana, S., Goldstone, A. P., Russell, S. H., Stanley, S. A., Smith, D. M., Yagaloff, K., Ghatei, M. A., and Bloom, S. R. (1998) A C-terminal fragment of Agouti-related protein increases feeding and antagonizes the effect of alpha-melanocyte stimulating hormone in vivo, *Endocrinology 139*, 4428-4431.
7. MacNeil, D. J., Howard, A. D., Guan, X., Fong, T. M., Nargund, R. P., Bednarek, M. A., Goulet, M. T., Weinberg, D. H., Strack, A. M., Marsh, D. J., Chen, H. Y., Shen, C. P., Chen, A. S., Rosenblum, C. I., MacNeil, T., Tota, M., MacIntyre, E. D., and Van der Ploeg, L. H. (2002) The role of melanocortins in body weight regulation: opportunities for the treatment of obesity, *Eur J Pharmacol 440*, 141-157.

8. Kiefer, L. L., Veal, J. M., Mountjoy, K. G., and Wilkison, W. O. (1998) Melanocortin receptor binding determinants in the agouti protein, *Biochemistry 37*, 991-997.
9. Tota, M. R., Smith, T. S., Mao, C., MacNeil, T., Mosley, R. T., Van der Ploeg, L. H., and Fong, T. M. (1999) Molecular interaction of Agouti protein and Agouti-related protein with human melanocortin receptors, *Biochemistry 38*, 897-904.
10. Bolin, K. A., Anderson, D. J., Trulson, J. A., Thompson, D. A., Wilken, J., Kent, S. B., Gantz, I., and Millhauser, G. L. (1999) NMR structure of a minimized human agouti related protein prepared by total chemical synthesis, *FEBS Lett 451*, 125-131.
11. Yang, Y. K., Fong, T. M., Dickinson, C. J., Mao, C., Li, J. Y., Tota, M. R., Mosley, R., Van Der Ploeg, L. H., and Gantz, I. (2000) Molecular determinants of ligand binding to the human melanocortin-4 receptor, *Biochemistry 39*, 14900-14911.
12. Haskell-Luevano, C., Cone, R. D., Monck, E. K., and Wan, Y. P. (2001) Structure activity studies of the melanocortin-4 receptor by in vitro mutagenesis: identification of agouti-related protein (AGRP), melanocortin agonist and synthetic peptide antagonist interaction determinants, *Biochemistry 40*, 6164-6179.
13. Jackson, P. J., McNulty, J. C., Yang, Y. K., Thompson, D. A., Chai, B., Gantz, I., Barsh, G. S., and Millhauser, G. L. (2002) Design, pharmacology, and NMR structure of a minimized cystine knot with agouti-related protein activity, *Biochemistry 41*, 7565-7572.
14. McNulty, J. C., Thompson, D. A., Bolin, K. A., Wilken, J., Barsh, G. S., and Millhauser, G. L. (2001) High-resolution NMR structure of the chemically-synthesized melanocortin receptor binding domain AGRP(87-132) of the agouti-related protein, *Biochemistry 40*, 15520-15527.
15. Mohle, K., and Hofmann, H. J. (1998) Secondary structure formation in N-substituted peptides, *J Pept Res 51*, 19-28.
16. Figliozzi, G. M., Goldsmith, R., Ng, S. C., Banville, S. C., and Zuckermann, R. N. (1996) Synthesis of N-substituted glycine peptoid libraries, *Methods Enzymol 267*, 437-447.
17. Miller, S. M., Simon, R. J., Ng, S., Zuckermann, R. N., Kerr, J. M., and Moos, W. H. (1994) Proteolytic Studies of Homologous Peptide and N-Substituted Glycine Peptoid Oligomers, *Bioorg Med Chem Lett 4*, 2657-2662.
18. Lipinski, C. A., Lombardo, F., Dominy, B. W., and Feeney, P. J. (1997) Experimental and computational approaches to estimate solubility and permeability in drug discovery and development settings, *Advanced Drug Delivery Reviews 23*, 3-25.
19. Haskell-Luevano, C., Rosenquist, A., Souers, A., Khong, K. C., Ellman, J. A., and Cone, R. D. (1999) Compounds that activate the mouse melanocortin-1

receptor identified by screening a small molecule library based upon the beta-turn, *J Med Chem 42*, 4380-4387.
20. Heizmann, G., Hildebrand, P., Tanner, H., Ketterer, S., Pansky, A., Froidevaux, S., Beglinger, C., and Eberle, A. N. (1999) A combinatorial peptoid library for the identification of novel MSH and GRP/bombesin receptor ligands, *Journal of Receptor and Signal Transduction Research 19*, 449-466.
21. Mutulis, F., Mutule, I., and Wikberg, J. E. (2002) N-alkylaminoacids and their derivatives interact with melanocortin receptors, *Bioorg Med Chem Lett 12*, 1039-1042.
22. Lee, J. H., Lim, S. K., Huh, S. H., Lee, D., and Lee, W. (1998) Solution structures of the melanocyte-stimulating hormones by two-dimensional NMR spectroscopy and dynamical simulated-annealing calculations, *Eur J Biochem 257*, 31-40.
23. Armand, P., Kirshenbaum, K., Falicov, A., Dunbrack, R. L., Jr., Dill, K. A., Zuckermann, R. N., and Cohen, F. E. (1997) Chiral N-substituted glycines can form stable helical conformations, *Fold Des 2*, 369-375.
24. Armand, P. (1998) *Dissertation*.
25. Adan, R. A., and Vink, T. (2001) Drug target discovery by pharmacogenetics: mutations in the melanocortin system and eating disorders, *Eur Neuropsychopharmacol 11*, 483-490.
26. Marks, D. L., Ling, N., and Cone, R. D. (2001) Role of the central melanocortin system in cachexia, *Cancer Res 61*, 1432-1438.

Epilogue

The experiments presented here are by no means exhaustive. If there is indeed a role for the N-terminus in the constitutive activity of most GPCRs, postulated in Chapter 1, then synthetic peptides corresponding to N-terminii of the other MCRs should agonize their respective receptors. Almost daily a new sequence of organismal genomes is completed, adding to the relatively large number of species specific agouti related protein sequences, one is described in Chapter 2. The simplified brain anatomy of fish and AgRP neuronal response induction of feeding behavior should permit endocrinologists to hypothesize about the origin of obesity in humans. Chapters 3 and 4 illustrate a bacterial expression system for mouse ASIP. Human ASIP preparation should follow similar techniques. The cDNA for human ASIP is in the Millhauser Lab freezer and was a gift from Greg Barsh. Once a protocol is established an inexperienced experimenter can manufacture multiple milligrams of material. This material can be used in a topical solution, probably containing DMSO, for the *in situ* antagonism of MC1R. Protein expression in minimal media containing stable isotopes will relieve congestion of the fingerprint region of the NOESY NMR spectrum and allow structural elucidation of the full length protein. In Yang Y-K et al. *Mol. Endo.* 1997 the authors find recombinant ASIP antagonizes MC2R and this inhibition cannot be reversed by addition of agonist, they term this "insurmountable" antagonism. In an equilibrium experiment this type of antagonism would be impossible, unless ASIP was irreversibly modifying MC2R in some way. I find such a scenario highly improbable and I would test my recombinant ASIP-YY for inhibition of MC2R activity. Finally,

chapter 5 discusses small molecules mimicking the active pharmacophore in AgRP, figure E.1 suggests a novel structure based on thioether cyclization. My second notebook details the synthesis of this molecule, however, it was never tested.

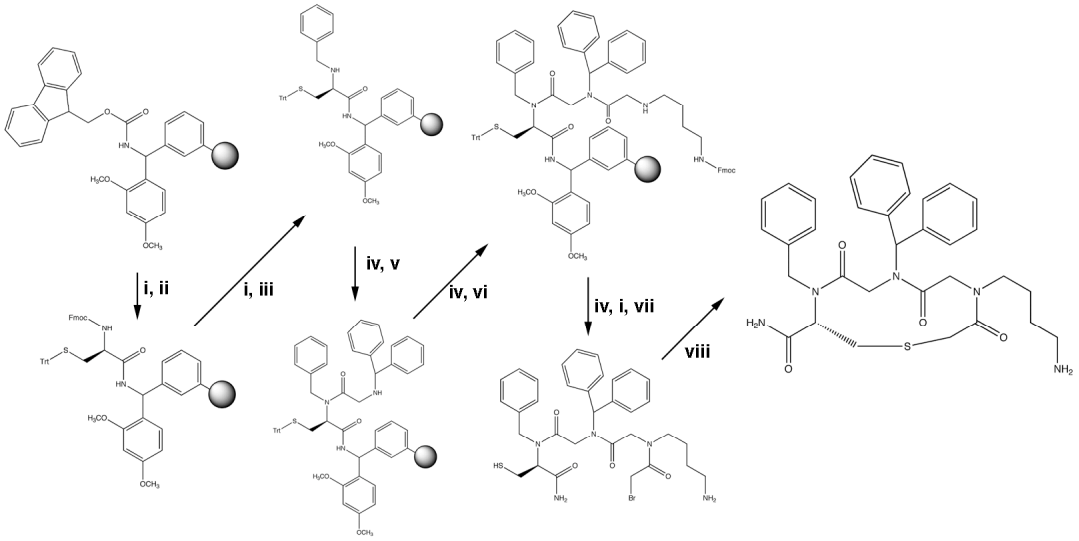

Total Potential Energy :	-18.3568 Kcal/mole	
Energy Component Breakdown :	Kcal/mole	Interactions
Bond Stretching	4.2503	86
Angle Bending	12.7642	151
Stretch-Bend	0.2611	138
Out-of-Plane Bend	0.2335	78
Torsional Angle	-7.8302	217
Van der Waals	7.3329	3166
Charge-Dipole	-6.0977	25
Dipole-Dipole	-29.2709	267
Total Electric Charge :	1.00000 Electrons	
Dipole Moment Magnitude :	29.327 Debyes	
Dipole X,Y,Z-Components :	-25.437 13.749	4.899
Total Accessible Area :	817.758 Square Angstroms	
Total Excluded Volume :	1566.547 Cubic Angstroms	

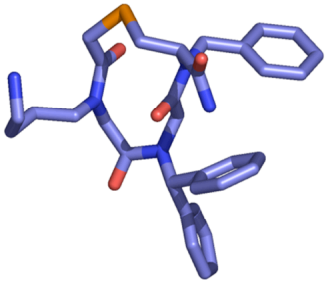

Figure E.1 (Top) Synthetic strategy for the preparation of thioether cyclized compounds. i) 20% v/v piperidine in DMF, ii) Fmoc-D-Cys(Trt)-OH, DIC, HOAt, iii) 7:2:1 DMF:Benzyl Bromide:DIEA, iv) bromoacetic acid, DIC, v) 20% v/v methyldiphenylamine in DMSO, vi) 20% Fmoc-diaminobutane in DMSO, vii) 95:5 TFA:TIS, viii) 3 M GuHCl 0.1 M Tris pH 6.7. (Bottom) DGEOM minimization of cyclic molecule with energy breakdown.